



AALBORG UNIVERSITET

*DETECTION OF
HYDRAULIC
CYLINDER
LEAKAGE*



THIS PAGE WAS LEFT INTENTIONALLY BLANK

Title:

Detection of Hydraulic cylinder leakage

Semester:

9th – 10th

Project period:

5/09/2015 - 9/06/2016

ECTS:

50

Supervisor:

Mohsen Soltani

Jesper Liniger

Project group:

OES10 – 2

Written by:**Synopsis:**

The main objective of this Master Thesis is to investigate the performance of fault detection and diagnosis (FDD) methods, by the use of the Extended Kalman Filter (EKF) and spectral analysis. A mathematical model is constructed and verified on the experimental setup. Signal processing of the FDD algorithms is done signal and model based. An EKF for each fault type is constructed, making it a bank of EKFs and isolating the faults. After parameter tuning and selecting fault thresholds system is tested for FDD purposes. The results show positive results for leakages above the threshold of Level 4 at 50bar and 100bar input pressures and 25°C. Fast Fourier Transformation (FFT) is used to analyze the spectral density of the EKF residual. It is possible to isolate the leakage. The pressure signal is analyzed in terms of spectral density to detect the leakage without prior manipulation. It is possible to detect a leakage

Arne Vietor

Dmitrij Lukjanec

Zoltan Balint

Number printed: 3

Pages: 137

Appendix: 27

Enclosures: 1 DVD

By signing this document, each member of the group confirms participation on equal terms in the process of writing the project. Thus, each member of the group is responsible for the all contents in the project.

Contents

1. Introduction.....	1
2. The Problem.....	2
2.1. Problem formulation	2
2.2. Delimitations.....	3
2.2.1. Overall.....	3
2.2.2. Software	3
2.2.3. Presentation.....	4
2.3. Task at hand	5
3. Theoretical model of the pantograph crane.....	6
3.1. The Setup	6
3.2. Planed model.....	6
3.3. The connected nonlinear model	7
3.4. Leakages in hydraulic systems.....	8
3.5. Fault choice	9
4. Mechanical System description	10
4.1. Introduction.....	10
4.2. Lagrangian and Newtonian approaches	10
5. Mechanical System Modeling.....	11
5.1. Geometrical constraints.....	12
5.1.1. Trigonometric functions.....	12
5.1.2. Curve fitting	14
5.1.3. Movement relationship between base and other frames	14
5.2. Setting up equations	15
5.2.1. Vector naming.....	17
5.2.2. Rod1	17
5.2.3. Rod3.....	19
5.2.4. Rod2.1	21
5.2.5. Rod2.2.....	22

5.2.6.	Lagrange method.....	24
6.	Hydraulic System description	25
6.1.	Hydraulic System Modeling	25
6.2.	Hydraulic system diagram	26
6.3.	Continuity equations	27
6.3.1.	Directional control valve.....	28
6.3.2.	Artificially implemented system leakage.....	31
6.3.3.	Cylinder leakage flow	31
6.3.4.	Bulk modulus	32
6.4.	Orifice equations	34
6.4.1.	K_v calculation.....	35
6.5.	Forces in the system.....	37
6.5.1.	Friction Force	38
7.	Model verification.....	40
7.1.	Verification of the mechanical model	40
7.2.	Verification of connected models	42
7.2.1.	Simulation conditions	42
7.2.2.	Results.....	43
8.	Fault Detection Diagnosis (FDD)	47
8.1.	Extended Kalman Filter based FDD	49
8.1.1.	Introduction.....	49
8.1.2.	Continuous-Discrete form model.....	52
8.1.3.	Extended Kalman Filter	57
8.1.4.	Bank of Extended Kalman Filters	60
9.	Experimental FDD implementation	65
9.1.	Data Gathering	65
9.2.	Experimental EKF results	69
9.2.1.	50bar – 25°C.....	72
9.2.2.	100 bar – 25°C.....	74

9.2.3.	50bar – 40°C.....	76
9.2.4.	100bar – 40°C.....	78
9.2.5.	50bar – 25°C – Tuned K_L 's	80
9.2.6.	Extended Kalman Filter conclusion	81
10.	Spectral analysis based FDD.....	82
10.1.	Introduction.....	82
10.2.	Fault detection using spectral analysis.....	82
10.3.	Residual analysis.....	85
10.4.	Spectral Analysis conclusion	88
11.	Comparison of the FDD methods	89
12.	Conclusion	90
13.	References.....	93
A.	Appendix.....	I
B.	Appendix.....	II
C.	Appendix.....	IV
D.	Appendix.....	VII
a.	Laboratory setup	VII
E.	Appendix.....	XVIII
a.	Step input 20%, 50 bar.....	XVIII
b.	Step input -20%, 50 bar.....	XIX
c.	Step input 40%, 50 bar.....	XX
d.	Step input -40%, 50 bar.....	XXI
e.	Step input 20%, 100 bar.....	XXII
F.	Appendix.....	XXIII
a.	EKF analysis – 50 bar – 25°C	XXIII
b.	EKF analysis – 50bar – 40°C	XXIV
c.	EKF analysis – 100bar – 25°C	XXV
d.	EKF analysis – 100bar – 40°C	XXVI
G.	Simulink diagrams	XXVII

Nomenclature

Mechanical Model

$[c_1] \cdot \ddot{x}_p$	- $[m/s^2]$	<i>Inertial part of the system</i>
$[c_2] \cdot \dot{x}_p^2$	- $[m/s]$	<i>Centripetal part of the system</i>
$[c_3] \cdot x_p$	- $[m]$	<i>Gravitational part of the system</i>
$d_{b \rightarrow cg1}^G y$	- $[m]$	<i>Only the second element of the vector, in the j_{base} direction</i>
$d_{b \rightarrow cg21}^G y$	- $[m]$	<i>Only the second element of the vector, in the j_{base} direction</i>
$d_{b \rightarrow cg22}^G y$	- $[m]$	<i>Only the second element of the vector, in the j_{base} direction</i>
$d_{b \rightarrow cg3}^G y$	- $[m]$	<i>Only the second element of the vector, in the j_{base} direction</i>
$d_{b \rightarrow r21}^G y$	0.155 $[m]$	<i>Y coordinate of global vector from base rotation frame to rod 2.1 rotation frame</i>
$d_{r1 \rightarrow cg1}^L x$	0.186 $[m]$	<i>X coordinate of local vector from rod 1 rotation frame to its center of mass</i>
$d_{r1 \rightarrow r22}^L x$	0.365 $[m]$	<i>X coordinate of local vector from rod 1 rotation frame to rod 2.2 rotation frame</i>
$d_{r21 \rightarrow cg21}^L x$	0.508 $[m]$	<i>X coordinate of local vector from rod 2.1 rotation frame to its center of mass</i>
$d_{r21 \rightarrow r1}^L x$	0.125 $[m]$	<i>X coordinate of local vector from rod 2.1 rotation frame to rod 1 rotation frame</i>
$d_{r21 \rightarrow r3}^L x$	1 $[m]$	<i>X coordinate of local vector from rod 2.1 rotation frame to rod 3 rotation frame</i>
$d_{r22 \rightarrow cg22}^L x$	0.44 $[m]$	<i>X coordinate of local vector from rod 2.2 rotation frame to its center of mass</i>
$d_{r3 \rightarrow cg3}^L x$	1.35 $[m]$	<i>X coordinate of local vector from rod 3 rotation frame to its center of mass</i>
g	9.81 $[kg/m^2]$	<i>Gravitational acceleration</i>
$i_{rod\#}$	1 $[-]$	<i>x direction unit vector</i>
$j_{rod\#}$	1 $[-]$	<i>y direction unit vector</i>
$k_{rod\#}$	1 $[-]$	<i>z direction unit vector</i>

L_0	$0.348[m]$	<i>Fixed length describing distance from pivot point to cylinders motion axis</i>
m_{r1}	$6.12844 [kg]$	<i>Mass of rod 1</i>
m_{r21}	$15.36792 [kg]$	<i>Mass of rod 2.1</i>
m_{r22}	$13.62235 [kg]$	<i>Mass of rod 2.2</i>
m_{r3}	$87.92456 [kg]$	<i>Mass of rod 3</i>
θ_1	$- [rad]$	<i>Angle between base frame x – coordinate and rotation frame x coordinate of rod 1 and 3</i>
θ_2	$- [rad]$	<i>Angle between base frame x – coordinate and rotation frame x coordinate of rod 2.1 and 2.2</i>

Hydraulic Model

A_p	$3.117e-3 [m^2]$	<i>Cross sectional area of the cylinder piston part</i>
A_r	$2.41e-3 [m^2]$	<i>Cross sectional area of the cylinder ring part</i>
B	$5000 [Nms]$	<i>Damping coefficient</i>
c_{ad}	$1.4 [-]$	<i>Adiabatic gas constant</i>
c_v	$10 [s/m]$	<i>Stribeck constant</i>
F_L	$- [N]$	<i>Load force</i>
F_{brk}	$- [N]$	<i>Breakaway friction force</i>
F_{cou}	$480 [N]$	<i>Coulomb friction</i>
F_f	$- [N]$	<i>Total Friction force</i>
F_v	$- [N]$	<i>Viscous friction</i>
K_{Lp}	$2.32e-9 [-]$	<i>Constant used in calculating Q_{Lp}</i>
K_{Lv}	$5.5e-13 [-]$	<i>Constant used in calculating Q_{Lv}</i>
K_v	$- [-]$	<i>Valve coefficient of the DCV spool</i>
P	$- [Pa]$	<i>Pressure in a particular node</i>
Q	$- [m^3/s]$	<i>Volume flow rate of oil through a particular node</i>
Q_{Lp}	$- [m^3/s]$	<i>Sealing leakage flow</i>
Q_{Lv}	$- [m^3/s]$	<i>DCV leakage flow</i>
V	$- [m^3]$	<i>Volume in general</i>
V_{p0}, V_{r0}	$- [m^3]$	<i>Initial fluid volumes in the control volumes</i>
u_v	<i>Reference $x_v [-]$</i>	<i>Valve input</i>
x_p	$- [m]$	<i>Position of the hydraulic cylinder</i>
x_v	$- [\% / 100\%]$	<i>Position inside the directional valve</i>

x_v	$-1 \leq x_v \leq 1 [-]$	Valve position
β_{eff}	- [bar]	Effective bulk modulus
β_{ideal}	16000 [bar]	Ideal bulk modulus
Δp	- [Pa]	Difference in pressure in a certain node
ε_a	- [%]	Volumetric air ratio
ε_{a0}	0-15 [%]	Air percentage in the system
ζ_v	0.92 [-]	Valve damping ratio
β	- [bar]	Compressibility – Bulk modulus
ρ	870 [kg/m ³]	Oil density
ω_v	280 π [rad/s]	Valve Eigen frequency

Fault detection

$\dot{\hat{\mathbf{x}}}$	Predicted state vector derivative
$\dot{\mathbf{x}}_k$	State vector derivative
$\hat{\mathbf{x}}_{k k}$	Updated state vector estimate
$\hat{\mathbf{x}}_{k k-1}$	Predicted state vector estimate
$\hat{\mathbf{y}}_k$	Innovation sequence or residual
\mathbf{H}_k	State selection matrix
\mathbf{K}_k	Kalman gain
$\mathbf{P}_{k k}$	Updated covariance estimate
$\mathbf{P}_{k k-1}$	Predicted covariance estimate
\mathbf{R}_k	Covariance matrix
\mathbf{S}_k	Innovation sequence or residual covariance
\mathbf{v}_k	Gaussian noise of 0 mean and diagonal covariance matrix in the output
\mathbf{y}_k	Output vector
\mathbf{z}_k	Measurement vector
$h(\mathbf{x}_{k k-1})$	Predicted output function
$h(\mathbf{x}_k)$	Output function
$\mathbf{A}(\hat{\mathbf{x}})$	Jacobian matrix of $\mathbf{f}(\mathbf{x}, \mathbf{u})$
\mathbf{I}	Identity matrix
$\mathbf{P}(t)$	Covariance prediction
\mathbf{Q}	Covariance matrix
$\mathbf{f}(\mathbf{x}, \mathbf{u})$	Differentiable system describing function vector
\mathbf{w}	Gaussian noise of 0 mean and diagonal covariance matrix in the states

Abstract

This Master Thesis explores the application of Fault Detection and Diagnosis (FDD) algorithm on a hydraulic crane setup. Extended Kalman Filter (EKF) and Spectral analysis were developed and tested, to see the role and the relationship between the leak magnitude and the chance of it being identified and possibly isolated. Laboratory experiments were conducted, followed by verification of the mathematical model and further offline model and signal based simulations. The findings in the research illustrate how the magnitude of the leak influences whether or not the fault can be detected and isolated. Choosing a threshold constant for the leak coefficients played a crucial role in determining the faults. The selected threshold proved to hold for leaks of level 4 and higher, while being inaccurate for lower levels. The results proved the superiority of the EKF over the spectral analysis. After further insight, it was concluded that spectral analysis is a very quantitative method that requires a lot of pre-analyzing for determining the faults, while EKF provides trustworthy results over the artificial leak level of 4 (0.1293 – 0.9853 l/min) at 25°C. Further research is prompt of re-thinking the EKF structure, with a possibility of implementing the leaks as a state with leak coefficients as an updating parameter estimates.

1. Introduction

It is not that difficult to recognize the wide range of hydraulic applications in industry and the role that they play in daily life. Hydraulics have been the mainstay of the modern world and, currently, they do not seem to have any competing technology to replace it.

Cylinder leakage can cause a lot of inconveniences or even put the process to a full stop. We are not talking simple pollution of the surroundings and the system itself, even though it is a major problem as well. Loss of liquid and pressure can lead to mechanical failures of the system which can result in immense damage, depending on the place and purpose for it is implemented.

Cylinder leakage can cause a lot of inconveniences or even put the process to a full stop. This master thesis focuses on the problems that can occur when loss of liquid and pressure leads to mechanical failures of the system which in turn can result in immense damage, depending on the location and purpose for which it is implemented. Clearly, other severe damage caused by cylinder leakage is possible, such as environmental pollution, risks for humans, animals and natural habitats. These are not dealt with in this master thesis.

Most hydraulic systems work under high pressure, which amplifies the damage that a single leak can cause both to the system, the surroundings and the operators.

Leakage can appear due to a number of factors, such as physical damage to the cylinder's components, contaminated liquid in the cylinder, too high or low operating temperatures, too high operating pressures or chemical reactions. The most common reason causing leakage is the premature rod seal failure.

Detecting early signs of leakage can prevent such accidents as well as increase the reliability of the system.

There are multiple methods for fault detection and diagnosis for hydraulic cylinder leakage. Still, there is no certain criterion for when it is better to use one method over another, nor the comparison of their effectiveness. Therefore, the aim of the project is to make a comparison between several most promising methods by implementing them on a pantograph crane and executing fault detection and diagnosis (FDD). The following approaches are to be implemented:

- Kalman filter
- Spectral analysis

2. The Problem

2.1. Problem formulation

The primary problem lies in the fact, that currently there are multiple ways used to do Fault Detection Diagnosis (FDD) on leakages in hydraulic cylinders. The problem lies in making a comparison and gain knowledge in terms of which method is more reliable, accurate or which should be used under specific circumstances.

The following questions match the description of the problems of this project:

- Which faults that cause the leakage, are to be covered by these FDD methods?
- Should the FDD algorithm be based on the theoretical model or the measured data?
- Which simulation/experimentation conditions are to be chosen, so neither FDD methods have an upper hand when implemented?
- Which data is to be recorded during the experimental procedure?

And the question, which would sum up the idea and the sole purpose behind this project:

- Where and when is it better to use a specific FDD method?

The secondary problem focuses on the intermediary problems, mostly technical, which need to be overcome in order to achieve any kind of results. This takes into consideration the problems, which occur when modeling, conducting research, experiments and implementation of the algorithm, when trying to acquire answers to the initial statement.

The following approach is used:

- Development of a hydraulic and a mechanical model of the system in a way that both can be interconnected
- Verification of the precision of the theoretical model with the data collected via experiments.
- Implementation of the FDD

The problem lies in the execution procedure and ways of modeling and collecting all the needed data. The following questions describe the occurring problems:

- Which modeling approaches are to be used to model the system?
- How should the faults be represented in the physical system during the experiments?
- How should the faults be modeled during the simulation?
- Which model precision suits the needs?
- For which methods FDD should be based on measured data and for which on the model?
- Do any FDD methods require linearizing the system/convert to state space?
- What are the cons, pros and results of each FDD method when they are implemented on the same experimental rig under the same initial conditions and performing the same tasks?

2.2. Delimitations

2.2.1. Overall

- Existing setup will be used with no modifications from our side.
- Any results achieved will be valid for this specific setup and the used parameters.
- Sensors of different precision will be used to gather the needed data.
- Sampling frequency will be chosen optimal for the process according to target PC limitations.
- Traditional methods will be used to model the hydraulic and mechanical systems.
- Mechanical parameters will be extracted from a 3D model of the exact crane.
- Models will be focused to be made accurate, though unknown parameters will/can be used as “tuning” parameters.
- Leakage detection is the primary purpose and leakage magnitude estimation is not

2.2.2. Software

- The symbolic mechanical model will be derived by the use of Maple.
- The numerical model will be ran and simulated by the use of Matlab.
- The hydraulic model will be assembled and simulated in Matlab Simulink.
- The connected models will be simulated in Matlab Simulink.
- The FDD methods will be applied in Matlab.
- SolidWorks will be used for technical drawings.
- Simulink Real Time will be used to gather the data during experiments.

2.2.3. Presentation

- The report will be written in Microsoft Word and converted to PDF format.
- The charts and tables in the report will be made by the use of Microsoft Excel where possible.
- Matlab simulation graphs will be presented in high resolution .eps format.
- Data from the experiments will be collected and assembled into a data base.
- Everything of secondary importance/relation to the project will be presented in the appendix.
- Everything referenced will be in the reference list or in the appendix.

Having as the main purpose of this project, developing a reliable fault detection diagnosis (FDD) on a hydraulic system, represented in our case by a hydraulic crane, some experiments are required to be executed in order to validate the FDD and the models used in the process. The laboratory setup is built using state of the art, or as close to state of the art equipment: flow meters, pressure gages, valves, pipes, hydraulic cylinders etc. Less accurate sensors will be used to measure the flow across the flow valve, while more precise flow meters will be placed to measure the leakage.

A way to log the movement of the cylinder has to be added to the system using position transducer connected, through an I/O card, to a computer which is using Matlab built in logging utility (Simulink Real-Time).

Sampling frequency is limited by the target computer. Through maximization of the target Pc CPU usage and allowing it to skip samples instead of overloading, sampling frequency was increased to 1000 Hz.

No modification of mechanical parts of the crane will be done, with the exception of adding sensors which, because of their positioning and reduced weight, will have little to no effect on the mechanical systems behavior.

The mechanical part of the system will be modeled using the Lagrangian mechanics while the hydraulic circuit by the use of orifice, continuity and Newton's second law equations.

Since there is a 3D model of the crane, dimensions will be taken from there, instead of measured from scratch. Hydraulic dimensions will be taken from data sheets and others measured, if possible. Parameters which are not possible to estimate, such as volumetric ratio of air, will be used as a "tuning" parameter and will be tuned to suit our means.

The mechanical model will be derived in Maple, due to the fact that it is more comfortable to work with symbolic equations. All simulations will later be simulated in Matlab and Simulink due to simplicity.

2.3. Task at hand

In order to build a reliable fault detection diagnosis model, some steps have to be taken before hand. To be able to predict the behavior of the system, some mathematical models have to be created. First step - a dynamic hydraulic model of the actual hydraulic system has to be done using continuity equations, force equilibrium equations, flow through restrictions (orifice equations), some factors have to be taken into account such as: losses in the pipeline, leakage losses in the cylinder and the non-linear dependency of the bulk modulus with regards to pressure.

The second step is the description of the mechanical system using Lagrangian kinematics. The movement of the mechanical parts has to be mathematically explained in order to understand the shifting of the load on the hydraulic cylinder.

After the completion of the models, they have to be implemented and tested on the test bench, which in the meanwhile will be constructed. The pantograph crane is used. There will be a series of sensors and measurement devices present on the crane such as: flow meters, pressure sensors, position sensors. These will allow real time measurements for future FDD analysis.

After the models have been verified the second phase of the process will begin, the implementing and testing of some FDD methods.

FDD methods can be divided into two types for our case:

- Signal based
- Model based

The first case involves the use of the data collected from the experiment. These qualitative and quantitative methods do not require the model and are carried out without it. Spectral analysis will be done manually through Matlab .m file, possibly with aid from Signal Processing toolbox from Matlab.

The second case, observer based FDD method, requires a model. The Extended Kalman Filter shall be made manually in a Matlab .m file with our chosen operation points.

3. Theoretical model of the pantograph crane

3.1. The Setup

The setup consists of a coupled mechanical system, which is a pantograph crane and a standard hydraulic circuit, which is the main driving force behind the entire system.

The interesting and ominous part of the system is the pantograph crane. Pantograph is a system, which is connected based on parallelogram principles. This principle was commonly used for duplication, as the first point is tracing a line trajectory, the other point will trace an enlarged or miniaturized same trajectory.

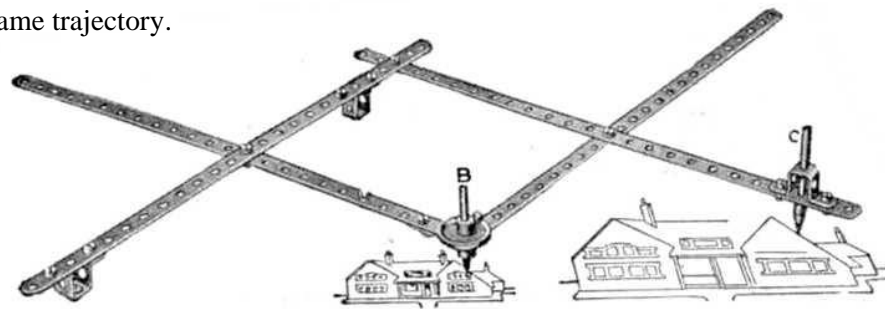


Figure 3-1 Sketch of a pantograph working principle [17]

In a pantograph, the horizontal and vertical bars are defined by the same angles, meaning, both horizontal bars move in the same manner, and both vertical bars move in the same manner, when they are driven by the hydraulic circuitry or any other movement producing actuator.

3.2. Planed model

The idea behind modeling the whole system is to have at the beginning a separate model for the mechanical part and a separate model for the hydraulic circuit. The two models would be interconnected via an iteration loop, where the hydraulic model would supply the load force to the mechanical, and in return the mechanical model would give out the position and velocity of the piston. Through being in the loop, the values would be constantly updated according to each other's magnitude.

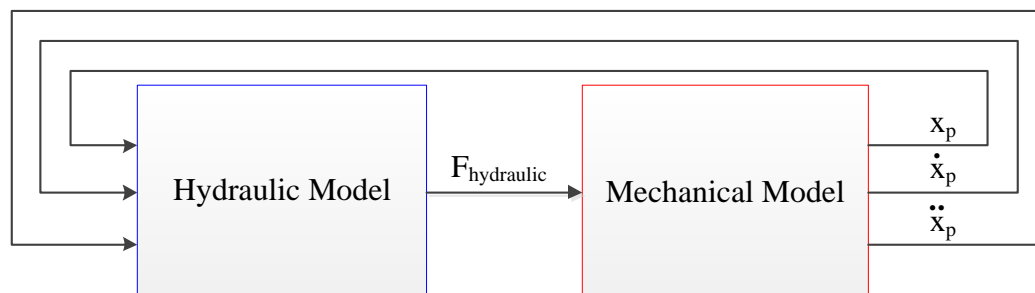


Figure 3-2 Simplified block diagram of the nonlinear models

All the properties of the mechanical model are known, due to the fact that the masses, dimensions are not changing and can be obtained from the 3D model and technical drawings. The hydraulic model is more difficult and for this the experimental rig is needed to be used. While some parameters given by the hydraulics can be measured, some, as the discharge coefficients have to be calculated, as they might be different from the ones specified in the manual, due to excessive exploitation.

Model verification will be done by comparing the data from the simulated model with the data, that the sensors will provide during experiments. Different patterns of crane movement are to be used and the data obtained to be compared, to estimate the model precision.

3.3. The connected nonlinear model

After the mechanical and hydraulic models have been completed, both of them need to be interconnected, as they are dependent on each other.

The hydraulic model will give the hydraulic forces in order for the mechanical model to be able to calculate the required acceleration, which after integrating, will serve as a feedback to the hydraulic model.

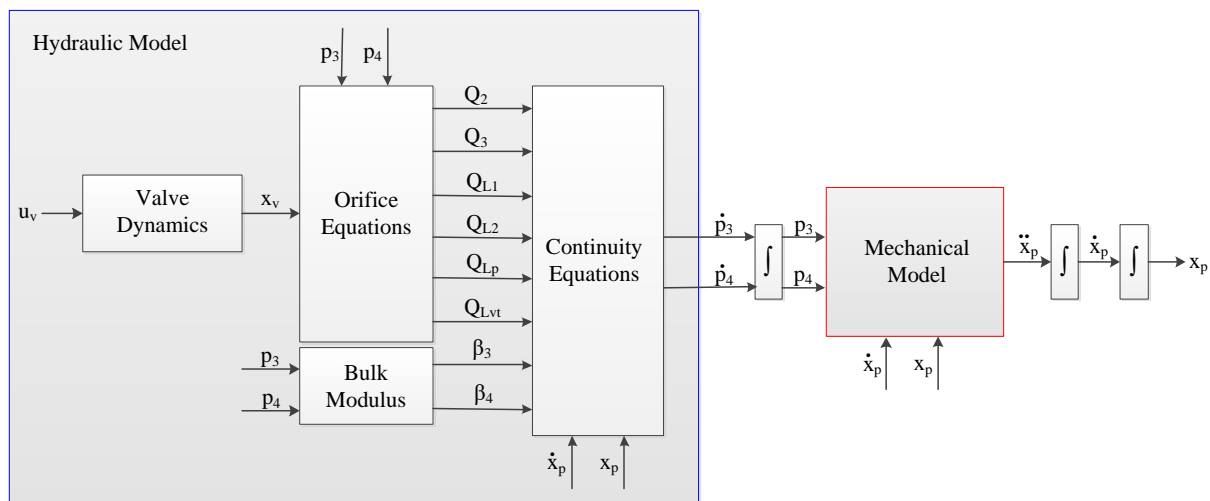


Figure 3-3 Block diagram explaining the process of combining the two models [13]

3.4. Leakages in hydraulic systems

Some leakages are constantly present in the system and are neglected unless their magnitude increases drastically to a point that it undermines the systems performance. Some leakages can appear over the course of time that the system is used, and may be the cause of puncture, corrosion, wear.

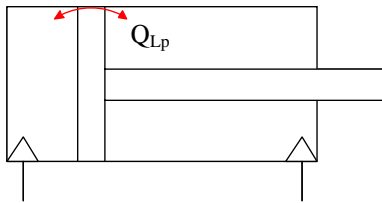
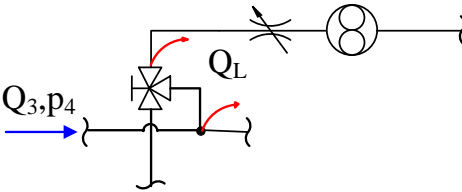
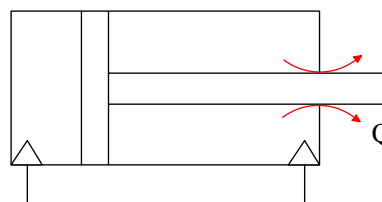
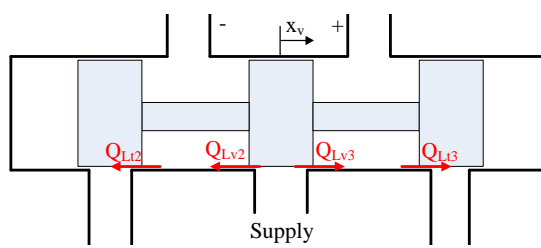
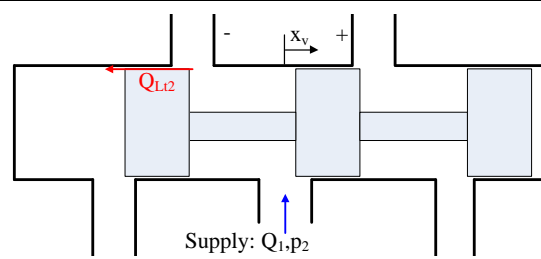
Cylinder leak		Cause: <ul style="list-style-type: none"> Defective seal
Hose leak		Cause: <ul style="list-style-type: none"> Defective fitting
Rod leak		Cause: <ul style="list-style-type: none"> Defective seal
Closed valve leak		Cause: <ul style="list-style-type: none"> Wear of the spool
Open valve leak		Cause: <ul style="list-style-type: none"> Wear of the spool

Table 3-1 Different types of leakages occurring in the hydraulic system [13]

3.5. Fault choice

In our setup, artificial faults, in the form of leaks, will be implemented into the system and are expected to be detected by FDD algorithms, as they can be controlled without damaging the system and be fully measured.

In addition to these artificial faults, system leaks will be present and will be modeled to get the most precise mathematical model of the system. These, permanent faults cannot be taken out and therefor will be acting alongside the artificial leaks.

Two artificial leaks will be implemented:

- Leak 1 - artificial leak along the valve
- Leak 2 - artificial leak across the hydraulic cylinder

Due to the big pressure in the system, leakages will occur alongside the artificial leaks. These are present mostly due to the seals or wear and are a common thing for any hydraulic system:

- Supply to port to tank – when the valve is closed
- Supply to tank – when the valve is open

As well as in the cylinder:

- Leak across the two hydraulic cylinder chambers

FDD requires a precise model, therefor all those leaks are to be taken into consideration and modeled. They can influence the flow, as well as the piston position and pressure changes.

4. Mechanical System description

4.1. Introduction

The Lagrange method will be used in order to derivate the dynamic model for the pantograph crane. The Lagrangian approach demands complex derivations, but the end result may be arranged in an equation form, which will consist of the, inertial part, centripetal force, gravity part. With the use of the Euler method, it is possible to determine the Euler angles and therefor position. A major assumption, when using this method, is that all elements of the system are rigid.

4.2. Lagrangian and Newtonian approaches

There are multiple methods for modeling, based on references [1, 2], a multi-dimensional mechanical system: the Newtonian approach, Lagrangian mechanics, which can be combined with Hamiltonian mechanics.

Newtonian mechanics mainly utilize the rectangular coordinate systems while considering all of the constraint forces of the system. The more constraints the system has the more complex the Newtonian model is.

Lagrange mechanics do not include the constraint forces and instead utilize any generalized coordinates, such as the angles, radial distances, where the amount of generalized coordinates is consistent with the amount of degrees of freedom of the system.

While both methods are supposed to give the same final results, it is sometimes more convenient to use one over another. Even though the Lagrangian approach requires utilizing the calculus of variations, the way to construct the model is simpler due to the possibility of using generalized coordinates, instead of standard like in the Newtonian approach.

Due to the fact, that the pantograph crane has mimicking motion of the parallel beams, which can be described through a trigonometric function, the Euler angle method shall be used. The rotation matrixes shall be placed at the joint around which the bars revolve. Due to the fact that parallel beams experience the same rotations and have equal angles, only two rotation matrixes have to be used, one for the vertical beams and one for the horizontal.

5. Mechanical System Modeling

The entire chapter 5 was built upon the information found in Y. Wang. (2015) *Dynamic Modeling and Simulation of Marine Satellite Tracking Antenna Using Lagrange Method* [1] and H. Goldstein, C. Poole, J. Safko (2002) *Classical Mechanics, 3rd Edition* [2].

Reference frame setup

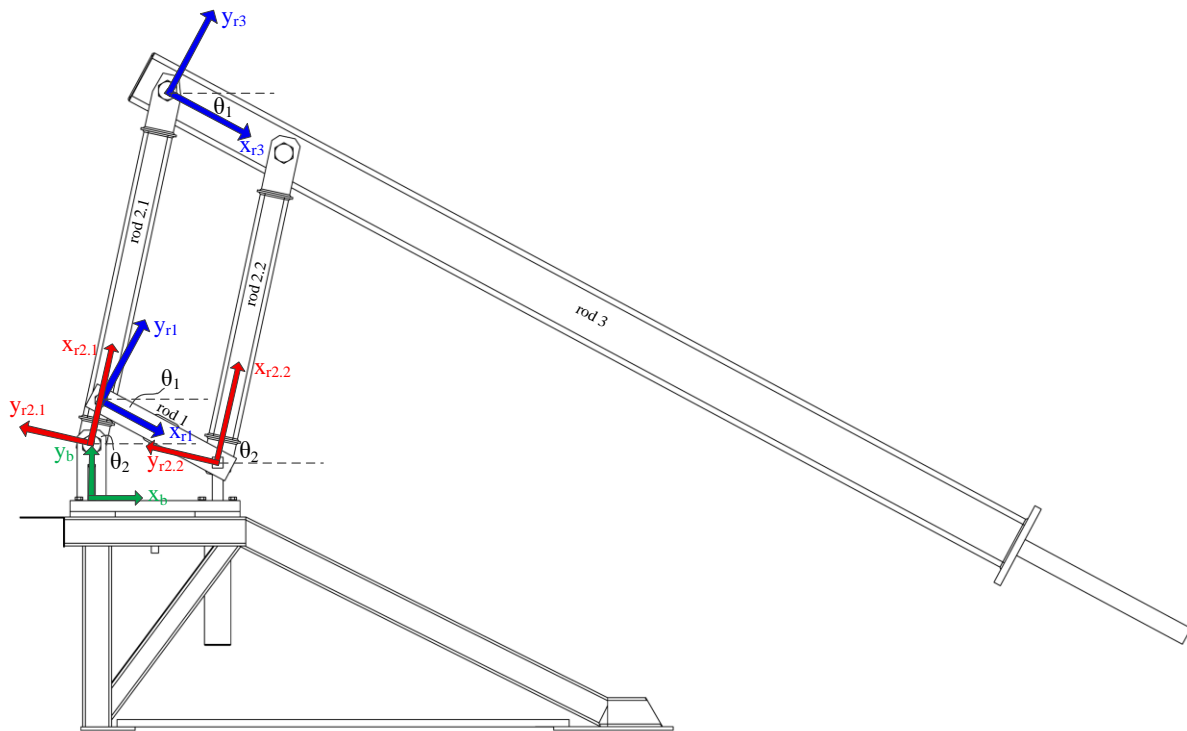


Figure 5-1 Positioning of global and local reference planes

All the components are interconnected in a way that they have only 1 degree of freedom. Relationship between the component movements will be done by making a vector, from a static reference frame to the centroid of a moving part, through the dynamic reference frame of the same moving part.

The static reference frame is placed on a fixed joint, around which the whole structure rotates, making it possible to have a static coordinate as a reference.

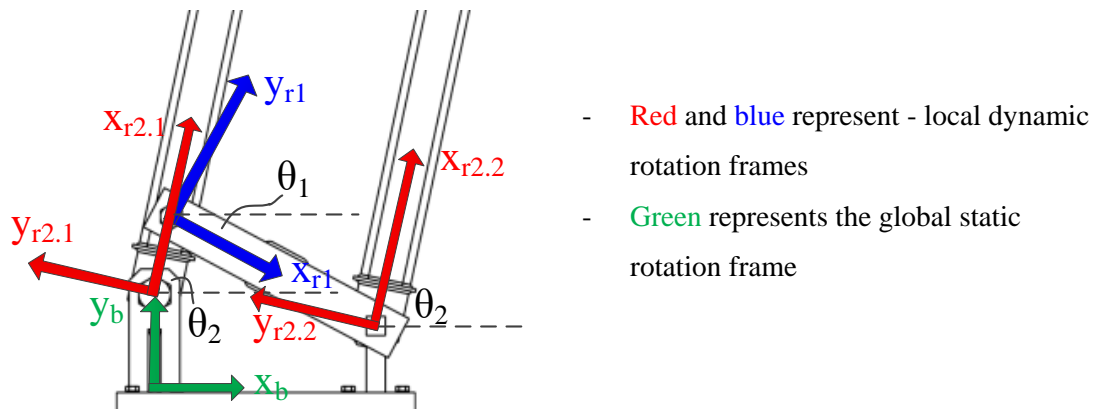


Figure 5-2 Static Base reference frame detail

The dynamic reference frames are placed at the closest joints to the base reference frame. Further, from this reference frame it is possible to make a vector to the centroid of the part. Since the physical dimensions of the components do not change, it will be a fixed value vector.

5.1. Geometrical constraints

5.1.1. Trigonometric functions

Using a combination of trigonometric functions such as Pythagoras theorem and cosine rule, a relationship between the angle change and the change in the hydraulic cylinder rod length can be found.

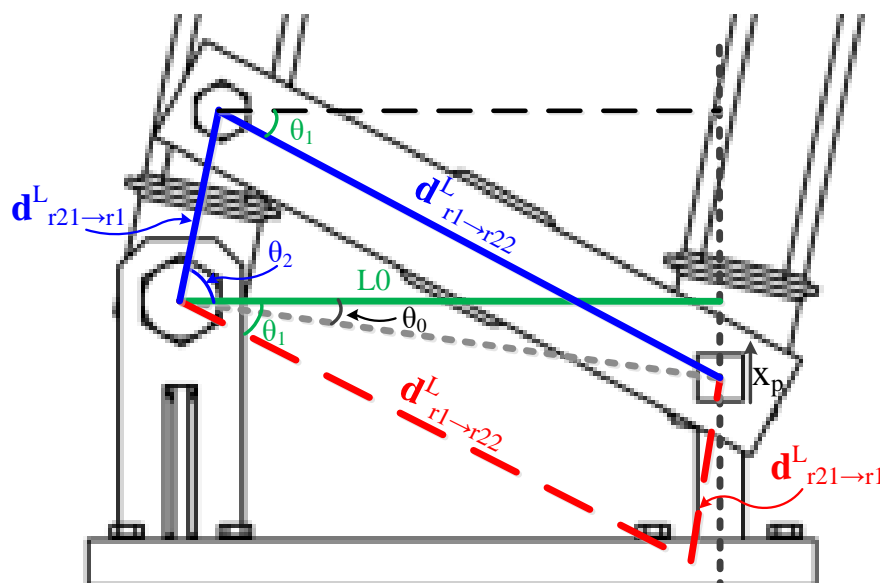


Figure 5-3 Theoretical triangles used in finding angle relationship

After applying the trigonometric functions, using the Figure 5-3 as reference we end up with the following expressions for the angles:

$$\cos(\theta_1) = -\frac{\mathbf{d}_{r1 \rightarrow r22}^L{}^2 - \mathbf{d}_{r21 \rightarrow r1}^L{}^2 + (L0^2 + xp^2)}{2 \cdot \mathbf{d}_{r1 \rightarrow r22}^L \sqrt{(L0^2 + xp^2)}} + \theta_0 \quad (5.1)$$

$$\cos(\theta_2) = \frac{\mathbf{d}_{r21 \rightarrow r1}^L{}^2 - \mathbf{d}_{r1 \rightarrow r22}^L{}^2 + (L0^2 + xp^2)}{2 \cdot \mathbf{d}_{r21 \rightarrow r1}^L \sqrt{(L0^2 + xp^2)}} + \theta_0 \quad (5.2)$$

<i>Variable Name</i>	<i>Value [Unit]</i>	<i>Description</i>
θ_1	- [rad]	Angle between base frame x – coordinate and rotation frame x coordinate of rod 1 and 3
θ_2	- [rad]	Angle between base frame x – coordinate and rotation frame x coordinate of rod 21 and 22
θ_0	- [rad]	Angle between L0 length and distance from the rotation axis to the piston position
\mathbf{d}	-[m]	Position vectors
xp	-[m]	Cylinder position
$L0$	0.348[m]	Fixed length describing distance from pivot point to cylinders motion axis

Due to the way the local coordinates work all vectors and angles become functions of the cylinder position. This occurs because the local reference frame rotates together with the rods, which makes the scalar distances the same no matter at which position you are as such giving a fixed relation between cylinder position and the rotation of each rod.

If the reference is the horizontal axis, it can be expressed with the extension of the hydraulic cylinder rod in the y axis and a fixed distance in the x direction between the cylinder and the static base reference frame:

$$\theta_0 = \text{atan} \frac{xp(t)}{L0} \quad (5.3)$$

5.1.2. Curve fitting

For optimisation and execution purposes, the calculated angle relationship from Eq.5.1 and 5.2, for θ_1 and θ_2 were curve fitted and been reduced to the following 1st and respectively 2nd order equations [Appendix A]:

$$\theta_1 = 162.5 \cdot xp - 19.99 \quad (5.4)$$

$$\theta_2 = -664.6 \cdot xp^2 + 163.9 \cdot xp + 87.71 \quad (5.5)$$

5.1.3. Movement relationship between base and other frames

Due to the planar motion of the system, the rotation relationship shall be the same for all of them, with an angle, corresponding to the specific rod present in it:

$$\mathbf{i}_{rod\#} = \cos(\theta_{rod\#}) \cdot \mathbf{i}_{base} - \sin(\theta_{rod\#}) \cdot \mathbf{j}_{base} \quad (5.6)$$

$$\mathbf{j}_{rod\#} = \sin(\theta_{rod\#}) \cdot \mathbf{i}_{base} + \cos(\theta_{rod\#}) \cdot \mathbf{j}_{base} \quad (5.7)$$

$$\mathbf{k}_{rod\#} = \mathbf{k}_{base} \quad (5.8)$$

<i>Variable Name</i>	<i>Value [Unit]</i>	<i>Description</i>
$\mathbf{i}_{rod\#}$	1[-]	<i>x direction unit vector</i>
$\mathbf{j}_{rod\#}$	1[-]	<i>y direction unit vector</i>
$\mathbf{k}_{rod\#}$	1[-]	<i>z direction unit vector</i>

While, the structure of the rotation matrixes will be exactly the same, the angles presented in them will differ, as every component has a specific symbolic angle assigned to it. From the above [Figure 5-3] mentioned dynamic reference frame movement to the static base frame it is possible to construct the following rotation matrixes:

Rotation matrix between the static base reference frame and dynamic rod 1 and rod 3 reference frame:

$$\mathbf{R}_1 = \begin{bmatrix} \cos(\theta_1) & -\sin(\theta_1) \\ \sin(\theta_1) & \cos(\theta_1) \end{bmatrix} \quad (5.9)$$

Rotation matrix between the static base reference frame and dynamic rod 2.1 and 2.2 reference frame:

$$\mathbf{R}_2 = \begin{bmatrix} \cos(\theta_2) & -\sin(\theta_2) \\ \sin(\theta_2) & \cos(\theta_2) \end{bmatrix} \quad (5.10)$$

5.2. Setting up equations

The Lagrangian mechanics are based on the energy difference principle method. This is represented in the Lagrangian, a function which summarizes the whole systems dynamics: the difference between the sum of rotational and translational kinetic energies of each component of the system and sum of potential energies of all the systems components.

In order to get the energy differences, it is necessary to track the motion of the center of gravity of each rod with respect to the global reference frame.

Global and local coordinate systems are used to represent the resultant vector and its components. Global coordinates represent the entire system that is being modeled and are fixed, making them a global reference point.

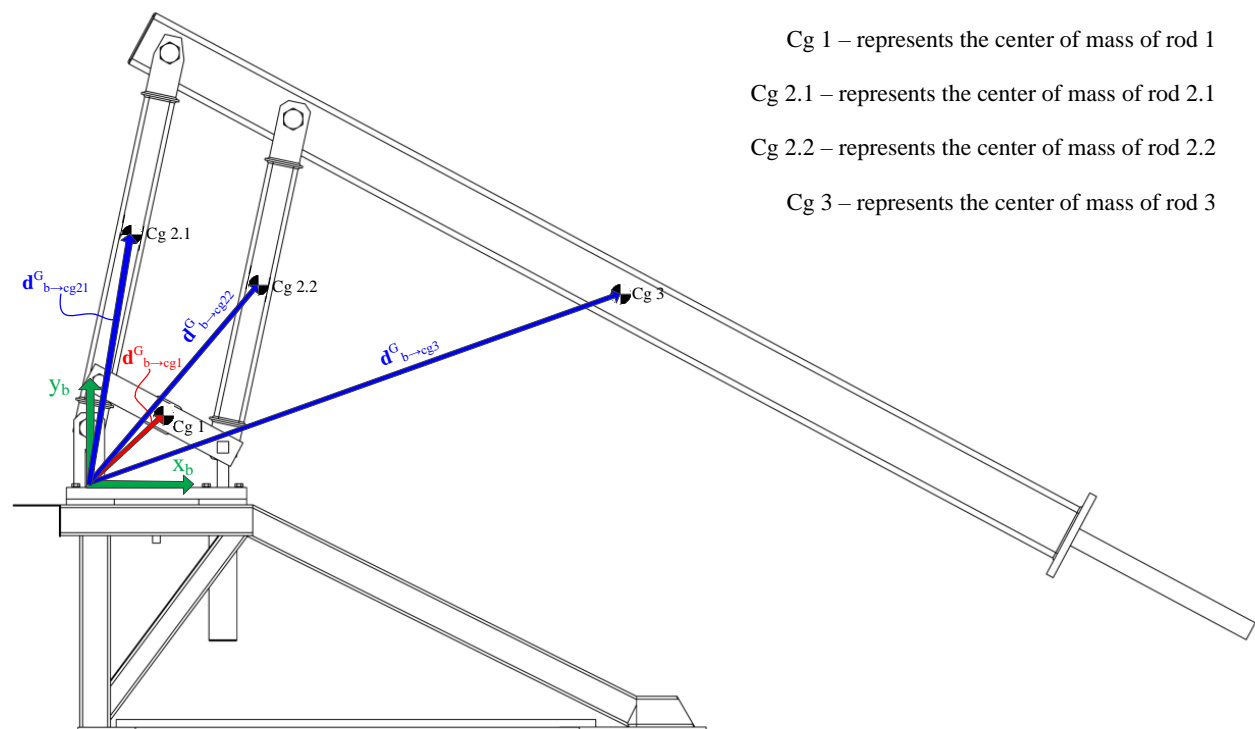


Figure 5-4 Representation of Global vectors linking the base frame origin with the centers of masses

Local coordinates are located within the global coordinates. The local origin may be located anywhere in the global coordinate system and can be both static and non-static. The kinematics of a local reference frame can be described through trigonometry.

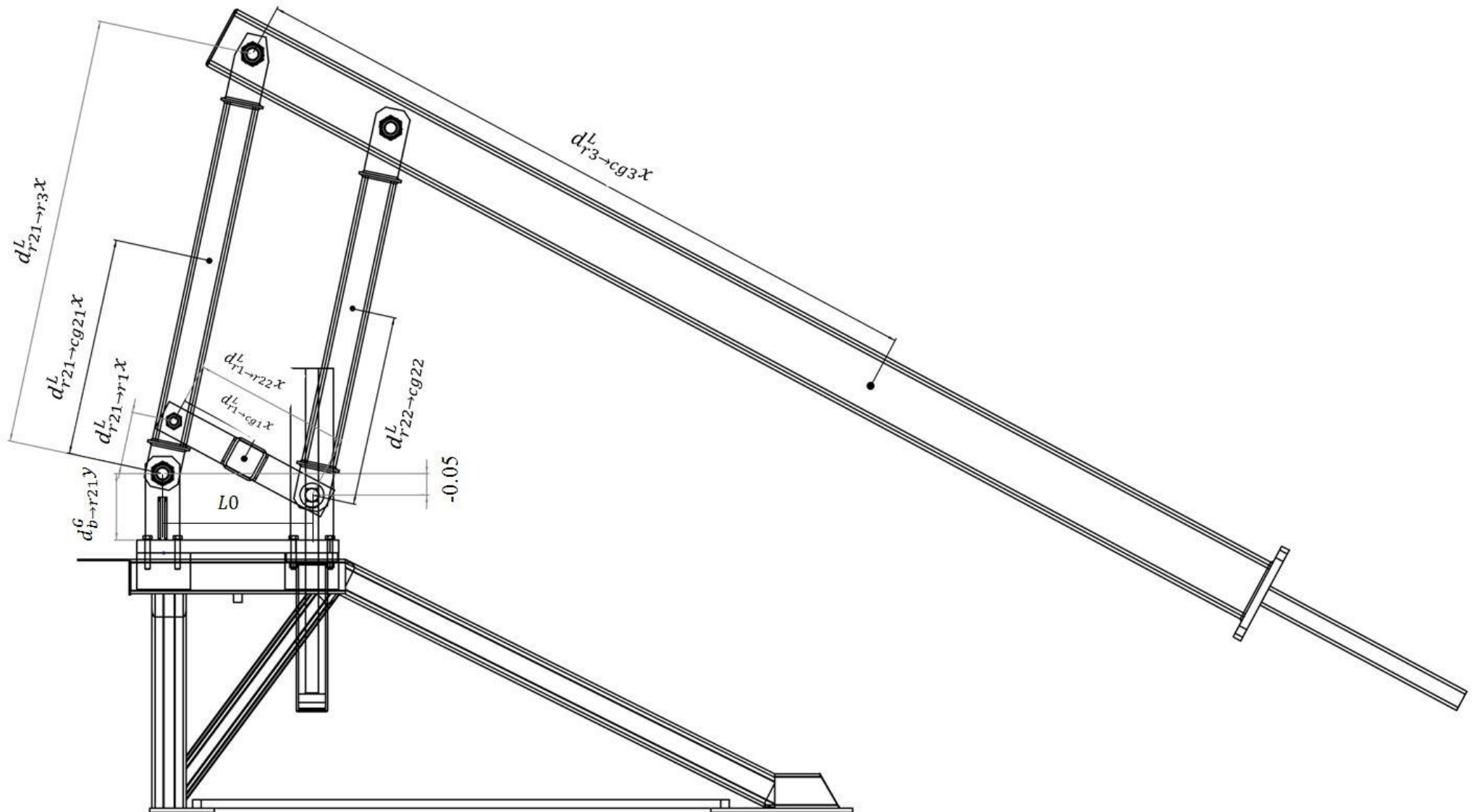


Figure 5-5 Representation of Local vectors

<i>Variable Name</i>	<i>Value [Unit]</i>	<i>Description</i>
$d_{r1 \rightarrow cg1}^L x$	0.186 [m]	X coordinate of local vector from rod 1 rotation frame to its center of mass
$d_{r3 \rightarrow cg3}^L x$	1.35 [m]	X coordinate of local vector from rod 3 rotation frame to its center of mass
$d_{r21 \rightarrow cg21}^L x$	0.508 [m]	X coordinate of local vector from rod 21 rotation frame to its center of mass
$d_{r22 \rightarrow cg22}^L x$	0.44 [m]	X coordinate of local vector from rod 22 rotation frame to its center of mass
$d_{r21 \rightarrow r1}^L x$	0.125 [m]	X coordinate of local vector from rod 21 rotation frame to rod 1 rotation frame
$d_{b \rightarrow r21}^G y$	0.155 [m]	Y coordinate of global vector from base rotation frame to rod 21 rotation frame
$d_{r21 \rightarrow r3}^L x$	1 [m]	X coordinate of local vector from rod 21 rotation frame to rod 3 rotation frame
$d_{r1 \rightarrow r22}^L x$	0.365 [m]	X coordinate of local vector from rod 1 rotation frame to rod 22 rotation frame

5.2.1. Vector naming

A vector is named by the use of superscripts and subscripts, as it can be seen in the example:

$$d_{r1 \rightarrow r22}^G$$

Where the upper script defines whether the vector is represented in the Global (G) reference frame or Local (L). The subscript shows the beginning and the end of the vector, with the arrow pointing from the first components reference frame origin to the end component reference frame origin or center of mass, this specific case being represented by a Global vector, from rod1 reference frame origin to the rod2.2 reference frame origin

5.2.2. Rod1

Global position vector from base reference frame origin to the rod 1 center of mass:

$$d_{b \rightarrow cg1}^G = d_{b \rightarrow r21}^G + d_{r21 \rightarrow r1}^G + d_{r1 \rightarrow cg1}^G \quad (5.11)$$

$$d_{b \rightarrow r21}^G = \begin{bmatrix} 0 \\ d_{b \rightarrow r21}^G y \end{bmatrix} \quad (5.12)$$

Global position vector from rod 2.1 reference frame origin to rod1 reference frame origin

$$\mathbf{d}_{r21 \rightarrow r1}^G = \mathbf{R}_2 \cdot \mathbf{d}_{r21 \rightarrow r1}^L \quad (5.13)$$

$$\mathbf{d}_{r21 \rightarrow r1}^L = \begin{bmatrix} d_{r21 \rightarrow r1}^L x \\ 0 \end{bmatrix} \quad (5.14)$$

Global position vector from rod 1 reference frame origin to rod1 center of mass:

$$\mathbf{d}_{r1 \rightarrow cg1}^G = \mathbf{R}_1 \cdot \mathbf{d}_{r1 \rightarrow cg1}^L \quad (5.15)$$

$$\mathbf{d}_{r1 \rightarrow cg1}^L = \begin{bmatrix} d_{r1 \rightarrow cg1}^L x \\ 0 \end{bmatrix} \quad (5.16)$$

Comparing how the vector's coordinates change from the mathematical model, with the one from SolidWorks, it can be seen that they are the same, meaning the vector construction is correct [Appendix B].

Mass center velocity of rod 1 in base reference frame is:

$$\mathbf{v}_{r1}^G = \frac{d(\mathbf{d}_{b \rightarrow cg1}^G)}{dt} \quad (5.17)$$

Kinetic energy due to translation:

$$E_{cg1}^k = \frac{1}{2} \cdot m_{r1} \cdot \|\mathbf{v}_{r1}^G\|_2^2 \quad (5.18)$$

<i>Variable Name</i>	<i>Value [Unit]</i>	<i>Description</i>
m_{r1}	6.12844 [kg]	Mass of rod 1

Angular velocity of rod 1 expressed in its own frame is:

$$\boldsymbol{\omega}_{r1}^{r1} = \dot{\theta}_1 \cdot \mathbf{k}_{base} \quad (5.19)$$

Kinetic energy due to rotation:

$$E_{r1I}^k = \frac{1}{2} \cdot (\boldsymbol{\omega}_{r1}^{r1})^T \cdot \mathbf{I}_{nr1} \cdot \boldsymbol{\omega}_{r1}^{r1} \quad (5.20)$$

Total kinetic energy of rod 1 part is equal to:

$$E_{r1}^k = \sum E_{r1}^k = E_{cg1}^k + E_{r1I}^k \quad (5.21)$$

Potential energy of rod 1:

$$E_{r1}^p = m_{r1} \cdot g \cdot \mathbf{d}_{b \rightarrow cg1}^G y \quad (5.22)$$

<i>Variable Name</i>	<i>Value [Unit]</i>	<i>Description</i>
g	$9.81 \text{ [kg/m}^2\text{]}$	<i>Gravitational constant</i>
$\mathbf{d}_{b \rightarrow cg1}^G y$	$- [m]$	<i>Only the second element of the vector, in the \mathbf{j}_{base} direction</i>

5.2.3. Rod3

Global position vector from base reference frame origin to the rod 3 center of mass:

$$\mathbf{d}_{b \rightarrow cg3}^G = \mathbf{d}_{b \rightarrow r21}^G + \mathbf{d}_{r21 \rightarrow r3}^G + \mathbf{d}_{r3 \rightarrow cg3}^G \quad (5.23)$$

Global position vector from rod 2.1 reference frame origin to rod 3 reference frame origin and its local component:

$$\mathbf{d}_{r21 \rightarrow r3}^G = \mathbf{R}_2 \cdot \mathbf{d}_{r21 \rightarrow r3}^L \quad (5.24)$$

$$\mathbf{d}_{r21 \rightarrow r3}^L = \begin{bmatrix} d_{r21 \rightarrow r3}^L x \\ 0 \end{bmatrix} \quad (5.25)$$

Global position vector from rod 3 reference frame origin to rod 3 center of mass and its local component:

$$\mathbf{d}_{r3 \rightarrow cg3}^G = \mathbf{R}_1 \cdot \mathbf{d}_{r3 \rightarrow cg3}^L \quad (5.26)$$

$$\mathbf{d}_{r3 \rightarrow cg3}^L = \begin{bmatrix} d_{r3 \rightarrow cg3}^L x \\ 0 \end{bmatrix} \quad (5.27)$$

Comparing how the vector's coordinates change from the mathematical model, with the one from SolidWorks, it can be seen that they are the same, meaning the vector construction is correct [Appendix B].

Mass center velocity of rod 3 in base reference frame is:

$$\mathbf{v}_{r3}^G = \frac{d(\mathbf{d}_{b \rightarrow cg3}^G)}{dt} \quad (5.28)$$

Kinetic energy of rod 3 due to translation:

$$E_{cg3}^k = \frac{1}{2} \cdot m_{r3} \cdot \|\mathbf{v}_{r3}^G\|_2^2 \quad (5.29)$$

<i>Variable Name</i>	<i>Value [Unit]</i>	<i>Description</i>
m_{r3}	87.92456 [kg]	Mass of rod 3

Angular velocity of rod 3 expressed in its own frame is:

$$\boldsymbol{\omega}_{r3}^{r3} = \dot{\theta}_1 \cdot \mathbf{k}_{base} \quad (5.30)$$

Kinetic energy of rod 3 due to rotation:

$$E_{r3I}^k = \frac{1}{2} \cdot (\boldsymbol{\omega}_{r3}^{r3})^T \cdot \mathbf{I}_{nr3} \cdot \boldsymbol{\omega}_{r3}^{r3} \quad (5.31)$$

Total kinetic energy of rod 3 part is equal to:

$$E_{r3}^k = \sum E_{r3}^k = E_{cg3}^k + E_{r3I}^k \quad (5.32)$$

Potential energy of rod 3:

$$E_{r3}^p = m_{r3} \cdot g \cdot \mathbf{d}_{b \rightarrow cg3}^G y \quad (5.33)$$

<i>Variable Name</i>	<i>Value [Unit]</i>	<i>Description</i>
g	9.81 [kg/m ²]	Gravitational constant
$\mathbf{d}_{b \rightarrow cg3}^G y$	- [m]	Only the second element of the vector, in the \mathbf{j}_{base} direction

5.2.4. Rod2.1

Global position vector from base reference frame origin to the rod 2.1 center of mass:

$$\mathbf{d}_{b \rightarrow cg21}^G = \mathbf{d}_{b \rightarrow r21}^G + \mathbf{d}_{r21 \rightarrow cg21}^G \quad (5.34)$$

Global position vector from rod 2.1 reference frame origin to rod 2.1 center of mass and its local component:

$$\mathbf{d}_{r21 \rightarrow cg21}^G = \mathbf{R}_2 \cdot \mathbf{d}_{r21 \rightarrow cg21}^L \quad (5.35)$$

$$\mathbf{d}_{r21 \rightarrow cg21}^L = \begin{bmatrix} d_{r21 \rightarrow cg21}^L x \\ 0 \end{bmatrix} \quad (5.36)$$

Comparing how the vector's coordinates change from the mathematical model, with the one from SolidWorks, it can be seen that they are the same, meaning the vector construction is correct [Appendix B].

Mass center velocity of rod 2.1 in base reference frame is:

$$\mathbf{v}_{cg21}^b = \frac{d(\mathbf{d}_{b \rightarrow cg21}^G)}{dt} \quad (5.37)$$

Kinetic energy of rod 2.1 due to translation:

$$E_{cg21}^k = \frac{1}{2} \cdot m_{r21} \cdot \|\mathbf{v}_{cg21}^b\|_2^2 \quad (5.38)$$

<i>Variable Name</i>	<i>Value [Unit]</i>	<i>Description</i>
m_{r21}	15.36792 [kg]	Mass of rod 2.1

Angular velocity of rod 21 expressed in its own frame is:

$$\boldsymbol{\omega}_{r21}^{r21} = \dot{\theta}_2 \cdot \mathbf{k}_{base} \quad (5.39)$$

Kinetic energy of rod 2.1 due to rotation:

$$E_{r21I}^k = \frac{1}{2} \cdot (\boldsymbol{\omega}_{r21}^{r21})^T \cdot \mathbf{I}nr21 \cdot \boldsymbol{\omega}_{r21}^{r21} \quad (5.40)$$

Total kinetic energy of rod 2.1 part is equal to:

$$E_{r21}^k = \sum E_{r21}^k = E_{cg21}^k + E_{r21l}^k \quad (5.41)$$

Potential energy of rod 2.1:

$$E_{r21}^p = m_{r21} \cdot g \cdot \mathbf{d}_{b \rightarrow cg21}^G y \quad (5.42)$$

<i>Variable Name</i>	<i>Value [Unit]</i>	<i>Description</i>
g	$9.81 \text{ [kg/m}^2\text{]}$	<i>Gravitational constant</i>
$\mathbf{d}_{b \rightarrow cg21}^G y$	$- [m]$	<i>Only the second element of the vector, in the \mathbf{j}_{base} direction</i>

5.2.5. Rod2.2

Global position vector from base reference frame origin to the rod 2.2 center of mass:

$$\mathbf{d}_{b \rightarrow cg22}^G = \mathbf{d}_{b \rightarrow r21}^G + \mathbf{d}_{r21 \rightarrow r1}^G + \mathbf{d}_{r1 \rightarrow r22}^G + \mathbf{d}_{r22 \rightarrow cg22}^G \quad (5.43)$$

Global position vector from rod 2.1 reference frame origin to rod1 reference frame origin:

$$\mathbf{d}_{r21 \rightarrow r1}^G = \mathbf{R}_2 \cdot \mathbf{d}_{r21 \rightarrow r1}^L \quad (5.44)$$

Global position vector from rod 1 reference frame origin to rod 2.2 reference frame origin and its local component:

$$\mathbf{d}_{r1 \rightarrow r22}^G = \mathbf{R}_1 \cdot \mathbf{d}_{r1 \rightarrow r22}^L \quad (5.45)$$

$$\mathbf{d}_{r1 \rightarrow r22}^L = \begin{bmatrix} d_{r1 \rightarrow r22}^L x \\ 0 \end{bmatrix} \quad (5.46)$$

Position vector from rod 2.2 reference frame origin to rod 2.2 center of mass and its local component:

$$\mathbf{d}_{r22 \rightarrow cg22}^G = \mathbf{R}_2 \cdot \mathbf{d}_{r22 \rightarrow cg22}^L \quad (5.47)$$

$$\mathbf{d}_{r22 \rightarrow cg22}^L = \begin{bmatrix} d_{r22 \rightarrow cg22}^L x \\ 0 \end{bmatrix} \quad (5.48)$$

Comparing how the vector's coordinates change from the mathematical model, with the one from SolidWorks, it can be seen that they are the same, meaning the vector construction is correct [Appendix B].

Mass center velocity of rod 2.2 in base reference frame is:

$$\mathbf{v}_{r22}^b = \frac{d(\mathbf{d}_{b \rightarrow cg22}^G)}{dt} \quad (5.49)$$

Kinetic energy of rod 2.2 due to translation:

$$E_{cg22}^k = \frac{1}{2} \cdot m_{r22} \cdot \|\mathbf{v}_{r22}^b\|_2^2 \quad (5.50)$$

<i>Variable Name</i>	<i>Value [Unit]</i>	<i>Description</i>
m_{r22}	13.62235 [kg]	Mass of rod 2.2

Angular velocity of rod 2.2 expressed in its own frame is:

$$\boldsymbol{\omega}_{r22}^{r22} = \dot{\theta}_2 \cdot \mathbf{k}_{base} \quad (5.51)$$

Kinetic energy of rod 2.2 due to rotation:

$$E_{r22I}^k = \frac{1}{2} \cdot (\boldsymbol{\omega}_{r22}^{r22})^T \cdot \mathbf{I}_{nr22} \cdot \boldsymbol{\omega}_{r22}^{r22} \quad (5.52)$$

Total kinetic energy of rod 2.2 part is equal to:

$$E_{r22}^k = \sum E_{r22}^k = E_{cg22}^k + E_{r22I}^k \quad (5.53)$$

Potential energy of rod 2.2:

$$E_{r22}^p = m_{r22} \cdot g \cdot \mathbf{d}_{b \rightarrow cg22}^G y \quad (5.54)$$

<i>Variable Name</i>	<i>Value [Unit]</i>	<i>Description</i>
g	9.81 [kg/m ²]	Gravitational constant
$\mathbf{d}_{b \rightarrow cg22}^G y$	- [m]	Only the second element of the vector, in the \mathbf{j}_{base} direction

5.2.6. Lagrange method

$$L = \sum E_{kinetic} - \sum E_{potential} = E_{r1}^k + E_{r3}^k + E_{r21}^k + E_{r22}^k - E_{r1}^p - E_{r3}^p - E_{r21}^p - E_{r22}^p \quad (5.55)$$

Applying the Lagrange method can obtain the force can be obtained in the following way:

$$M_{Lagrange} = \frac{d}{dt} \cdot \frac{\partial L}{\partial \dot{x}_p} - \frac{\partial L}{\partial x_p} \quad (5.56)$$

Further, the final Lagrangian can be represented in the following way:

$$F_{Load} = [c_1] \cdot \ddot{x}_p + [c_2] \cdot \dot{x}_p^2 + [c_3] \cdot x_p \quad (5.57)$$

<i>Variable Name</i>	<i>Value [Unit]</i>	<i>Description</i>
$[c_1] \cdot \ddot{x}_p$	- [m/s ²]	<i>Inertial part of the system</i>
$[c_2] \cdot \dot{x}_p^2$	- [m/s]	<i>Centripetal part of the system</i>
$[c_3] \cdot x_p$	- [m]	<i>Gravitational part of the system</i>

6. Hydraulic System description

The entire chapter 6 was built upon the information found in T.O. Andersen, M.R. Hansen (2007) *Fluid power circuits: system design and analysis* [6].

6.1. Hydraulic System Modeling

The idea behind hydraulics is to transfer power via pressurized liquids. Hydraulics are widely used due to their ability to handle big loads, therefore they are the backbone of lifting structures, such as cranes. Modeling hydraulic systems is done by the application of continuity equation, orifice equation and Newton's second law to the specific system.

This particular system consists of:

- the hydraulic fluid, which allows to transmit power.
- the reservoir, which acts as a storage unit for the hydraulic fluid, as well as a filter for any solid, bigger sized contaminants. Additionally, it allows the fluid to cool off.
- the pump, which acts as a converter from mechanical energy to hydraulic energy, which eventually moves the system.
- the valve, which directs the flow of the hydraulic fluid.
- the cylinder, which converts hydraulic energy back to the mechanical work, that is acting upon the load.
- two adjustable needle valves which allow to simulate external valve leakage and internal cylinder leakage.

Due to the fact that the experiments and the FDD implementation will be made on two cases with different leakages, in the ideal case, none of them will be occurring simultaneously. This leads to having two models of the hydraulic circuit with different leakages.

6.2. Hydraulic system diagram

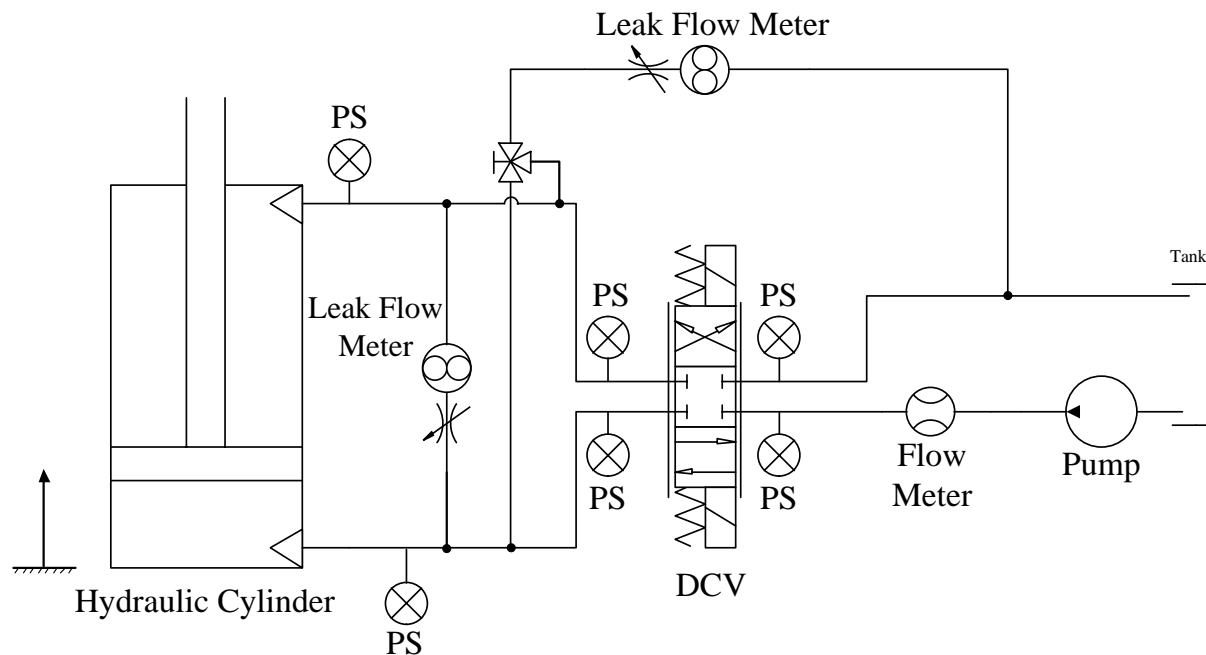


Figure 6-1 Hydraulic circuit schematic view

The hydraulic loop which has been used in the experimentation is described by Figure 6-1. It consists of:

<i>Sensors</i>	<i>Number</i>	<i>Description</i>
<i>Pressure sensor</i>	<i>6</i>	<i>Measure pressure inside the hydraulic loop</i>
<i>Flow meter</i>	<i>1</i>	<i>Measure flow of oil given by pump</i>
<i>Leak Flow meter</i>	<i>2</i>	<i>Measure flow of oil when artificial leakage is implemented</i>
<i>Position transducer</i>	<i>1</i>	<i>Measure position of cylinder</i>

*More about the laboratory setup and how it was build can be found in Appendix D.a

6.3. Continuity equations

The continuity equation is the expression which represents the principle of conservation of mass. For the control volumes present in our case, with a single inlet and single outlet, the mass flow rate entering the control volume is different from the one exiting it. This way the pressure in the system is built up and the crane is driven.

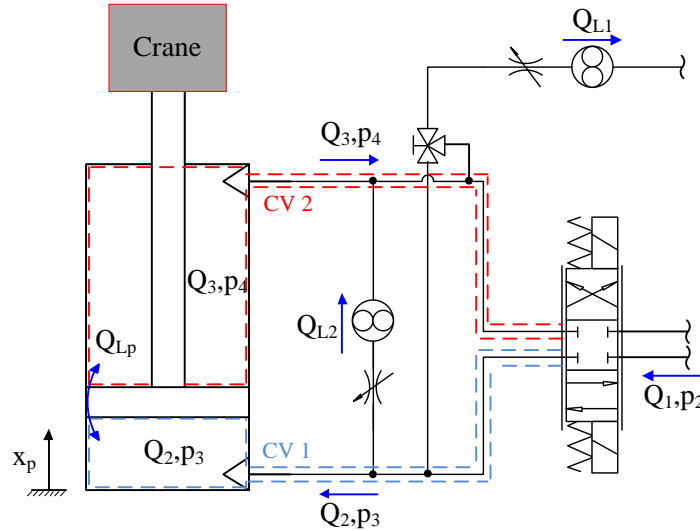


Figure 6-2 Hydraulic circuit schematic view with visual representation of control volumes, flows and pressures

The two different control volumes in the hydraulic system, assuming constant tank and pump pressures, are written as:

$$Q_2 - Q_{Lp} + Q_{LvTotal} - Q_{L1} - Q_{L2} = A_p \cdot \dot{x}_p + \frac{A_p \cdot x_p + V_{p0}}{\beta} \cdot \dot{p}_3 \quad (6.1)$$

$$Q_{Lp} - Q_3 + Q_{LvTotal} - Q_{L1} + Q_{L2} = -A_r \cdot \dot{x}_p + \frac{V_{r0} - A_r \cdot x_p}{\beta} \cdot \dot{p}_4 \quad (6.2)$$

Variable Name	Value [Unit]	Description
Q_{Lp}	- [m^3/s]	Sealing leakage flow
$Q_{LvTotal}$	- [m^3/s]	DCV leakage flow
Q_L	- [m^3/s]	Implement artificial leakage
V_{p0}, V_{r0}	- [m^3]	Initial fluid volumes in the control volumes
β	- [bar]	Compressibility – Bulk modulus
\dot{x}_p	- [m/s]	Velocity of the hydraulic cylinder
A_p	$3.117e-3$ [m^2]	Cross sectional area of the cylinder piston part
A_r	$2.41e-3$ [m^2]	Cross sectional area of the cylinder ring part
p	- [Pa]	Pressure in a particular node

6.3.1. Directional control valve

In order to model the servo directional control valve (DCV) behavior as accurate as possible it was needed to define the valve dynamics, which are commonly done by a second order system as shown below [14]:

$$u_v \cdot \omega_v^2 = \ddot{x}_v + 2 \cdot \zeta_v \cdot \omega_v \cdot \dot{x}_v + \omega_v^2 x_v \quad (6.3)$$

<i>Variable Name</i>	<i>Value [Unit]</i>	<i>Description</i>
u_v	Desired x_v [%/100%]	Valve input
ω_v	280π [rad/s]	Valve Eigen frequency
x_v	$-1 \leq x_v \leq 1$	Valve position
ζ_v	0.92 [-]	Valve damping ratio

To verify the valve dynamics it was necessary to simulate a step response with a specific slew rate to reach the desired behavior in different opening positions of 25%, 50%, 75% and 100% as shown in the data sheet of the valve [Appendix C].

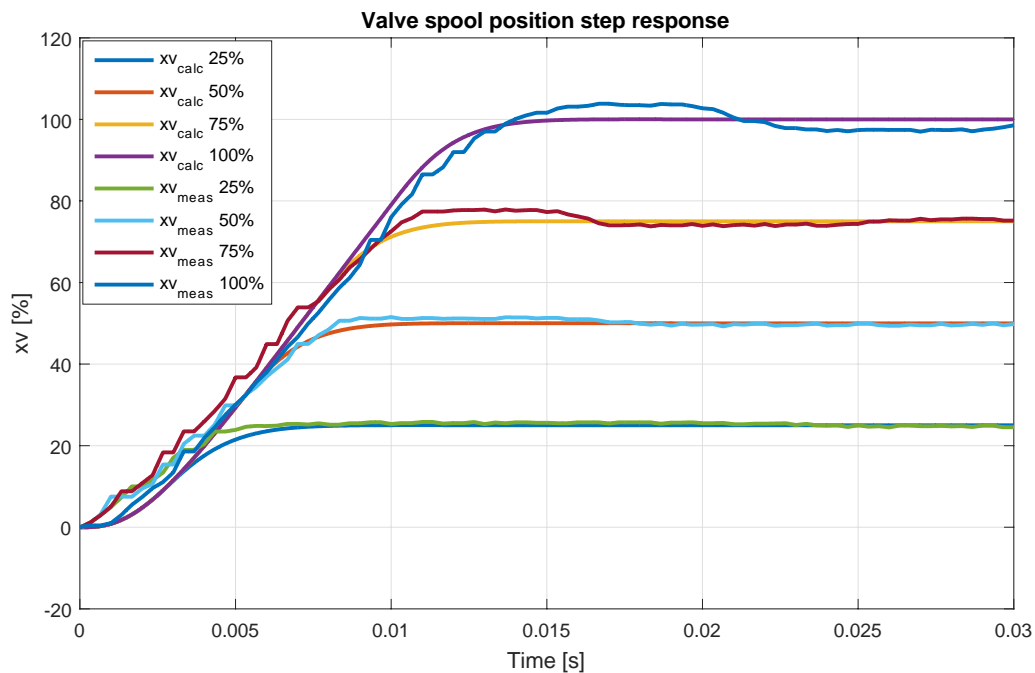


Figure 6-3 Step response of the DFV spool dynamics

6.3.1.1. DCV Dead zone

This particular directional control valve has a dead zone, a region around the 0% position where the spool doesn't actually move, even if a certain input is delivered to it. This exact region is hard to determine. By using the experimental setup, increasing the u_v in small increments starting from 0.1% and upwards (downwards) we observed that the cylinder was not reacting until $u_v \approx \pm 0.015$ (1.5%). It can be concluded that a good approximation of $\pm 1.5\%$ dead zone was acceptable [15].

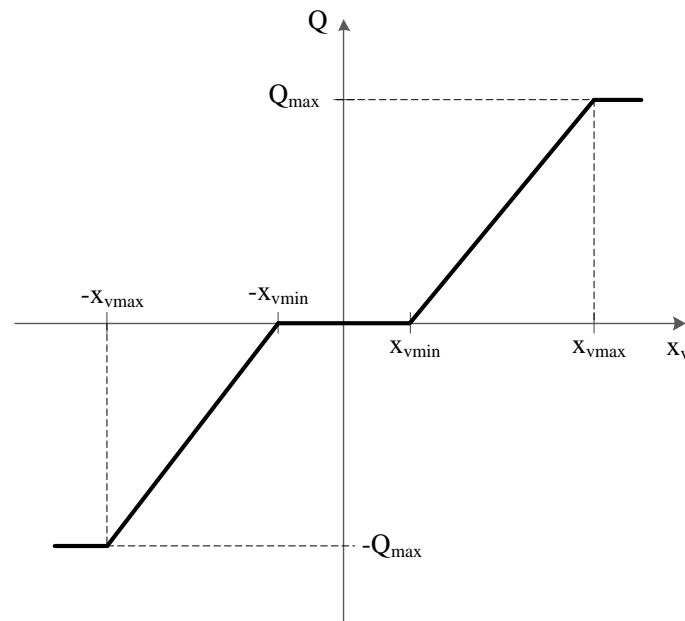


Figure 6-4 Representation of the dead zones inside the DCV

6.3.1.2. DCV internal leaks

The leaks inside the DCV occur because of multiple aspects such as:

- Seal of the spool does not seal properly
- Usage over time, make the surfaces inside the valve become rough
- Oil can deposit residue over time
- The speed of the spool is very high and because of this it cannot be fitted too tightly inside the casing

In order to achieve better results and simulate close to real scenarios the small leakages inside the directional control valve are assumed to be of a laminar nature and their mathematical equations have been implemented as such:

$$Q_{LvTotal2} = \begin{cases} Q_{Lv2} = K_{Lv2} \cdot (p_2 - p_3), & -0.015 < x_v < 0.015 \\ -Q_{Lt2} = K_{Lt2} \cdot (p_3 - p_5), & -0.015 < x_v < 0.015 \end{cases} \quad (6.4)$$

$$Q_{LvTotal3} = \begin{cases} Q_{Lv3} = K_{Lv3} \cdot (p_2 - p_4), & -0.015 < x_v < 0.015 \\ -Q_{Lt3} = K_{Lt3} \cdot (p_4 - p_5), & -0.015 < x_v < 0.015 \end{cases} \quad (6.5)$$

<i>Variable Name</i>	<i>Value [Unit]</i>	<i>Description</i>
Q_{Lv}	- [l/min]	Valve leak from supply to port
Q_{Lt}	- [l/min]	Valve leak from port to tank
K_{Lv2}	$1.1e-12$ [-]	Leak constant for valve leak supply-port with x_v negative
K_{Lt2}	$4.776 e-12$ [-]	Leak constant for valve leak port-tank with x_v negative
K_{Lv3}	$3.882e-11$ [-]	Leak constant for valve leak supply-port with x_v positive
K_{Lt3}	$2.5e-11$ [-]	Leak constant for valve leak port-tank with x_v positive

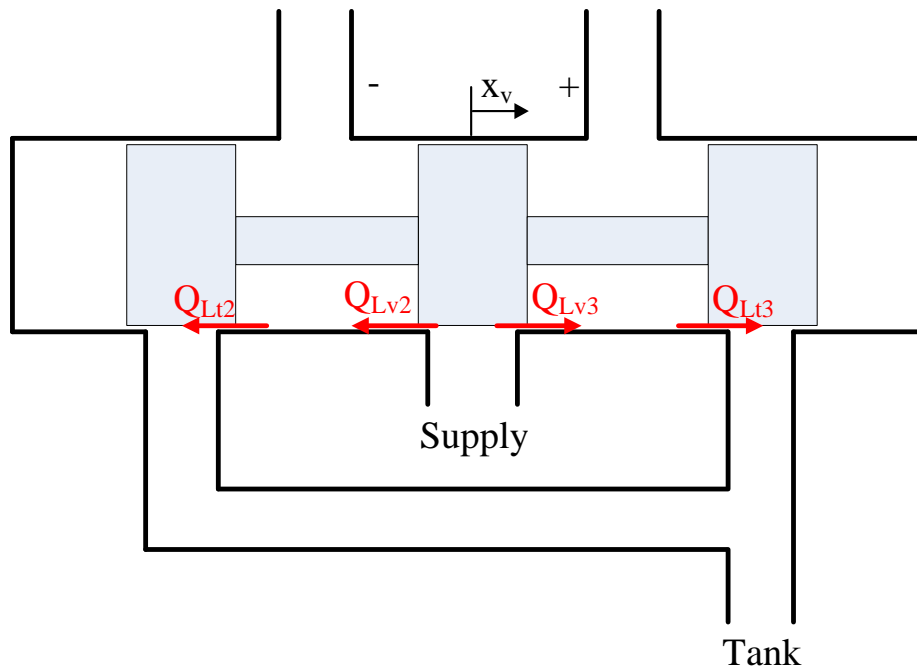


Figure 6-5 Description of DCV internal leakage

6.3.2. Artificially implemented system leakage

For the purpose of using these leaks later for different fault detection methods, some leaks which occur in the system artificially have been modeled. These represent failures inside the cylinder (Q_{L2}) and failure inside the DCV (Q_{L1}) other than the already modeled leaks, which occur normally and are assumed to be laminar. There are 2 x Q_{L1} leaks occurring which are controlled by the 3 way selector valve [Figure 6-2]

$$Q_{L1} = \begin{cases} K_{L1} \cdot (p_3 - p_5) \\ K_{L1} \cdot (p_4 - p_5) \end{cases} \quad (6.6)$$

$$Q_{L2} = K_{L2} \cdot (p_3 - p_4) \quad (6.7)$$

Variable Name	Value [Unit]	Description
Q_{L1}	- [l/min]	Artificial leak simulating valve failure
Q_{L2}	- [l/min]	Artificial leak simulating cylinder failure
K_L	- [-]	Leak constant for artificial leak

6.3.3. Cylinder leakage flow

Some leakage across the seal of the hydraulic cylinder also occurs normally inside the circuit, so a similar method has been chosen, as for the DCV leakage, to be implemented into the model. The mathematical formula is also based on the relationship between constant K_{Lp} , the pressure drop across the cylinder and is considered to be laminar:

$$Q_{Lp} = K_{Lp} \cdot (p_3 - p_4) \quad (6.8)$$

Variable Name	Value [Unit]	Description
Q_{Lp}	- [l/min]	Internal cylinder seal leakage
K_{Lp}	1e-12[-]	Leak constant cylinder leakage

6.3.4. Bulk modulus

Applying pressure to a volume of fluid, an amount of energy is expected to squeeze the hydraulic oil molecules closer to each other – compress the fluid. Not taking into consideration, i.e not modeling it, the bulk modulus can lead to delayed response, as the structure will not move until the hydraulic oil compresses.

The hydraulic oil gets aerated while being in use and air has a big effect on bulk modulus, due to its low compressibility. The air in the oil reduces the bulk modulus.

It takes 2 steps to calculate the bulk modulus. First, the volumetric air ratio, ε_a , is calculated [Eq. 6.9], followed by effective stiffness β_{eff} [Eq. 6.10].

$$\varepsilon_a(p) = \frac{1}{\frac{1 - \varepsilon_{a0}}{\varepsilon_{a0}} + \left(\frac{p_{atm}}{p}\right)^{c_{ad}} + 1} \quad (6.9)$$

$$\beta_{eff} = \frac{1}{\frac{1}{\beta_{ideal}} + \frac{\varepsilon_a(p)}{c_{ad} \cdot p_a}} \quad (6.10)$$

Variable Name	Value [Unit]	Description
β_{eff}	- [bar]	Effective bulk modulus
β_{ideal}	16000 [bar]	Ideal bulk modulus
ε_a	- [%]	Volumetric air ratio
ε_{a0}	0-15 [%]	Air percentage in the system
c_{ad}	1.4 [-]	Adiabatic gas constant

Plotting the bulk modulus from [Eq. 6.9], [Eq. 6.10] a graph can be obtained showing how bulk modulus changes with both pressure and air concentration in the hydraulic fluid.

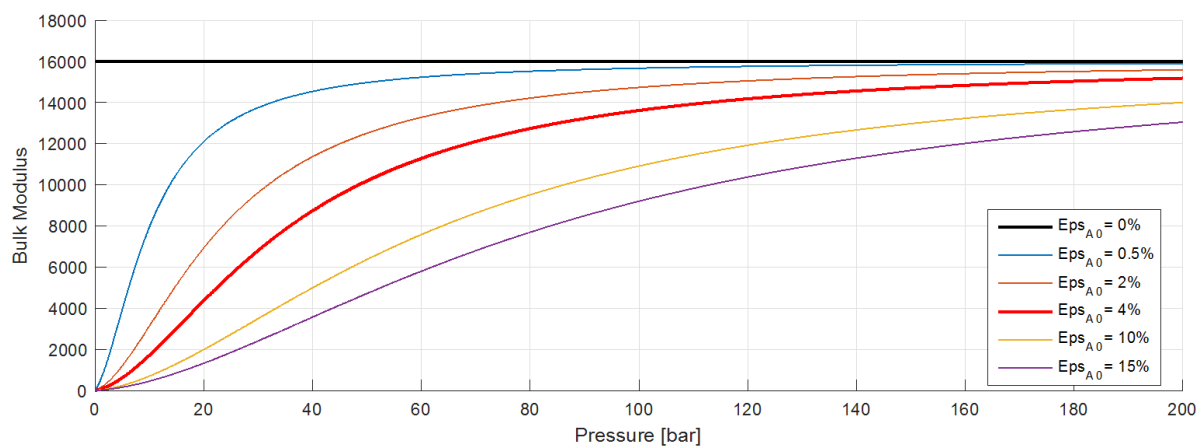


Figure 6-6 Bulk modulus compared to pressure, at different volumetric air ratios

It is possible to see that the differences between 0% air and any other concentration are substantially big, especially at lower pressures. Maximum value at 0% air in the hydraulic fluid leads to bulk modulus with a magnitude of 16000 bar. This is an ideal case and is not suitable for our model. For our case bulk modulus will be chosen so that it suits our model and improves if possible its behavior. Furthermore, hoses and their expansion under pressure are not modeled, meaning, in reality a bulk modulus of lower value should be used to suit the experimental and validation conditions better.

In order to implement a bulk modulus as accurately as possible while not increasing computational time by a lot, the complex bulk modulus equation has been simplified around (or as close as possible) to the operating pressures inside the cylinder. As later on, for model validation, it was decided that the use of two different supply pressures (50 bar and 100 bar) was suitable. It was approximated using simple first order equations giving us a piecewise linear curve, as follows:

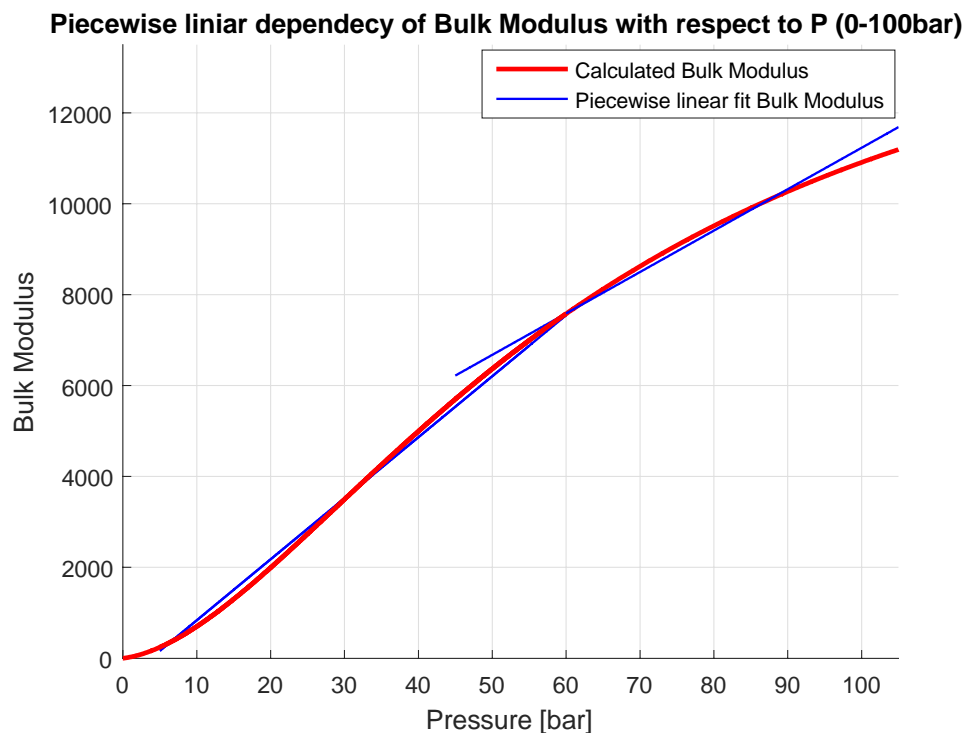


Figure 6-7 Piecewise linearization of bulk modulus for 50 and 100 bar input pressure

6.4. Orifice equations

The hydraulic model is calculated by using the orifice equation for the valve and flow meter, which defines the flow due to a pressure difference. The equation that will be used to do these calculations, are only valid for sharp shaped orifices which have a turbulent flow passing through them. This also implies linear opening behavior of the valve.

The hydraulic system contains one directional flow valve. The flows are dependent on the valve position x_v and the pressure drop:

$$Q_1 = \begin{cases} K_{v1} \cdot x_v \sqrt{|p_2 - p_3|} \cdot \text{sign}(p_2 - p_3), (x_v \geq 0.015) \\ -K_{v2} \cdot x_v \sqrt{|p_2 - p_4|} \cdot \text{sign}(p_2 - p_4), (x_v \leq 0.015) \end{cases} \quad (6.11)$$

$$Q_4 = \begin{cases} K_{v1} \cdot x_v \sqrt{|p_4 - p_5|} \cdot \text{sign}(p_4 - p_5), (x_v \geq 0.015) \\ K_{v2} \cdot x_v \sqrt{|p_3 - p_5|} \cdot \text{sign}(p_3 - p_5), (x_v \leq 0.015) \end{cases} \quad (6.12)$$

$$Q_2 = \begin{cases} K_{v1} \cdot x_v \sqrt{|p_2 - p_3|} \cdot \text{sign}(p_2 - p_3), (x_v \geq 0.015) \\ K_{v2} \cdot x_v \sqrt{|p_3 - p_5|} \cdot \text{sign}(p_3 - p_5), (x_v \leq 0.015) \end{cases} \quad (6.13)$$

$$Q_3 = \begin{cases} K_{v1} \cdot x_v \sqrt{|p_4 - p_5|} \cdot \text{sign}(p_4 - p_5), (x_v \geq 0.015) \\ -K_{v2} \cdot x_v \sqrt{|p_2 - p_4|} \cdot \text{sign}(p_2 - p_4), (x_v \leq 0.015) \end{cases} \quad (6.14)$$

<i>Variable Name</i>	<i>Value [Unit]</i>	<i>Description</i>
K_{v1}	$4.165e-7 [-]$	Valve coefficient 1 of the DCV
K_{v2}	$3.91e-7 [-]$	Valve coefficient 2 of the DCV
x_v	$- [\% / 100\%]$	Spool position inside the DCV
p	$- [Pa]$	Pressure in a certain node

6.4.1. K_v calculation

The K_v is a valve coefficient which includes the C_d - discharge coefficient - of the valve, the square root of half density and the discharge area inside the directional control valve.

$$Q = C_d \cdot A_d \cdot x_v \cdot \sqrt{\frac{2}{\rho} \cdot (\Delta p)} \rightarrow Q = K_v \cdot x_v \cdot \sqrt{\Delta p}$$

$$K_v = C_d \cdot A_d \cdot \sqrt{\frac{2}{\rho}} \quad (6.15)$$

<i>Variable Name</i>	<i>Value [Unit]</i>	<i>Description</i>
K_v	- [-]	Valve coefficient
x_v	- [%/100%]	Valve spool position
C_d	- [-]	Discharge coefficient
A_d	- [m^2]	Discharge area
ρ	- [kg/m^3]	Density of fluid
Q	- [m^3/s]	Volumetric flow

Due to the fact that the C_d might be different from what is described in the datasheets, because of the wear which occurs inside the valve on the edges of the flow ports, the correct discharge area was hard to determine because of the lack of information from the datasheet of this particular valve [Appendix D.a].

An experimental procedure was developed in order to more accurately approximate the K_v .

The pump delivers a pressure of 50 bars, and the valve is set to multiple openings ranging from -80% to +80%, in such a way it is possible to get better results across a bigger dynamic range of the valve. Each direction of the flow will give a different valve coefficient.

The pressures across the DCV and the flow can be measured using the sensors in the system and knowing that x_v has a value between -0.8 and 0.8, the K_v can then be calculated, giving two different coefficients depending on the position of the spool, either being in the positive side, or the negative side.

After the preliminary calculations were done using the measured data and the equation in Eq. 6-15, it has been decided the K_v will be used as a tuning parameter in order to tune the flow in the hydraulic model. Figure 6-8 shows the result of the calculated piston position with the calculated K_v compared with the measured K_v . It can be seen that the results using the calculated K_v are less than acceptable. By the use of the trial and error method it was possible to tune the K_v in such manner, that the calculated data fits the measured data. Figure 6-9 shows the difference between the calculated and tuned K_v .

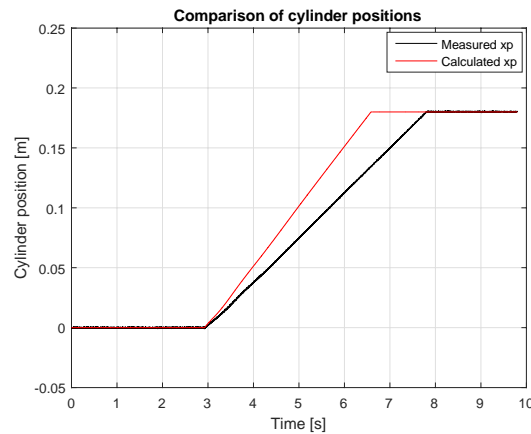


Figure 6-8 - Comparison of Piston Position using Calculated K_v coefficient

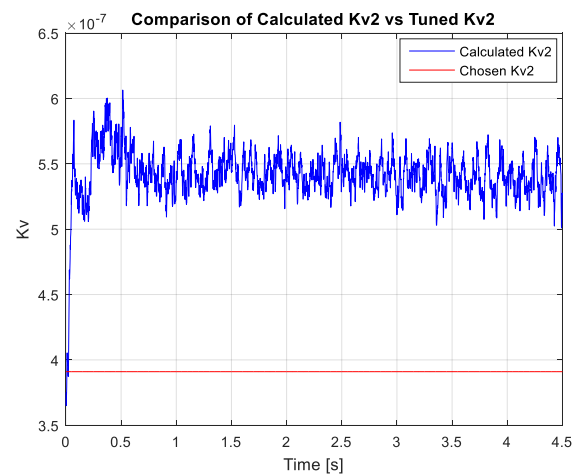
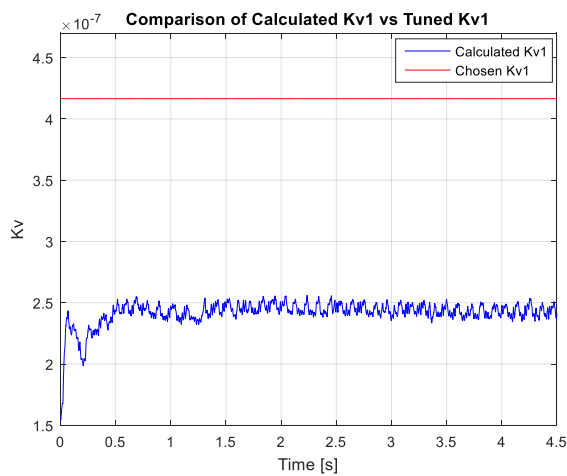


Figure 6-9 - Comparison of calculated K_v 's and tuned K_v 's

6.5. Forces in the system

Newton's second law states, that an unbalanced force, which is acting on an object, will result in that objects momentum change over a period of time. The magnitude of this unbalanced force determined the velocity and acceleration of the object. In this specific case, the force balance consists of the load, frictional force, which is acting in the opposite of the velocity vector and the 2 forces inside the hydraulic cylinder, one of which is the lifting force. Due to the fact that there is always pressure in the chambers, their direction will always be constant; piston side will be acting upwards while ring side is acting downwards, unless a vacuum is made within them.

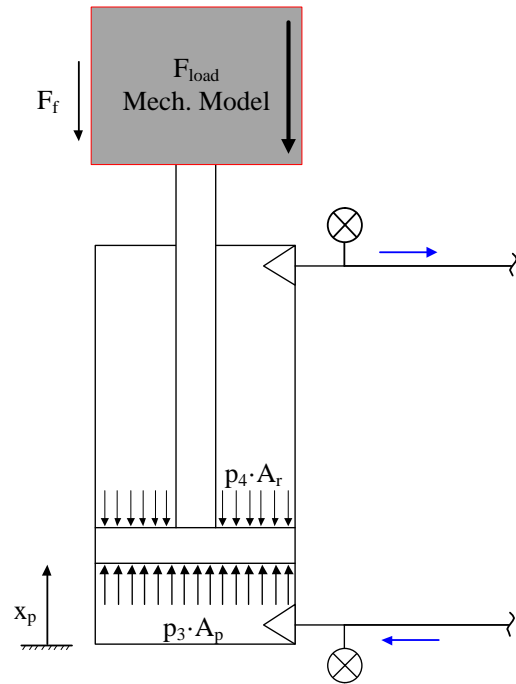


Figure 6-10 Force balance

$$F_{Load} = p_3 \cdot A_p - p_4 \cdot A_r \pm F_f \quad (6.16)$$

Variable Name	Value [Unit]	Description
F_{Load}	- [N]	Load force
A_p	$3.117e-3 [m^2]$	Area of cylinder piston side
A_r	$2.41e-3 [m^2]$	Area of cylinder ring side
F_f	- [N]	Total friction force
p	- [Pa]	Pressure in a particular volume

6.5.1. Friction Force

The friction forces [16] in the system are composed of multiple forces, such as Coulomb friction [Figure 6-11a], viscous friction [Figure 6-11b] and Stribeck friction [Figure 6-11c], which act together making a generalized friction force simplified by [Eq.6.17, Figure 6-11d].

$$F_f = (F_{cou} + F_{stb}) \cdot \text{sign}(\dot{x}_p) + F_v$$

$$F_{stb} = (F_{cou} - F_{brk}) \cdot e^{-c_v \cdot |\dot{x}_p|}$$

$$F_v = B \cdot \dot{x}_p$$
(6.17)

Variable Name	Value [Unit]	Description
F_f	- [N]	Total friction force
F_{cou}	480 [N]	Coulomb friction
F_v	- [N]	Viscous friction
F_{stb}	990 [N]	Stribeck friction
F_{brk}	- [N]	Breakaway friction force
c_v	10 [s/m]	Stribeck constant
B	5000 [Nms]	Damping coefficient

A generalized representation of these frictions can be seen in the following graph [16]:

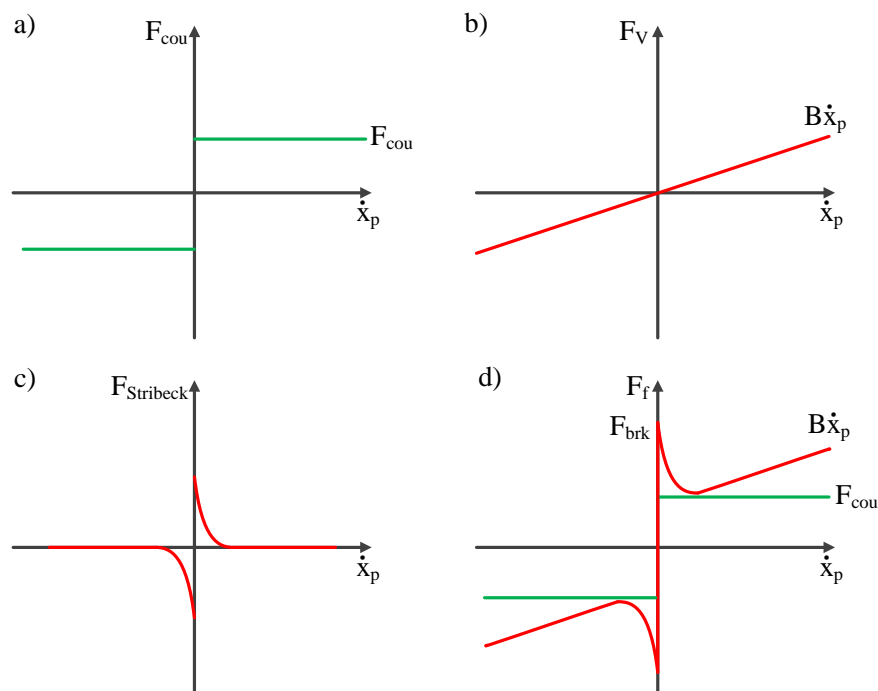


Figure 6-11 Different types of friction forces represented in visual form

Half of the difference between the lifting and lowering hydraulic forces results in the Coulomb friction [Chapter 7.1]. Friction force is a force that resists the relative motion of elements sliding against each other. Meaning, it is crucial to have it in the force equilibrium to get a simulation as accurate as possible.

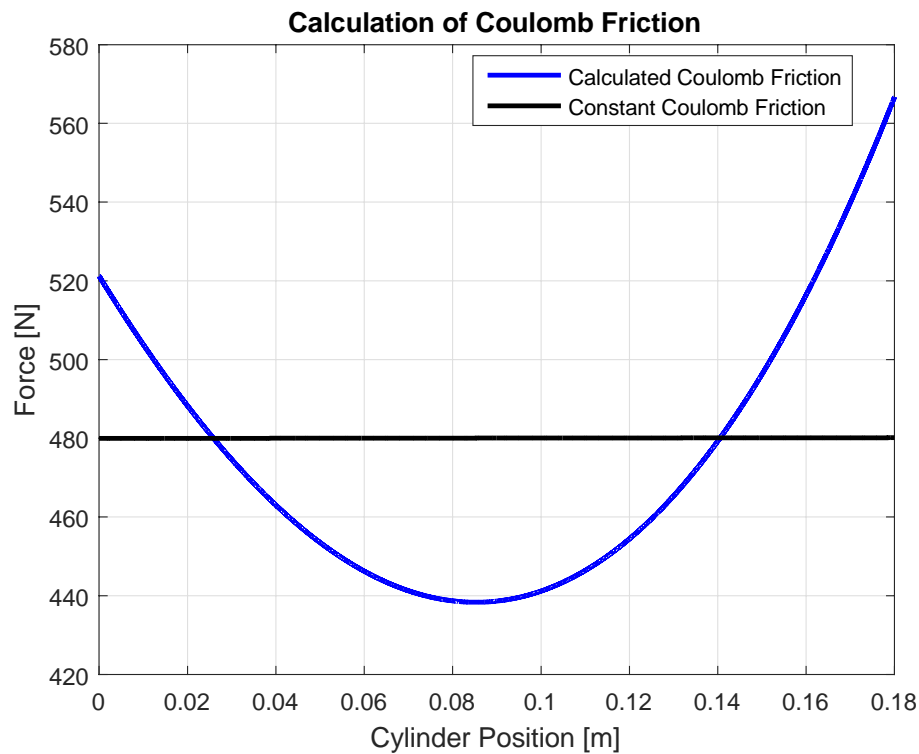


Figure 6-12 Approximated Coulomb friction

Figure 6-12 explains how the coulomb friction changes over the cylinder position. Because of its complexity and because of practical reasons, this has been approximated to be a constant of 480 N which suits the best over the entire range of the cylinder stroke.

7. Model verification

7.1. Verification of the mechanical model

The only way to verify the model through the data collected during the experiments is through combination of the two models. An experiment can be conducted by moving the pantograph crane in a quazi-static way, meaning it will move in such a slow manner that the gravitational part and the coulomb friction will have the biggest impact on the load the hydraulic cylinder is experiencing, while influences from the velocity and other friction forces are reduced to a point where they can be neglected.

Knowing the hydraulic cylinders ring and piston areas, while having the reading of the pressure sensors, the load the crane is giving can be determined while it is moving up and down. This has been done using 10 runs of the same experiment and averaging them, giving a better and more realistic spread of the measured data.

The hydraulic force given out by the hydraulic cylinder when the crane is performing an upward motion should be bigger than the force while it is going downwards. Half the difference between these loads would give up the friction force of the system. These loads have been curve fitted the data that was gathered, in order for ease of use. This leaves us working with roughly the mean of the data set:

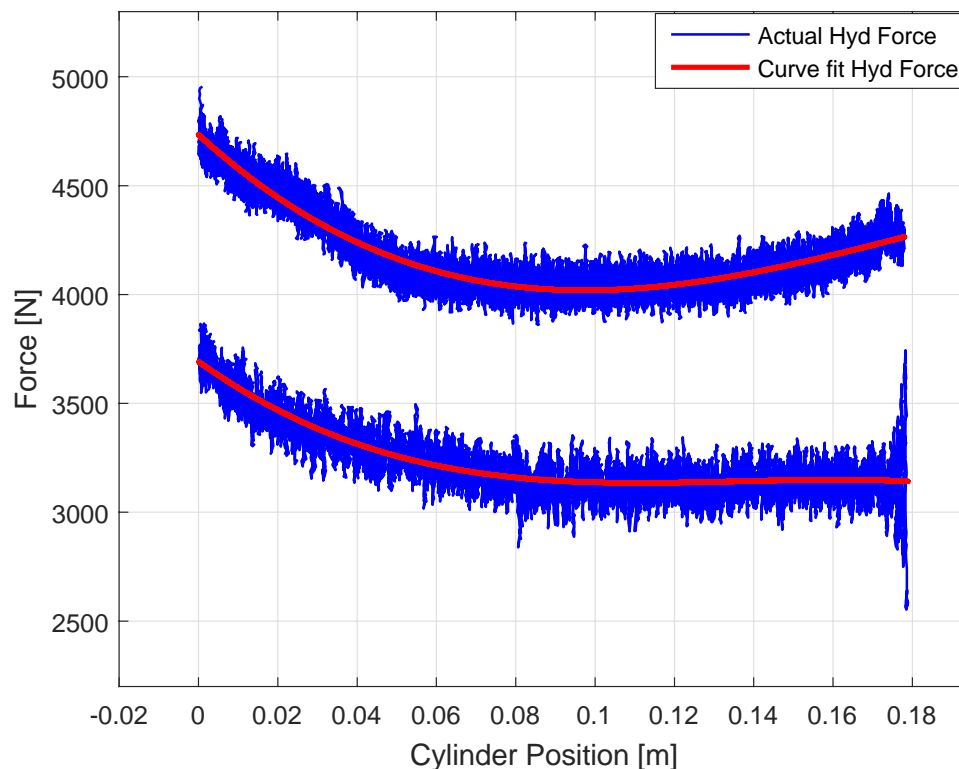


Figure 7-1 Curve fit of hydraulic force s upward motion and downward motion

The gravitational forces change of the crane load due to the piston position is almost constant due to the fact that the crane experiences only upward motion. Extracting only the gravitational part of our system and plotting it with the above mentioned quazi-static loads, it is expected to be in-between them and having same nearly-linear behavior.

In an ideal case, plotting these three curves together should resolve in having the gravitational load of the crane in between the two hydraulic forces, the lifting one being with the highest magnitude and lowering one with the lowest.

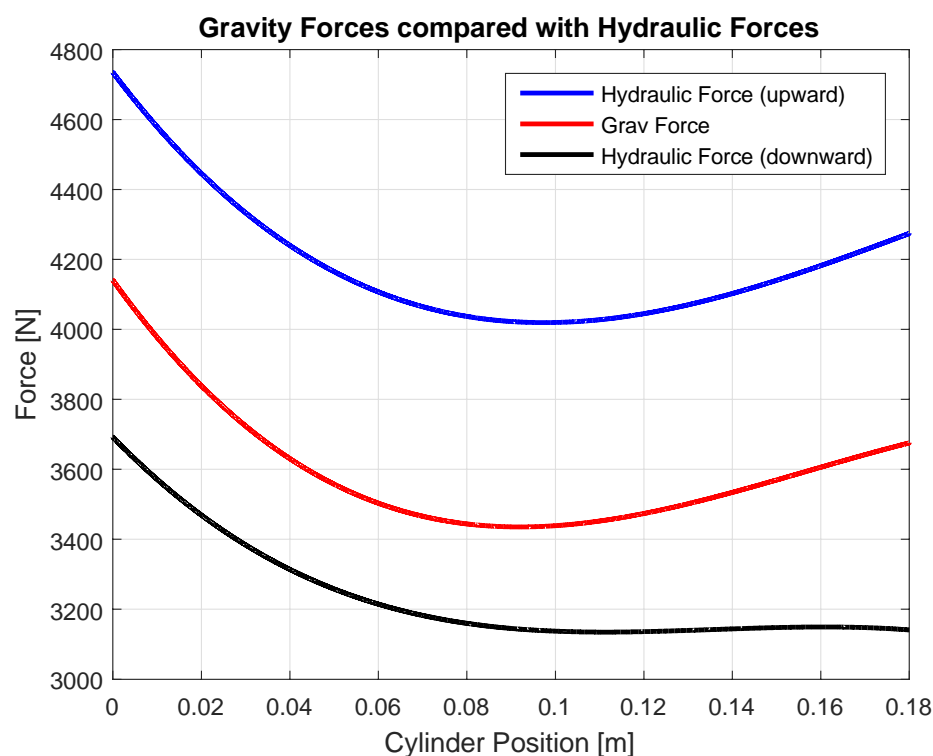


Figure 7-2 Gravity force compared to Hydraulic forces

It can be observed that the gravitational load is located in-between the hydraulic force, but not exactly in the middle. This might be due to the fact that certain masses have not been accounted for: paint, welds, not precise estimation of the bolt and nut weights. Gravitational force is shifted downwards from the ideal position by roughly 50 N, which, is can be compensated due to the unaccounted weights.

Even though the gravitational force is shifted downwards, it is still following a close to constant shape, similar to the hydraulic forces. The difference between the lifting and lowering hydraulic forces is distinguishable after the cylinder position reaches 0.12 meters and is the biggest shape discrepancy between the 2 forces. Gravitational force shape is closer to the top frictional force shape, which might be due to the bigger velocity contribution when lowering the crane due to gravity.

7.2. Verification of connected models

The main objective of carrying out non-linear model verification is to verify the dynamics and steady state properties of the hydraulic cylinder, flow and pressures, which were obtained during the experiments, with the ones obtained during the simulation of the mathematical model. Valve dynamics are to be represented with positive and negative step inputs, as they cover all the system conditions in terms of the valve position and cover all the frequencies, as opposed to other inputs.

Because of the fact that the mathematical crane model has a direct influence on the force balance part of the hydraulic model, the hydraulic model has to be verified combined with the mechanical model, representing the whole system. This is to be done in an open loop simulation.

7.2.1. Simulation conditions

Multiple simulations have been executed using data from some of the experiments that have been done (Appendix E). A 9.8 second simulation time has been chosen (and not a round number such as “10 sec”, as some of the collected data had to be discarded). The nonlinear model will be excited with using a step input as the reference spool position (“ u_v ”, [Eq. 6-3]). A step input has been chosen over a sinusoid or other pseudo random inputs because of the fact that it perfectly expresses the transition between two steady states. Unlike a sinusoidal input, which is limited to one single frequency, the step input covers a range of frequencies as such, validating the model using this type of signal made sense.

Different steps will be used in the experiments -40%, -20%, 20%, 40% openings [eg. Figure 7-5]. All the steps start at zero position and open the valve at 3 seconds. There will be also other variables taken into account, input pressure of 50 bar and 100 bar, as such giving us a bigger range of different scenarios in which will give an overview over the accuracy of the model. [Appendix D]

7.2.2. Results

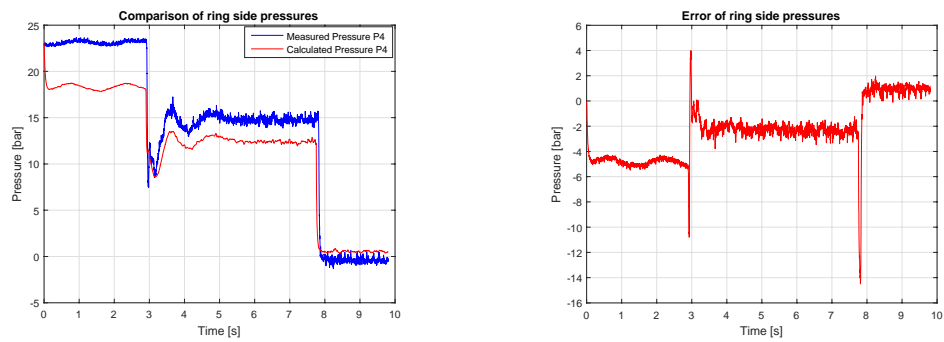


Figure 7-3 Step input 20%, 50bar – Comparison of Ring side pressures [Appendix D.a]

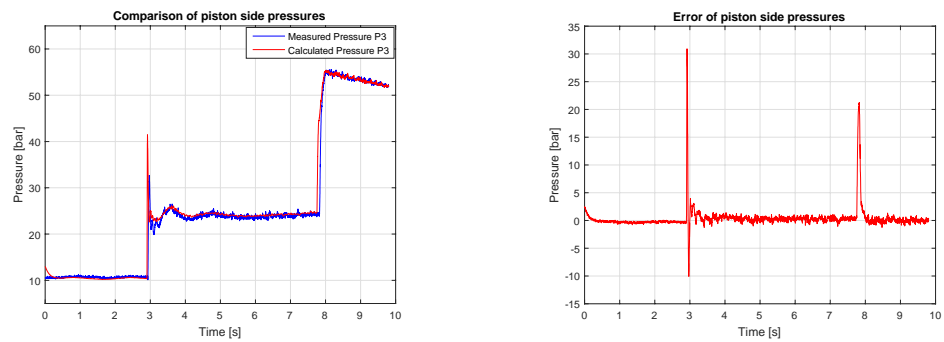


Figure 7-4 Step input 20%, 50 bar – Comparison of Piston side pressures [Appendix D.a]

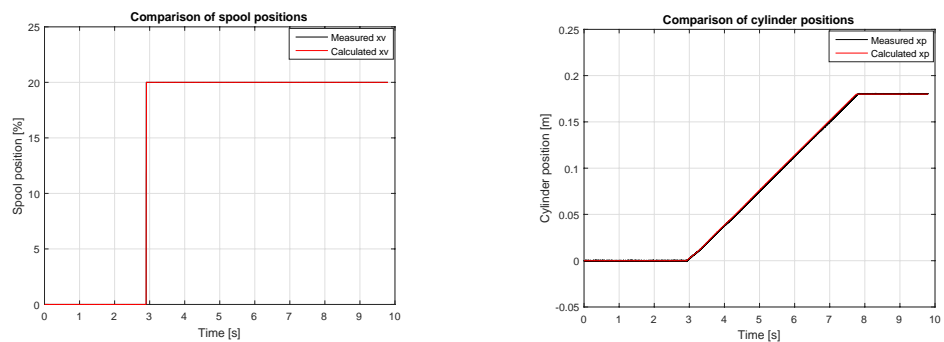


Figure 7-5 Step input 20%, 50bar – Comparison of Spool and Piston positions [Appendix D.a]

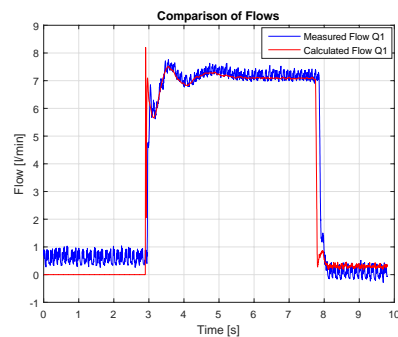


Figure 7-6 Step input 20%, 50 bar – Comparison of Measured flow with Calculated flow (Q1) [Appendix D.a]

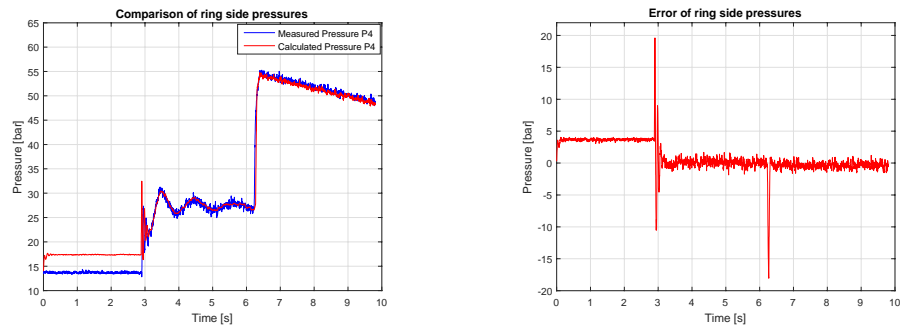


Figure 7-7 Step input -20%, 50bar - Comparison of Ring side pressures [Appendix D.b]

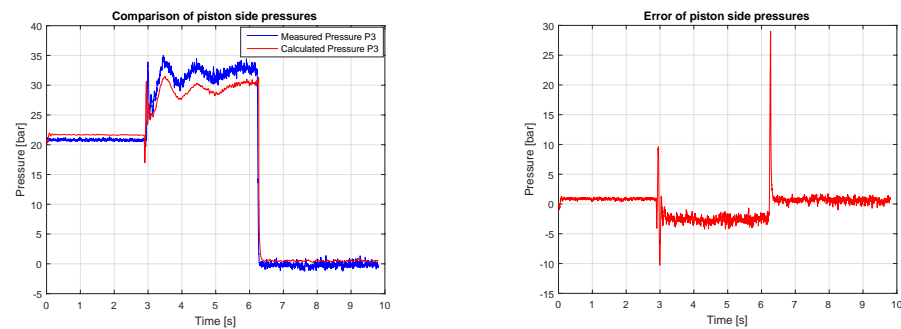


Figure 7-8 Step input -20%, 50bar - Comparison of Piston side pressures [Appendix D.b]

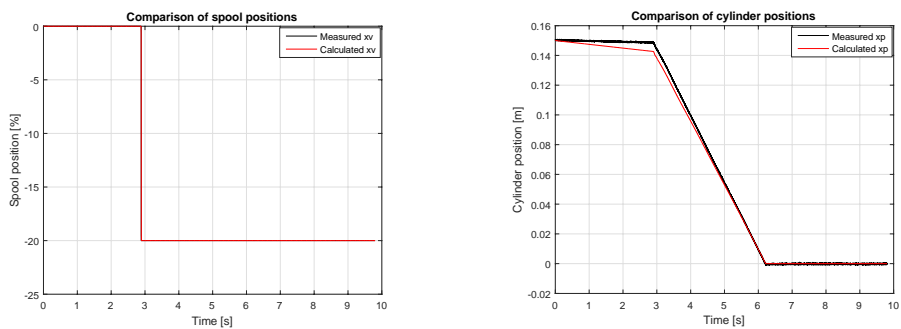


Figure 7-9 Step input -20%, 50bar – Comparison of Spool and Piston positions [Appendix D.b]

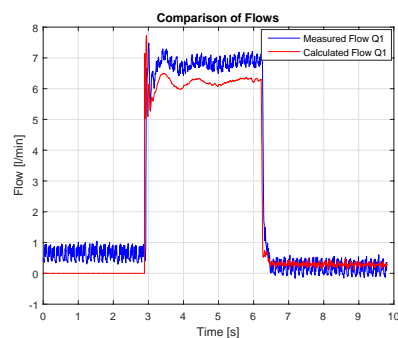


Figure 7-10 Step input -20%, 50 bar – Comarison of Measured flow with Calculated flow (Q1) [Appendix D.b]

The results show an acceptable behavior of the combined model. An offset is present in the 0 spool position in p_4 [Figure 7-3] that can be explained with a leakage or shift in spool position. It was not possible to narrow it down without influencing the other parameters in the system. The test results show as well that there is a bigger error in the pressure of the chamber, which is not driven by the pump directly. For example the error in the lowering case is bigger in p_3 [Figure 7-8] (approximately 3 bar) than in p_4 that is driven by the supply pressure. In the lifting case it is the other way around. p_3 [Figure 7-4] is connected to the supply pressure and shows less error than p_4 (approximately 5 bar in the region 0 to 3sec and approximately 2 bar in the region 3 to 8 sec).

As it can be determined from [Figure 7-5, 7-9] the accuracy of the cylinder position is high in both cases step 20% and step -20%.

The biggest inconsistencies can be seen in the pressures. As the error plots show [Figure 7-3, 7-4, 7-7, 7-8] the error fluctuations are minor compared to the operating pressure. The highest pressure difference occurs at two peaks, which occur due to a slight delay between the simulated and measured results. This is caused by the fact that the pressure transducers have a 4 ms delay and the filter applied to the signals to reduce the noise, will also have an impact. [Appendix D]

Other reasons for inconsistencies:

- Calculation of the valve coefficient: Some approximations have been done in order to get a valve coefficient that would suit our needs. Because of the fact that the datasheet of the DCV was not giving the parameters needed to calculate the flows with the general valve equation which uses discharge coefficient and discharge area, it was necessary to make some compromises. The value of the valve coefficient was fluctuating a lot. Having multiple measurements with different valve openings gave us a range of values for the coefficient. The one that fit best was selected
- Leakage coefficients: These were tuning parameters
- Signal input accuracy to the valve
- Noise
- Sampling frequency: A higher sample frequency when doing the experiments would have helped with the accuracy
- Bulk modulus and friction forces approximations: Because of the complicated non-linear equations, these had to be simplified to help with computation time
- Weight of the crane: The crane was not disassembled for us to make accurate weight measurements
- Hydraulic damping

The step input at 100 bar [Appendix E.e] supply pressure shows a similar behavior in the error dynamics. Due to the higher pressure a bigger error is present. It varies from 0 - 10 bar, which is acceptable.

Previous research papers show error dynamics of ~5 to 7 bar [8]. Due to the fact that the error in the combined model is smaller compared to the one in previous researches it can be assumed that the model works how it should.

The model captures the driving dynamic aspects of the combined hydraulic and mechanical system in terms of the piston position change, pressure and flow dynamics. The model is to be assumed accurate to a level to carry out FDD.

8. Fault Detection Diagnosis (FDD)

FDD is a one of the areas of control engineering which focuses on monitoring systems, detection an occurrence of a fault, detecting the type of fault and isolating it. Faults can be detected in a number of ways, which are qualitative or quantitative based.

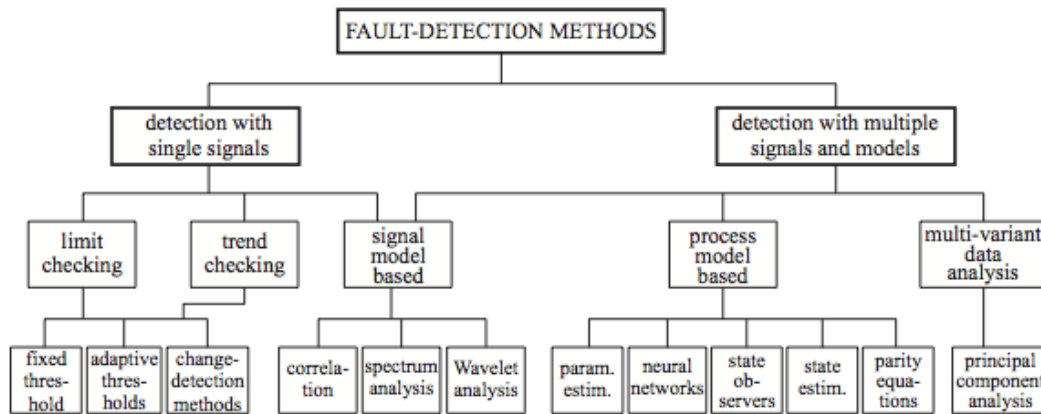


Figure 8-1 Fault Detection methods [4]

FDD can be classified into 2 groups [4]:

- Model based FDD

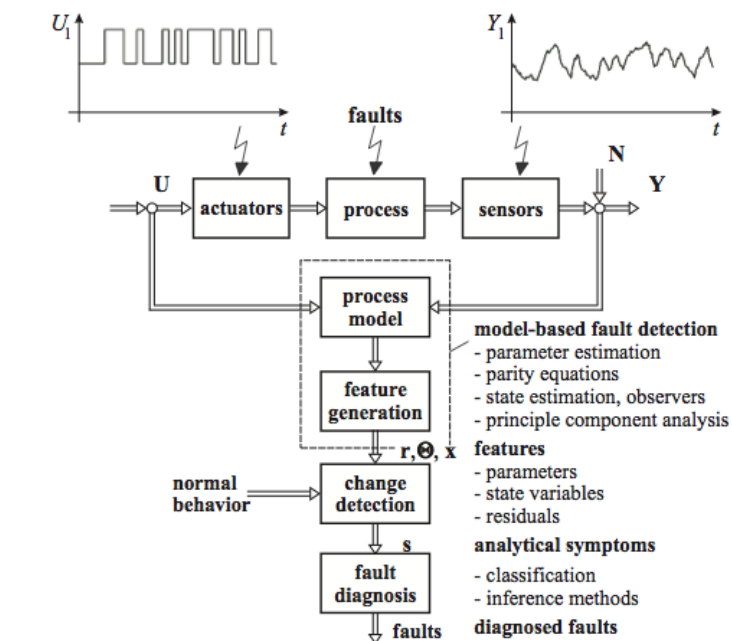


Figure 8-2 Model based FDD block diagram representation [4]

Model based approaches require the use of a mathematical model, to detect a fault. These include observers, parameter identification methods and parity space methods.

Model based FDD takes into consideration the dynamics of the system. Model accuracy has a high impact on its performance. This FDD method utilizes relationships between multiple variable to detect possible changes caused by the faults. The relationship between the input and output signal is made through the mathematical model and special features, such as states, are extracted, and their observed values are compared with the nominal to generate residuals or other symptoms.

- Signal based FDD

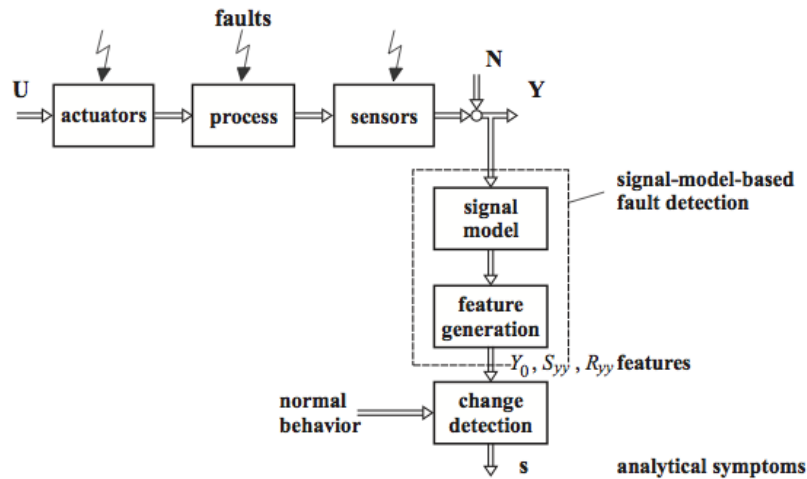


Figure 8-3 Signal based FDD block diagram representation [4]

Signal based approaches are based on statistical and mathematical approaches. These include time domain reflectometry, signal based artificial neural networks.

Signal based approaches are usually applied on periodic signals, constant periodic parts and stochastic signals. They only take into consideration the signal outputs, meaning the sensor accuracy, noise have an impact on its performance.

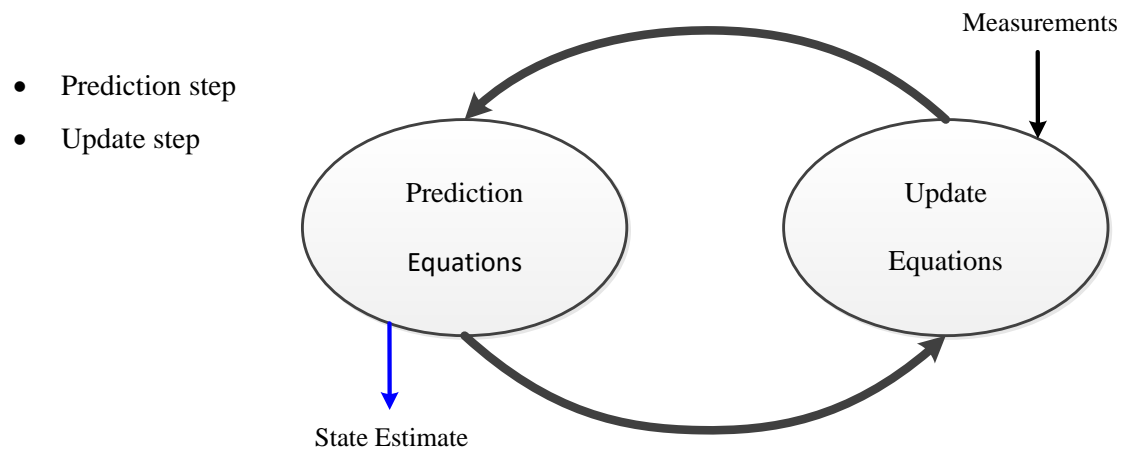
Assumptions are made of the mathematical models based on the measured output and selected features are calculated, such as amplitudes and spectrum frequencies.

In this report both ways will be applied to the model constructed and data collected and analyzed in terms of their performance on the same setup under the same conditions. To enhance the performance of FDD methods, they will be combined to increase the effectiveness.

8.1. Extended Kalman Filter based FDD

8.1.1. Introduction

Extended Kalman Filter is a non-linear version of the Kalman Filter, which itself linearizes around the estimates of mean and covariance, after each step of the iteration loop the filter re-linearizes. It is a predictor – corrector algorithm which consists of 2 steps:



The objective of implementing the Extended Kalman Filter is to get the systems residuals based on the inputs, measured outputs and certain assumptions made to the process noises and output noises, based on which FDD will be concluded.

The prediction step estimates the current state based on the estimate of the error covariance and most recent state estimate.

The update step corrects the predicted state estimate based on a new measurement.

Due to the non-linearity of the process, covariance and update predictions use the Jacobian matrix, instead of differentiable system equations.

Biggest drawback of the Extended Kalman Filter (EKF) is that if the process is linear, the equations become the same as the linear Kalman Filter, making it a non-optimal estimator. As well, inaccurate process model will lead to poor convergence results due to the Jacobian matrix.

For the pantograph crane system, EKF, which linearizes around the current mean at every step, is an excellent tool to closely and precisely estimate the state trajectories. The system is non-linear, differentiable and thus an EKF is applicable, as we assume that a linear approximation for our system would be not too detrimental.

Similar steps in using the EKF to detect leakages in hydraulic circuits have been taken in different scientific papers such as: An & Sepheri (2005) [7] and Choux, Tyapin & Hovland (2012) [11] scientific papers. The work done in this report has taken into consideration the results, pros and cons, from the previously mentioned paper. Instead of a Sinusoidal input, it has been opted to use a more complicated pseudo-random input and a step, which better highlights the dynamic characteristics of a real life hydraulic circuit. The formulas used in building the EKFs are using a combination of continuous and discrete time equations. The mechanical model is more complicated and multiple levels of internal and external leaks have been inputted artificially.

For verification purposes an EKF [Figure 8-4] has been implemented without the artificial leaks Q_{L1} and Q_{L2} . So the artificial leaks have been disregarded in the state equation.

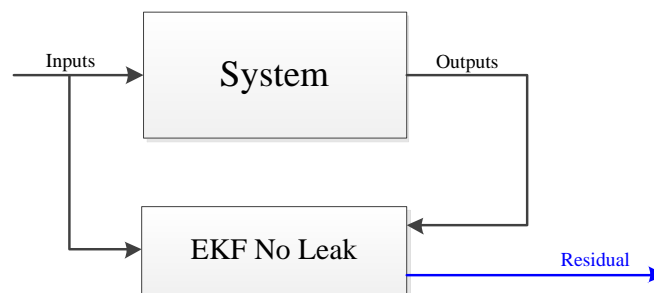


Figure 8-4 Block diagram of EKF implementation

In doing so, it is expected that the EKF will give a close to zero residual when the system is not faulty, and the exact opposite when leak is introduced. These assumptions are confirmed in the 8.1.3 subchapter.

With the implementation of just one EKF the leak that can be detected in the system although there is a certain amount of uncertainty in determining the exact source of the leak. Thus multiple EKF have been developed, or so called Bank of Kalman Filters, as seen in Figure 8-5.

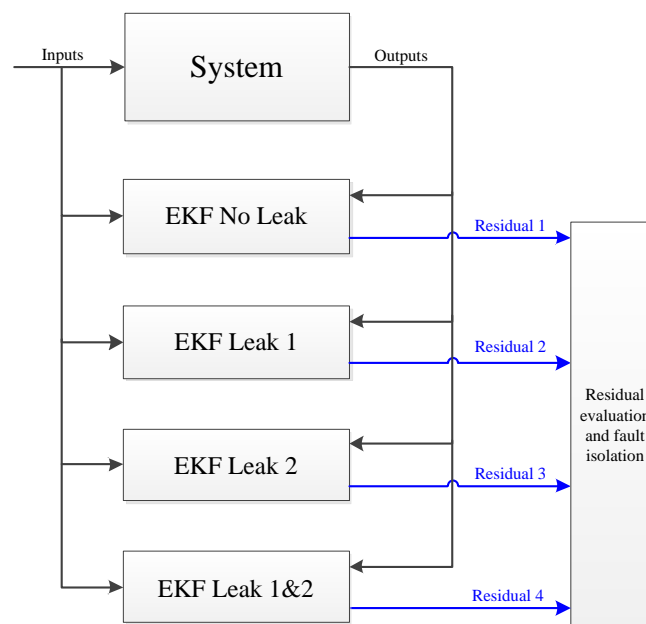


Figure 8-5 Block diagram of Bank EKF implementation

Three EKF have been implemented. The difference between them is that first EKF is using no leaks in the state equations, the second one implements the artificial leak which occurs in the valve, and the third one implements the artificial leak which simulates leakage across the seal of the cylinder.

In theory, by evaluating each of the residuals, it can clearly be denoted where exactly in the system the leak occurs. This is confirmed in practice also in the subchapter 8.1.4.

Because of the fact that there are several conditions under which the hydraulic model has to operate, these conditions had to be replicated inside the EKF's. The valve leakage (which is internal leakage inside the valve, modeled in Chapter 6.3.1.2., Eq.6-4, 6-5) can only occur when the valve spool position is inside the dead zone (between -1.5% and 1.5%). Other two conditions had to be implemented to express the directional changes in the hydraulic cylinder (covered in Chapter 6.4, Eq.6-11 through 6-14).

It is important to mention that in this first phase of the verification stage the systems measured states are direct outputs of the combined model of the hydraulic system and mechanical model, and only the input to the system has measured data (similar to model validation in Chapter 7).

The validation of the EKF with experimental data will be carried out in [Chapter 9.2] in the report.

8.1.2. Continuous-Discrete form model

As mentioned above, in the Extended Kalman Filter state models are to be non-linear, therefor they are represented as differentiable functions as [3]:

$$\begin{aligned}\dot{\mathbf{x}}_k &= \mathbf{f}(\mathbf{x}, \mathbf{u}) + \mathbf{w} \\ \mathbf{y}_k &= \mathbf{h}(\mathbf{x}_k) + \mathbf{v}_k\end{aligned}\tag{8.1}$$

\mathbf{w} and \mathbf{v}_k are assumed to be Gaussian noises of zero mean and $\mathbf{Q} = \text{diag}[0.001 \ 0.001 \ 0.001 \ 0.001 \ 1e5 \ 1e5]$ and $\mathbf{R}_k = [0.001 \ 0.001 \ 0.001 \ 0.001 \ 0.5e5 \ 2e5]$ covariance matrixes, these matrixes can be adjusted via simulation and are to be diagonal. These have been taken as tuning parameters and have been chosen with such values that gave the most accurate EKF results.

The constructed model, allows having continuous processes while having discrete outputs which are measured at sampling times k , due to the fact that the Jacobian matrix is continuous while the other steps in the EKF are discretized.

In our case, the non-linear state space model is represented in the following way [7]:

$$\mathbf{X} = \begin{bmatrix} x_1 \\ x_2 \\ x_3 \\ x_4 \\ x_5 \\ x_6 \end{bmatrix} = \begin{bmatrix} x_p \\ \dot{x}_p \\ x_v \\ \dot{x}_v \\ p_3 \\ p_4 \end{bmatrix} \quad \mathbf{u} = \begin{bmatrix} p_2 \\ p_5 \\ u_v \end{bmatrix}\tag{8.2}$$

$$\dot{\mathbf{X}} = \begin{bmatrix} \dot{x}_1 \\ \dot{x}_2 \\ \dot{x}_3 \\ \dot{x}_4 \\ \dot{x}_5 \\ \dot{x}_6 \end{bmatrix} = \begin{bmatrix} \dot{x}_p \\ \ddot{x}_p \\ \dot{x}_v \\ \ddot{x}_v \\ \dot{p}_3 \\ \dot{p}_4 \end{bmatrix}\tag{8.3}$$

Inserting Eq. 6-1 through 6-17 from Chapter 6 into Eq. 8.3 in the case of the single EKF without implemented leaks the state equations become:

$$\begin{aligned} \dot{\mathbf{x}} &= \mathbf{f}(\mathbf{x}, \mathbf{u}) \\ &= \begin{bmatrix} \frac{x1}{[c_1]} \cdot \frac{x5 \cdot A_p - x6 \cdot A_r - F_f - ([c_2] \cdot x2^2 + [c_3] \cdot x1)}{x4} \\ uv \cdot \omega n^2 + 2 \cdot \zeta \cdot \omega n \cdot x4 + \omega n^2 \cdot x3 \\ \left(\frac{\beta}{A_p \cdot x1 + V_{p0}} \cdot \left((kv \cdot x3 \cdot \sqrt{p_2 - x5}) - Q_{Lp}(\mathbf{x}) - Q_{LvTotal}(\mathbf{x}) - A_p x2 \right) \right. \\ \left. \frac{\beta}{A_p \cdot x1 + V_{p0}} \cdot \left((kv \cdot x3 \cdot \sqrt{x5 - p_5}) - Q_{Lp}(\mathbf{x}) - Q_{LvTotal}(\mathbf{x}) - A_p x2 \right) \right. \\ \left. \frac{\beta}{-A_r \cdot x1 + V_{r0}} \cdot \left(- (kv \cdot x3 \cdot \sqrt{x6 - p_5}) + Q_{Lp}(\mathbf{x}) + Q_{LvTotal}(\mathbf{x}) + A_r x2 \right) \right. \\ \left. \frac{\beta}{-A_r \cdot x1 + V_{r0}} \cdot \left(- (kv \cdot x3 \cdot \sqrt{p_2 - x6}) + Q_{Lp}(\mathbf{x}) + Q_{LvTotal}(\mathbf{x}) + A_r x2 \right) \right] \end{bmatrix} \quad (8.4) \end{aligned}$$

Inserting Eq. 6-1 through 6-17 from Chapter 6 into Eq. 8.3 in the case of the EKF with only the Leak 1 implemented the state equations become:

$$\begin{aligned} \dot{\mathbf{x}} &= \mathbf{f}(\mathbf{x}, \mathbf{u}) \\ &= \begin{bmatrix} \frac{x1}{[c_1]} \cdot \frac{x5 \cdot A_p - x6 \cdot A_r - F_f - ([c_2] \cdot x2^2 + [c_3] \cdot x1)}{x4} \\ uv \cdot \omega n^2 + 2 \cdot \zeta \cdot \omega n \cdot x4 + \omega n^2 \cdot x3 \\ \left(\frac{\beta}{A_p \cdot x1 + V_{p0}} \cdot \left((kv \cdot x3 \cdot \sqrt{p_2 - x5}) - Q_{Lp}(\mathbf{x}) - Q_{LvTotal}(\mathbf{x}) - Q_{L1}(\mathbf{x}) - A_p x2 \right) \right. \\ \left. \frac{\beta}{A_p \cdot x1 + V_{p0}} \cdot \left((kv \cdot x3 \cdot \sqrt{x5 - p_5}) - Q_{Lp}(\mathbf{x}) - Q_{LvTotal}(\mathbf{x}) - Q_{L1}(\mathbf{x}) - A_p x2 \right) \right. \\ \left. \frac{\beta}{-A_r \cdot x1 + V_{r0}} \cdot \left(- (kv \cdot x3 \cdot \sqrt{x6 - p_5}) + Q_{Lp}(\mathbf{x}) + Q_{LvTotal}(\mathbf{x}) - Q_{L1}(\mathbf{x}) + A_r x2 \right) \right. \\ \left. \frac{\beta}{-A_r \cdot x1 + V_{r0}} \cdot \left(- (kv \cdot x3 \cdot \sqrt{p_2 - x6}) + Q_{Lp}(\mathbf{x}) + Q_{LvTotal}(\mathbf{x}) - Q_{L1}(\mathbf{x}) + A_r x2 \right) \right] \end{bmatrix} \quad (8.5) \end{aligned}$$

Inserting Eq. 6-1 through 6-17 from Chapter 6 into Eq. 8.3 in the case of the EKF with only the Leak 2 implemented the state equations become:

$$\begin{aligned} \dot{\mathbf{X}} &= \mathbf{f}(\mathbf{x}, \mathbf{u}) \\ &= \begin{bmatrix} \frac{x1}{[c_1]} \cdot \frac{x5 \cdot A_p - x6 \cdot A_r - F_f - ([c_2] \cdot x2^2 + [c_3] \cdot x1)}{x4} \\ uv \cdot \omega n^2 + 2 \cdot \zeta \cdot \omega n \cdot x4 + \omega n^2 \cdot x3 \\ \left(\frac{\beta}{A_p \cdot x1 + V_{p0}} \cdot \left((kv \cdot x3 \cdot \sqrt{p_2 - x5}) - Q_{Lp}(\mathbf{x}) - Q_{LvTotal}(\mathbf{x}) - Q_{L2}(\mathbf{x}) - A_p x2 \right) \right) \\ \left(\frac{\beta}{A_p \cdot x1 + V_{p0}} \cdot \left((kv \cdot x3 \cdot \sqrt{x5 - p_5}) - Q_{Lp}(\mathbf{x}) - Q_{LvTotal}(\mathbf{x}) - Q_{L2}(\mathbf{x}) - A_p x2 \right) \right) \\ \left(\frac{\beta}{-A_r \cdot x1 + V_{r0}} \cdot \left(- (kv \cdot x3 \cdot \sqrt{x6 - p_5}) + Q_{Lp}(\mathbf{x}) + Q_{LvTotal}(\mathbf{x}) + Q_{L2}(\mathbf{x}) + A_r x2 \right) \right) \\ \left(\frac{\beta}{-A_r \cdot x1 + V_{r0}} \cdot \left(- (kv \cdot x3 \cdot \sqrt{p_2 - x6}) + Q_{Lp}(\mathbf{x}) + Q_{LvTotal}(\mathbf{x}) + Q_{L2}(\mathbf{x}) + A_r x2 \right) \right) \end{bmatrix} \quad (8.6) \end{aligned}$$

Inserting Eq. 6-1 through 6-17 from Chapter 6 into Eq. 8.3 in the case of the EKF with both Leak 1 and Leak 2 implemented the state equations become:

$$\begin{aligned} \dot{\mathbf{X}} &= \mathbf{f}(\mathbf{x}, \mathbf{u}) \\ &= \begin{bmatrix} \frac{x1}{[c_1]} \cdot \frac{x5 \cdot A_p - x6 \cdot A_r - F_f - ([c_2] \cdot x2^2 + [c_3] \cdot x1)}{x4} \\ uv \cdot \omega n^2 + 2 \cdot \zeta \cdot \omega n \cdot x4 + \omega n^2 \cdot x3 \\ \left(\frac{\beta}{A_p \cdot x1 + V_{p0}} \cdot \left((kv \cdot x3 \cdot \sqrt{p_2 - x5}) + Q_{TL1} - A_p x2 \right) \right) \\ \left(\frac{\beta}{A_p \cdot x1 + V_{p0}} \cdot \left((kv \cdot x3 \cdot \sqrt{x5 - p_5}) + Q_{TL1} - A_p x2 \right) \right) \\ \left(\frac{\beta}{-A_r \cdot x1 + V_{r0}} \cdot \left(- (kv \cdot x3 \cdot \sqrt{x6 - p_5}) + Q_{TL2} + A_r x2 \right) \right) \\ \left(\frac{\beta}{-A_r \cdot x1 + V_{r0}} \cdot \left(- (kv \cdot x3 \cdot \sqrt{p_2 - x6}) + Q_{TL2} + A_r x2 \right) \right) \end{bmatrix} \quad (8.7) \end{aligned}$$

Where for writing practicality, the system leakages and artificial leakages have been replaced with:

$$Q_{TL1} = -Q_{Lp}(\mathbf{x}) - Q_{LvTotal}(\mathbf{x}) - Q_{L1}(\mathbf{x}) - Q_{L2}(\mathbf{x})$$

$$Q_{TL2} = Q_{Lp}(\mathbf{x}) + Q_{LvTotal}(\mathbf{x}) - Q_{L1}(\mathbf{x}) + Q_{L2}(\mathbf{x})$$

8.1.2.1. Prediction

As expressed in Process Control, J.P.Corriou [3] the prediction phase of the Extended Kalman Filter is defined:

- State prediction

$$\dot{\hat{\mathbf{x}}} = \mathbf{f}(\hat{\mathbf{x}}, \mathbf{u}) \quad (8.8)$$

- Covariance prediction

$$\mathbf{P}_k = \mathbf{A}(\hat{\mathbf{x}}, t) \cdot \mathbf{P}_{k|k-1} + \mathbf{P}_{k|k-1} \cdot \mathbf{A}^T(\hat{\mathbf{x}}, t) + \mathbf{Q}(t) \quad (8.9)$$

Where \mathbf{A} is the Jacobian matrix of \mathbf{f}

$$\mathbf{A}(\hat{\mathbf{x}}, t) = \left. \frac{\delta \mathbf{f}}{\delta \mathbf{x}} \right|_{\mathbf{x}=\hat{\mathbf{x}}} \quad (8.10)$$

8.1.2.2. Update

As expressed in Process Control, J.P.Corriou [3] the update phase of the Extended Kalman Filter is defined:

- Innovation sequence or residual

$$\hat{\mathbf{y}}_k = \mathbf{z}_k - h(\mathbf{x}_{k|k-1}) \quad (8.11)$$

Where \mathbf{z}_k is the measurement vector.

- Innovation sequence or residual covariance (covariance of the estimated outputs)

$$\mathbf{S}_k = \mathbf{H}_k \cdot \mathbf{P}_{k|k-1} \cdot \mathbf{H}_k^T + \mathbf{R}_k \quad (8.12)$$

- Kalman gain

$$\mathbf{K}_k = \mathbf{P}_{k|k-1} \cdot \mathbf{H}_k^T \cdot \mathbf{S}_k^{-1} \quad (8.13)$$

- Updated state estimate

$$\hat{\mathbf{x}}_{k|k} = \hat{\mathbf{x}}_{k|k-1} + \mathbf{K}_k \cdot \hat{\mathbf{y}}_k \quad (8.14)$$

- Updated covariance estimate

$$\mathbf{P}_{k|k} = (\mathbf{I} - \mathbf{K}_k \cdot \mathbf{H}_k) \cdot \mathbf{P}_{k|k-1} \quad (8.15)$$

8.1.2.3. Artificial Leaks used

In order to validate the claims that the implemented EKF's are giving correct results, some fault had to be added to the system. As discussed in previous chapters these faults take the form of artificial leaks. Leak 1 represents leakage in the valve [Figure 8-6]; Leak 2 represents the leakage across the seal of the cylinder [Figure 8-7].

It is important to mention that the Leak 1 representing the valve leak is assumed present only in the p_4 (ring pressure) side to tank section of the hydraulic system.

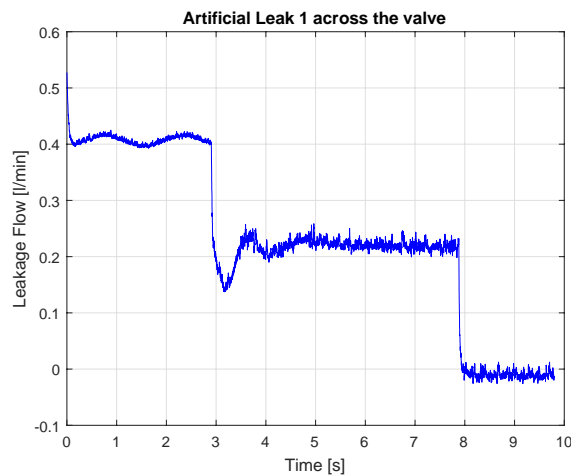


Figure 8-6 - External artificial Leak 1 - across the valve

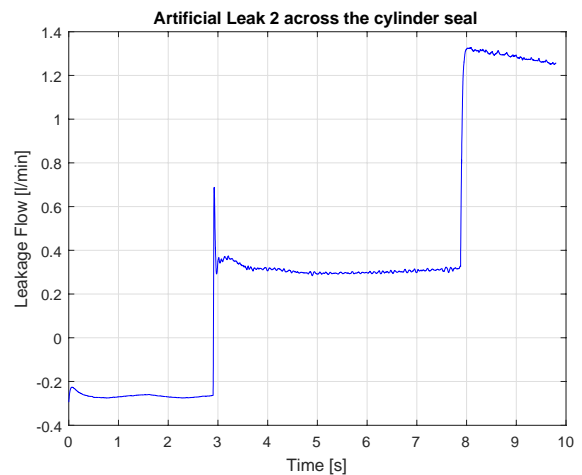


Figure 8-7 - Internal artificial Leak 2 - across the cylinder seal

8.1.3. Extended Kalman Filter

Due to the implementation of the Extended Kalman Filter it is possible to show the error residuals of the different states. State x_5 (p_3) and x_6 (p_4) were chosen to represent the system error. The evaluation of the residuals shows that the previously mentioned states were the most suitable states to detect an error. In the displayed time range ~3 to 7 sec the lifting movement of the crane occurs. The time before and after this movement, the crane is stationary and is not relevant to the results evaluation.

8.1.3.1. p_3 evaluation

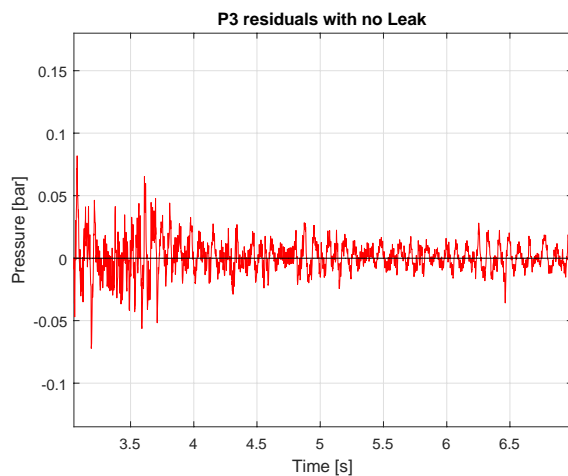


Figure 8-8 p_3 residual with no leak implemented

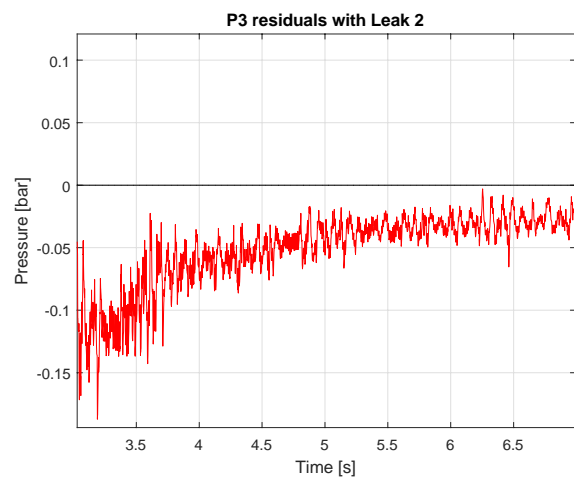


Figure 8-9 p_3 residual with implemented artificial leak across the cylinder

Figure 8-8 shows the simulation result with no artificial leak. It is visible that the residual fluctuates around zero, which indicates a fault free system.

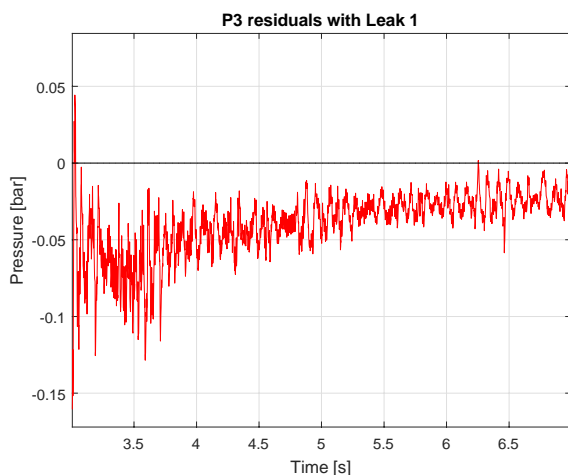


Figure 8-10 p_3 residual with implemented artificial leak across the valve

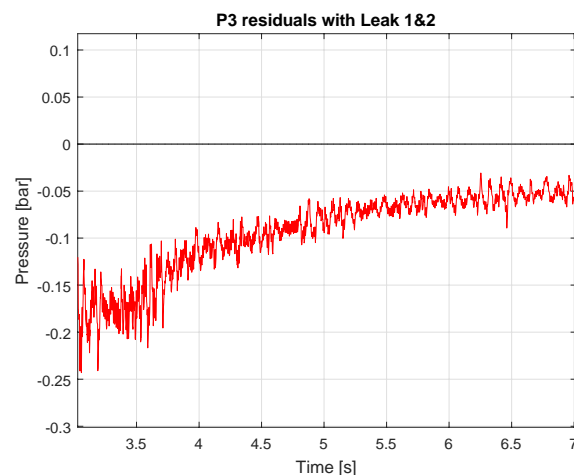


Figure 8-11 p_3 residual with both artificial leaks implemented

Figure 8-9 and 8-10 represent the simulation situations in which an artificial Leak 1 (across the valve) and artificial Leak 2 (across the piston sealing) are implemented. In the first case it is simulated as a valve leak from the ring chamber to the tank. The second represents a leakage over the piston. It can be seen that the residual is non-zero, which represents a difference between the faulty system and the estimated value from the EKF. It can be concluded that a fault is detected in the system.

Figure 8-11 represents a situation where both artificial leaks are present simultaneously. As it can be seen the residual of the EKF with both leaks is the worst from the previously mentioned situations, having the biggest error. It can be concluded that there exists a bigger fault in the system however it cannot distinguish exactly which leaks are present.

8.1.3.2. p_4 evaluation

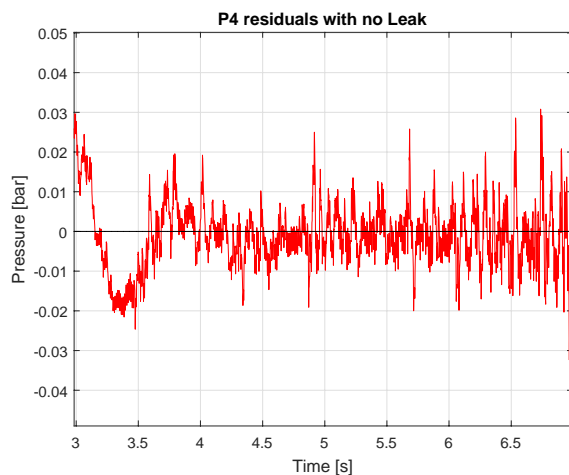


Figure 8-12 p_4 residual with no leak implemented

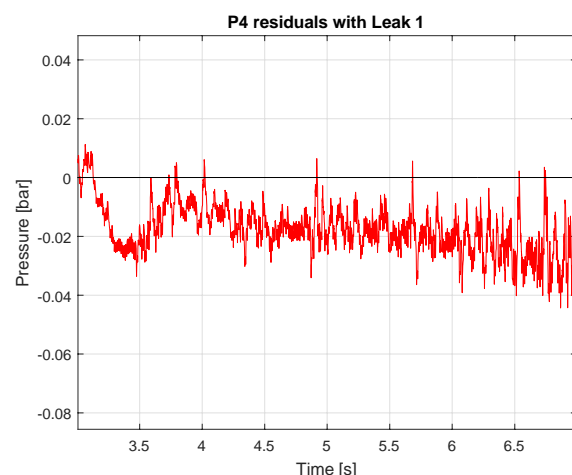


Figure 8-13 p_4 residual with implemented artificial leak across the valve

Figure 8-12 shows the simulation result with no artificial leak. It is shown that the residual is around zero, which indicates a fault free system.

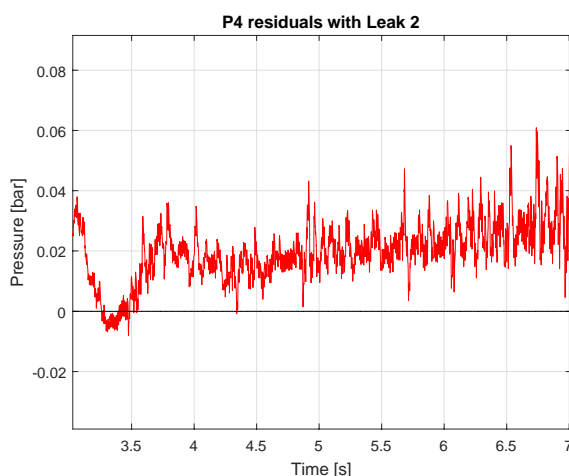


Figure 8-14 p_4 residual with implemented artificial leak across the valve

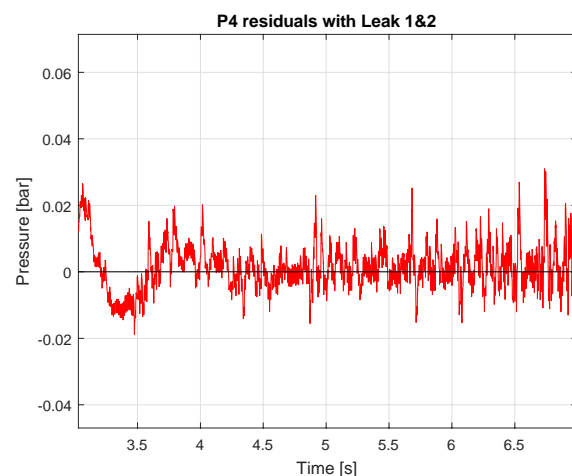


Figure 8-15 p_4 residual with both artificial leaks implemented

Figures 8-13, 8-14 and 8-15 represent the simulation results with implemented artificial Leak 1 (across the valve from the ring chamber to the tank), artificial Leak 2 (across the piston sealing) and both leaks implemented simultaneously. It can be seen that the residuals are non-zero which represents a difference between the faulty system and the estimated value from the EKF. It can be concluded that a fault is detected in the system.

Residuals of the states x_5 (p_3) and x_6 (p_4) will always have a difference, simply due to the fact that at a moment in time there is only one leak present, which influences mostly either the piston, or the ring chamber pressure. In an instance, where both leaks are present, residuals are to be expected to be similar, unless leak magnitudes differ significantly.

As it can be seen state variable x_6 (p_4) is less suitable for detection purposes in this particular scenario, as the influence of the leaks on the ring side pressure is less than on the piston side pressure x_5 (p_3), because of the fact that it delivers the main driving force for upward motion .

8.1.4. Bank of Extended Kalman Filters

Bank of Extended Kalman Filters (BEKF) are several Extended Kalman Filters implemented on the same system to aid with fault isolation based on the individual residuals, which are divided by separate leakage implementation. This helps to isolate the fault in the system to the root of it, however it cannot precisely detect the magnitude of the fault. BEKF is to be implemented on the model, as well as on the experiments for better performance evaluation.

BEKF as mentioned in the M. Choux (2012) [11] paper is a method which will in addition also isolate the fault and can be refined by introducing a bigger number of EKF's.

8.1.4.1. *p3 evaluation*

The simulation result of the BEKF shows the expected results. It was possible to isolate the fault in the system.

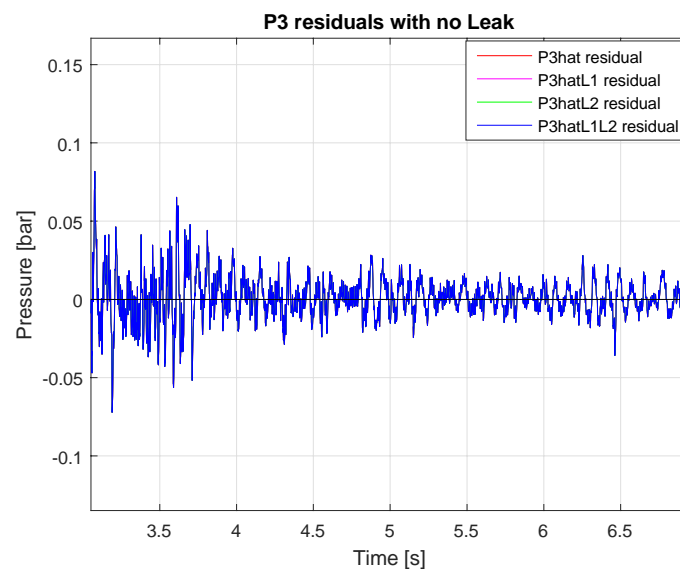


Figure 8-16 p3 residual of BEKF with no leak implemented

Figure 8-16 represents a non-faulty system. For this scenario, it is expected that all residuals should fluctuate around zero. It can be seen that it behaves as it should. It can be concluded that the system runs fault free. All residuals perfectly stack on each other, which is an indicator that the same should appear if any residuals cross-over a certain leakage.

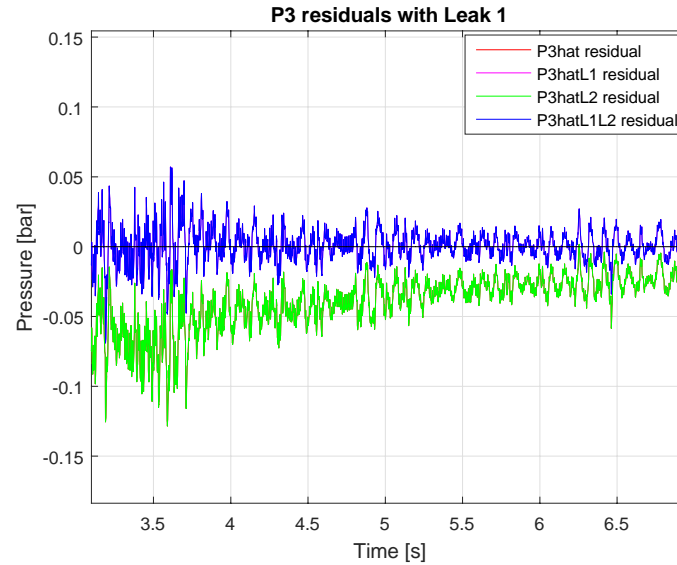


Figure 8-17 p3 residual of BEKF with implemented artificial leak across the valve

Figure 8-17 shows the simulation result with an artificial Leak 1 (across the valve). This shows that the manipulated EKF, the one which the equations of state take into account set leak, gives a residual around zero where the other EKFs show bigger differences. The fact that the Leak 1 EKF gives a zero residual indicates that there is a fault in the valve of the system. Therefore, the fault is detected and isolated.

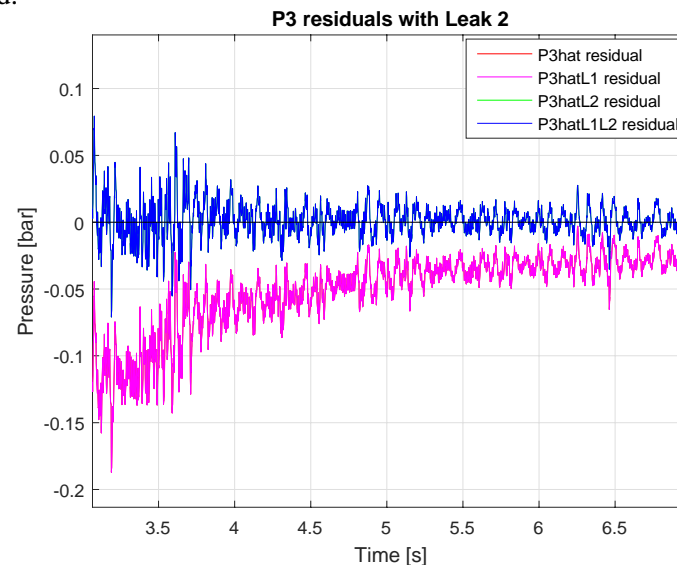


Figure 8-18 p3 residual of BEKF with implemented artificial leak across the cylinder

Figure 8-18 shows the simulation result with an artificial Leak 2 (across the cylinder seal). It can be seen that the manipulated EKF gives a residual around zero where the other EKFs show bigger differences. The fact the Leak 2 EKF gives a zero residual indicates that there is a fault in the piston of the system. Therefore, the fault is detected and isolated.

It is important to mention that the residual that are not visible in the graphs are behind the line which is furthest from the zero line of the graph.

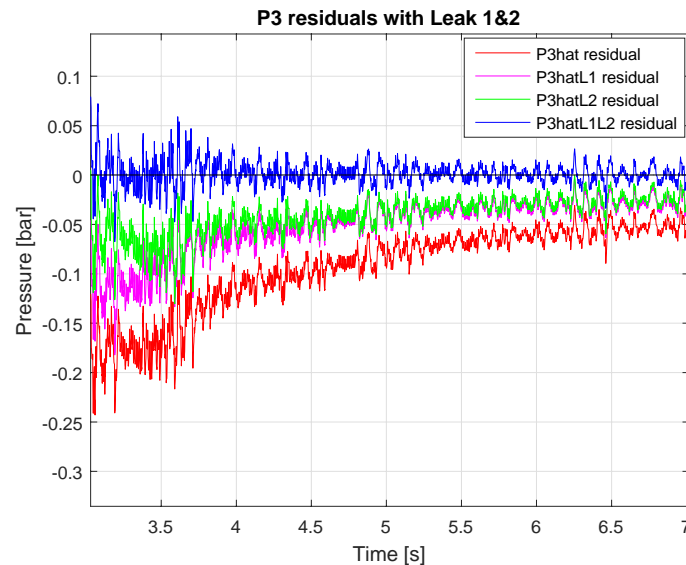


Figure 8-19 p3 residual of BEKF with both leaks implemented at the same time

Figure 8-19 shows the simulation result with an artificial Leak 1 and 2 combined. It can be seen that the manipulated EKF which has both leaks implemented, gives a residual closer to zero where the non-fault EKF shows bigger differences. The fact the Leak 1&2 EKF gives a closer to zero residual indicates that there is a fault in the valve and piston of the system. Therefore, the faults are detected and isolated. Leak 1 and Leak 2 EKF's also deliver a closer to zero residual because of the fact that both set leaks are present in the system.

8.1.4.2. *p4 evaluation*

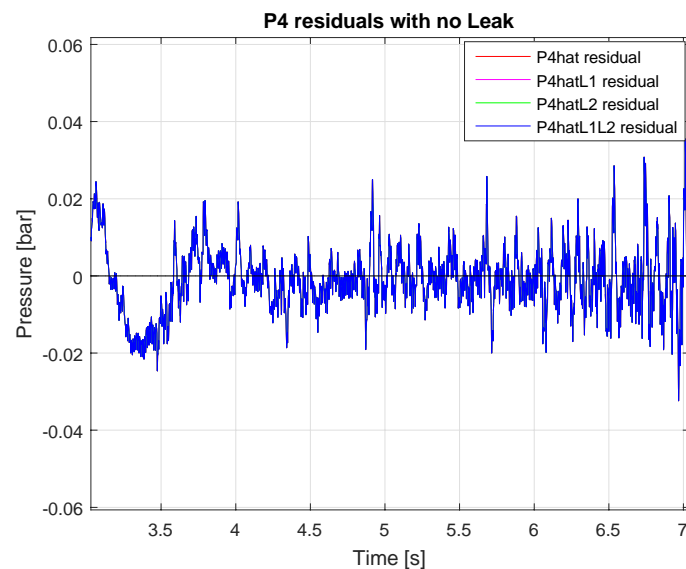


Figure 8-20 p4 residual of BEKF with no leak implemented in the system

Figure 8-20 represents a non-faulty system. The expected p_4 residual should fluctuate around zero. It can be seen that it behaves closely to what is expected. It can be concluded that the system runs fault free.

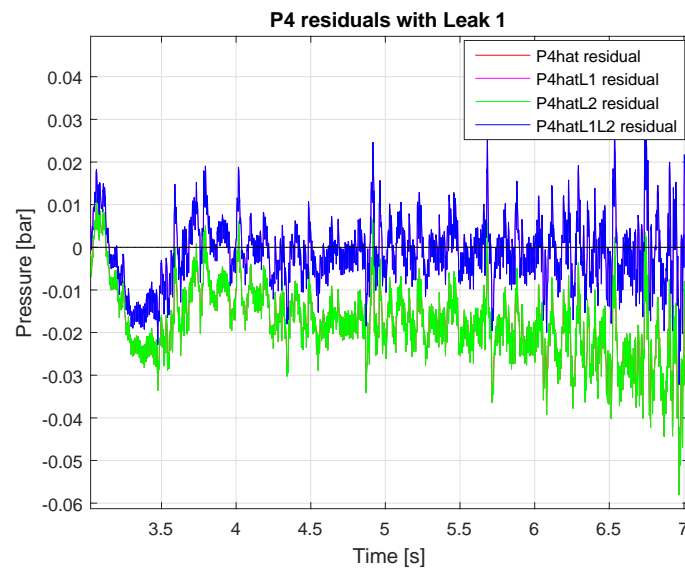


Figure 8-21 p_4 residual of BEKF with implemented artificial leak across the valve

Figure 8-21 shows the simulation result with an artificial Leak 1. Similar to p_3 residual graph, it shows that the manipulated EKF gives a residual around zero where the other EKFs show bigger differences. The fact the Leak 1 EKF gives a zero residual indicates that there is a fault in the valve of the system. Therefore, the fault is detected and isolated.

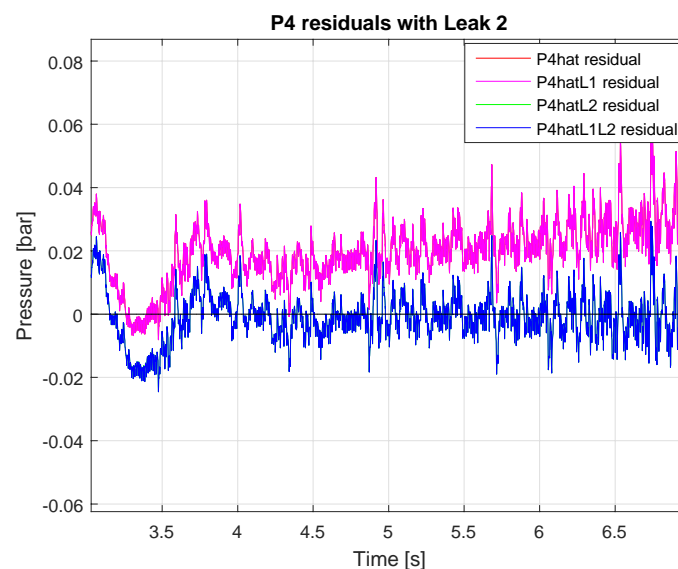


Figure 8-22 p_4 residual of BEKF with implemented artificial leak across the cylinder

Figure 8-22 shows the simulation result with an artificial Leak 2. The graph shows, that the manipulated EKF gives a residual around zero where the other EKFs show bigger differences. The fact the Leak 2 EKF gives a zero residual indicates that there is a fault in the piston of the system. Therefore the fault is detected and isolated.

It is important to mention that the residual that are not visible in the graphs are behind the line which is furthest from the zero line of the graph.

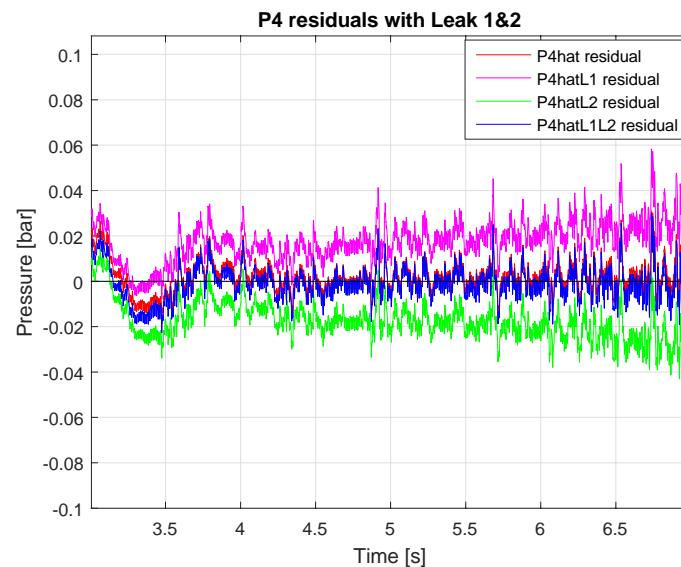


Figure 8-23 p4 residual of BEKF with both leaks implemented at the same time

Figure 8-23 shows the simulation result with an artificial Leak 1 and 2 combined. It can be seen that the manipulated EKF which has both leaks implemented, gives a residual closer to zero where the non-fault EKF shows bigger differences. The fact the Leak 1&2 EKF gives a closer to zero residual indicates that there is a fault in the valve and piston of the system. Therefore, the faults are detected and isolated. Leak 1 and Leak 2 EKF's also deliver a closer to zero residual because of the fact that both set leaks are present in the system.

As it can be seen the state variable x_6 (p_4) is less suitable for detection purposes in this particular scenario, as the influence of the leaks on the ring side pressure is a lot less than on the piston side pressure x_5 (p_3).

9. Experimental FDD implementation

9.1. Data Gathering

For FDD and Model validation, different data variations have to be gathered, in order to later on find the lowest parameters at which fault detection is possible. The purpose of the experiment is to simulate a real world work environment for a hydraulic actuator with different kinds of leakage in the system. These leakages are designed with flow valves that are controlled manually.

Materials

- Hydraulic system
- Simulink real time control unit

In order to simulate a close to real work environment behavior of the hydraulic system, a curve for a changing x_p was chosen. The design was chosen to perform different speeds of changing and reaching different height. Four sets of experiments were performed. They differ in supply pressure and in oil temperature. A supply pressure of 50 bar and of 100 bar was chosen to simulate different operating conditions. The oil temperature was chosen to be 25°C and 40°C.

To simulate a bigger variety of leakage conditions five different artificial leakage levels of each leak were chosen. The Table 9-1 below shows the different valve openings of the leakage conditions. Each experiment setting includes several samples, which were saved automatically to an Excel sheet.

	Leakage 1	Leakage 2		Leakage 1	Leakage 2
Setting 1	closed	closed	Setting 9	closed	2
Setting 2	0.2	closed	Setting 10	closed	3
Setting 3	0.4	closed	Setting 11	closed	4.5
Setting 4	0.6	closed	Setting 12	0.2	1
Setting 5	1.5	closed	Setting 13	0.4	1.5
Setting 6	2.5	closed	Setting 14	0.6	2
Setting 7	closed	1	Setting 15	1.5	3
Setting 8	closed	1.5	Setting 16	2.5	4.5

Table 9-1 Description of different valve openings used in implementing artificial leak

Data collection [Table 9-2] will be conducted at two different temperatures; at each temperature five different leakage levels will be utilized (with the exception of the step input ones, which only have 1 level of leakage). Each experiment at specific operation conditions will be conducted several times, for precision purpose.

Test #	Pressure	Temperature	Input	Amount	Leak	Levels
Test 1.10	50 Bar	25°C	Step	5	No Leak	X
Test 1.11	50 Bar	25°C	Step	5	Leak 1	X
Test 1.12	50 Bar	25°C	Step	5	Leak 2	X
Test 1.13	50 Bar	25°C	Step	5	Leak 1&2	X
Test 1.14	100 Bar	25°C	Step	5	No Leak	X
Test 1.20	50 Bar	25°C	Custom	10	No Leak	X
Test 1.21	50 Bar	25°C	Custom	5-10	Leak 1	1-5
Test 1.22	50 Bar	25°C	Custom	5-10	Leak 2	1-5
Test 1.23	50 Bar	25°C	Custom	3	Leak 1&2	1-5
Test 1.30	100 Bar	25°C	Custom	5-10	No Leak	1-5
Test 1.31	100 Bar	25°C	Custom	5-10	Leak 1	1-5
Test 1.32	100 Bar	25°C	Custom	5	Leak 2	1-5
Test 1.33	100 Bar	25°C	Custom	3	Leak 1&2	1-5
Test 2.20	50 Bar	40°C	Custom	3	No Leak	X
Test 2.21	50 Bar	40°C	Custom	3	Leak 1	4 & 5
Test 2.22	50 Bar	40°C	Custom	3	Leak 2	4 & 5
Test 2.30	100 Bar	40°C	Custom	3	No Leak	X
Test 2.31	100 Bar	40°C	Custom	3	Leak 1	4 & 5
Test 2.32	100 Bar	40°C	Custom	3	Leak 2	4 & 5

Table 9-2 – Different experimental tests done under different conditions

During each experiment varying valve opening will be utilized, this is needed for FDD purposes, in order to see whether FDD is valid for different valve opening under the exact same operation conditions. In such case, leakage might be detected when the system is running with a higher valve opening, rather than a small one. Furthermore, the experiment will follow a position curve, which will have both abrupt position changed as well as smooth transitions. Due to this we will see how FDD methods react to intervals when a smaller amount of samples is present.

For model validation a step input was selected as reference valve position, rather than the complicated position reference for the FDD purpose.

The step input reference [Figure 9-1] will bypass the controller used in the FDD [Figure 9-2] validation and will act as a direct valve position reference.

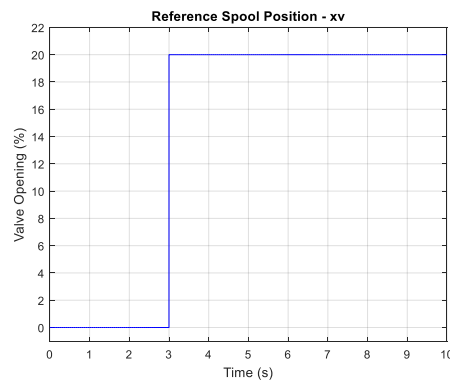


Figure 9-1 xv - reference spool position used in model validation

For the purpose of keeping a system in operational conditions, a simple controller was constructed that prevented the pantograph crane from reaching its maximum and minimum stroke limits and therefore not compromising its structural integrity due to vibrations. A simple proportional controller was made, which took into consideration the current position and the reference position.

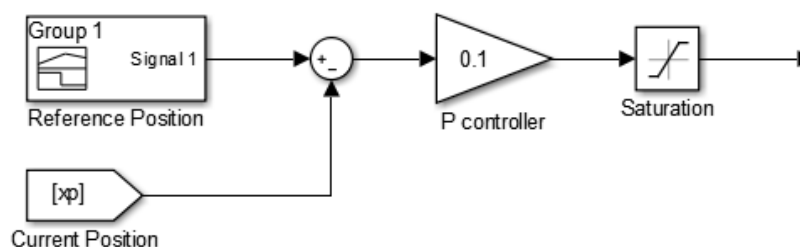
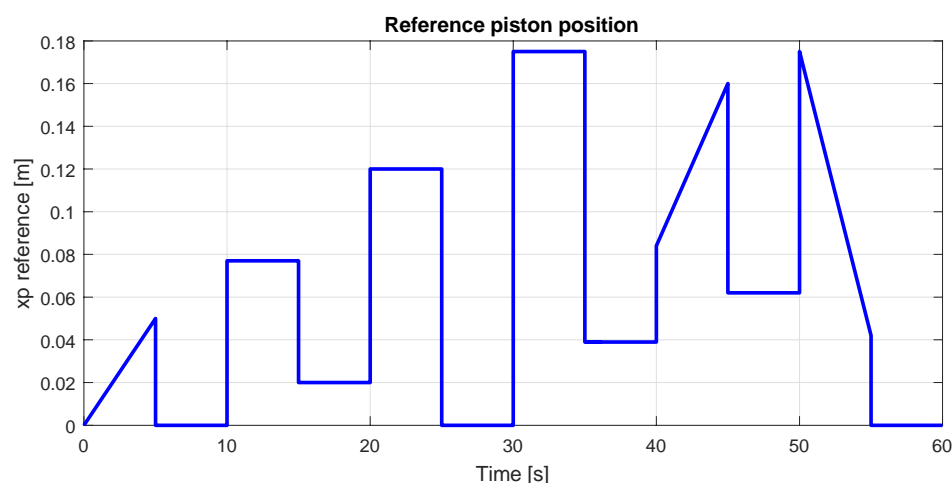


Figure 9-2 Reference piston position - xp - and P controller used for position control

Due to the fact, that the sensors stopped collecting data at different time, the crane was made to stay still for an additional 3 seconds, which were later cut out in order to equal up the samples for each sensor.

Sensors that were used have different accuracies, therefor it is needed to know in which places bigger deviations are to be expected.

Sensor type	Type	Precision	Number Used
Position transducer	Analog	± 1 mm	1
Pressure sensor	Analog	0.5% - 1%	6
Flow meter	Analog	$\pm 2\%$	1
Leak flow meter	Digital	$\pm 0.05\%$	2

Table 9-3 Sensor precision chart

Furthermore, the temperature sensor could not be connected to the setup. Therefor the only temperature reference source was the pump control display. Only a range could be defined on the display, therefor fluctuations within 2 degrees Celsius were present during the experiments.

More information about the experimental setup can be found in Appendix D.

9.2. Experimental EKF results

To test the accuracy of the developed EKF it was necessary to implement the measured data from the laboratory setup into the EKF. Different data sets were implemented. Starting with a non-faulty dataset followed by datasets containing the different artificial leakages 1 and 2. In order to more easily evaluate the residual it was decided to filter the residual signal with a running mean.

To tune the EKF for the real world environment it is necessary to give them a critical K_L coefficient. This means, that it is needed to find a Leakage level of the valve and the piston at which the system does not operate properly anymore, depending on the working requirements of the system.

It was chosen to set the residual threshold at leak level 4. The K_L coefficients were tuned to give a reasonable value at leak Level 4 and Level 5. Figures 9-3 through 9-6 and Table 9-4 show the magnitude of the artificial leakages in different pressure conditions. Leakage Level 4 is shown as the purple colored curve.

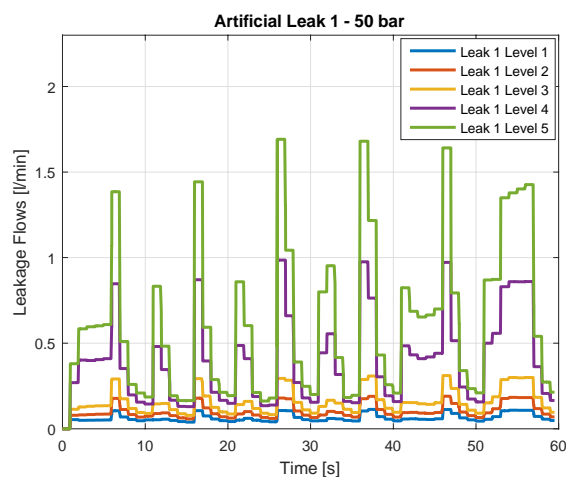


Figure 9-3 Measured external artificial leak through the valve at 50 bar operating pressure and 25°C

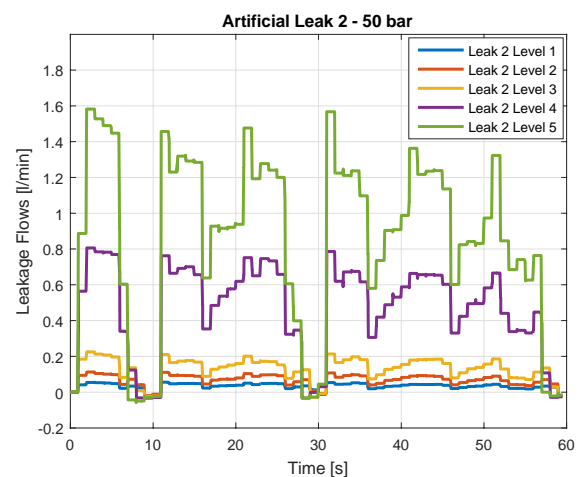


Figure 9-4 Measured internal artificial leak through the cylinder seal at 50 bar operating pressure and 25°C

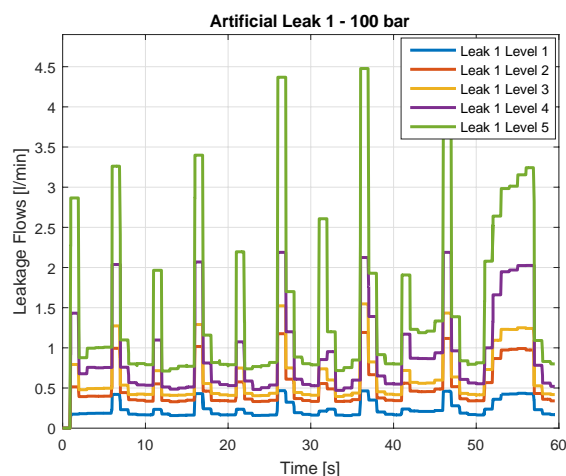


Figure 9-5 Measured external artificial leak through the valve at 100 bar operating pressure and 25°C

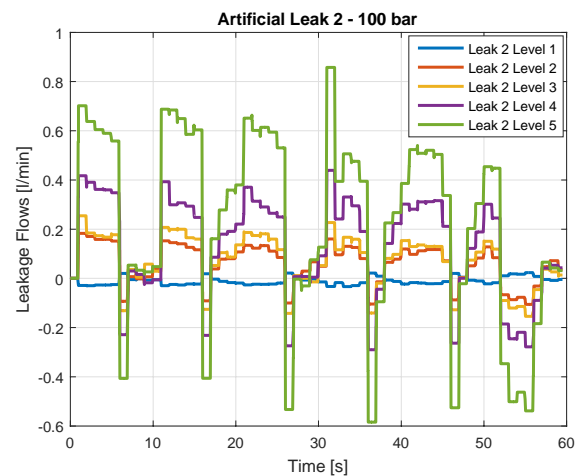


Figure 9-6 Measured internal artificial leak through the cylinder seal at 50 bar operating pressure and 25°C

Leak 1	50bar - 25°C			100bar - 25°C		
	Min [l/min]	Max [l/min]	Mean [l/min]	Min [l/min]	Max [l/min]	Mean [l/min]
Level1	0.0388	0.1133	0.0634	0.157	0.4658	0.2315
Level2	0.0573	0.1894	0.1025	0.3273	1.1905	0.5069
Level3	0.0784	0.3082	0.1589	0.394	1.5463	0.6352
Level4	0.1293	0.9853	0.3973	0.4686	2.1884	0.927
Level5	0.1643	1.692	0.6187	0.7105	4.4762	1.4868

Leak 2	50bar - 25°C			100bar - 25°C		
	Min [l/min]	Max [l/min]	Mean [l/min]	Min [l/min]	Max [l/min]	Mean [l/min]
Level1	5.10E-04	0.0558	0.0341	9.00E-05	0.0334	1.72E-02
Level2	3.75E-04	0.01125	0.0694	3.60E-04	0.1829	0.0903
Level3	9.30E-04	0.2252	1.326	3.00E-05	0.2542	0.1145
Level4	0.0012	0.8062	0.4826	5.70E-04	0.4389	0.216
Level5	3.00E-04	1.5824	0.8779	0.0031	0.8573	0.3895

Table 9-4 Minimum, Maximum and Mean values of Leak 1 and Leak 2 at different levels and input pressures

It was necessary to choose different sets of K_L coefficients to match the operating conditions of 50bar and 100bar supply pressure as well as 25°C and 40°C [Table 9-5].

	50bar	100bar
K_{L1} 25°C	3,12E-11	2,48E-12
K_{L2} 25°C	6,44E-11	6,44E-11
K_{L1} 40°C	3,12E-11	2,48E-12
K_{L2} 40°C	6,44E-11	6,44E-11

Table 9-5 Values of K_L coefficients at different input pressures

To analyze the measurement in all conditions it was not sufficient to take the residual only from p_3 or p_4 or x_p to detect and isolate a leakage [Figures 9-7, 9-8, 9-9]. Analyzing EKF results can also be difficult if multiple residuals have the same or close magnitudes as they proceed through the simulation. In this case statistical analysis can prove to be a useful tool. Multiple popular methods were tried and the best were chosen.

- Root mean square (RMS)
 - it is a statistical tool, which, if applied on the residual would make a data set undergo a square root of the mean of the squares. This method should smooth out the residual, making it easier to analyze and isolate the fault.
- Power/Probability density function (PDF)
 - when applied to the residual, PDF should residual value distribution over the whole simulation. Applying it for each case residual it should be possible to isolate the fault, as it would point out which has its magnitudes closest to the 0.

- Running mean / Moving average
 - is a way to analyze a dataset by making averages of different subsets. It smooths out fluctuations making it easier to analyze the residuals.

Running mean was chosen to be used for residual analysis in further simulations, as it seemed to be visually an easier tool for residual analysis. Furthermore, compared to the PDF, it was still possible to see the behavior of the residual during the simulations, rather than just the numerical distribution of data.

As a solution to this the residuals were designed as a combination of the p_3 residual, the p_4 residual and the x_p residual. The sum of these gave a reasonable solution to the different leakage situations. The following Figure 9-10 shows the average magnitude of the residuals generated by the EKF's.

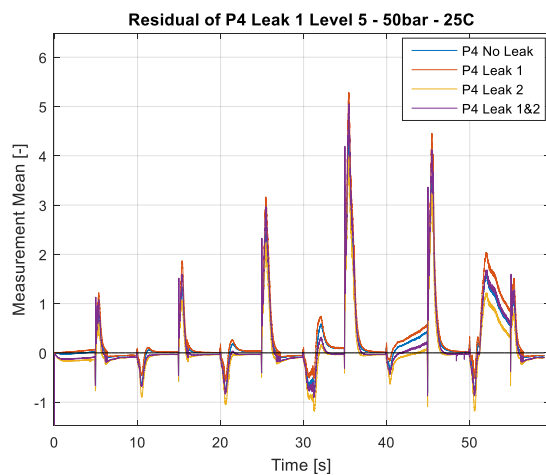


Figure 9-5 p_4 residuals from all EKF's at 50 bar and 25°C operating conditions with artificial Leak 1 Level 5

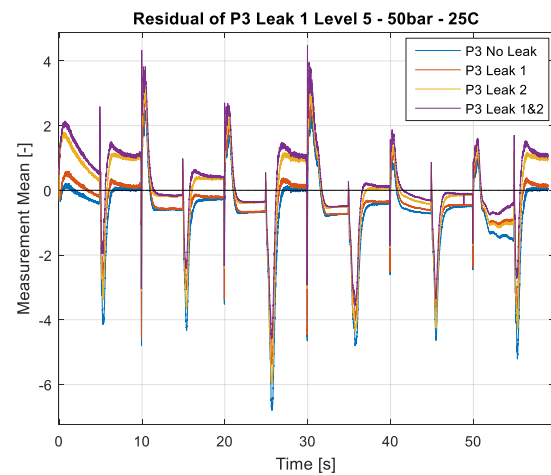


Figure 9-6 p_3 residuals from all EKF's at 50 bar and 25°C operating conditions with artificial Leak 1 Level 5

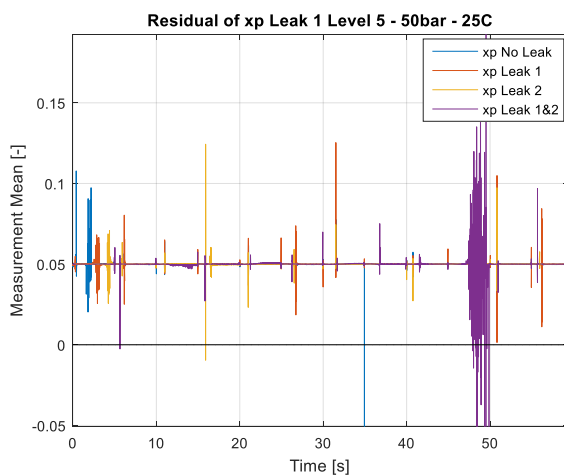


Figure 9-7 x_p residuals from all EKF's at 50 bar and 25°C operating conditions with artificial Leak 1 Level 5

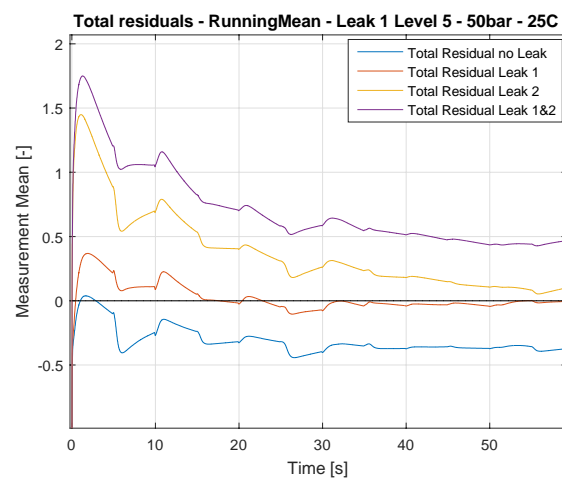


Figure 9-8 Total residuals from all EKF's at 50 bar and 25°C operating conditions with artificial Leak 1 Level 5

9.2.1. 50bar – 25°C

Following the results given in Table 9-6 the smallest residual is marked green. It can be seen, that for Leakage 1 and 2 in Level 4 and 5, the smallest residual is given by the corresponding EKF. Residuals for the Leakage Level 1, 2 and 3 were not good enough. In this case the non-faulty EKF gave the smallest residual which means the system seems to run fault free even when there are small leakages.

In case of a fault free system, the non-faulty EKF residual works as it should. It has the smallest magnitude of all four residuals and indicates a fault free system.

The Fault simulation with Leak 1 and 2 combined shows less promising results. Here it was not possible for the corresponding EKF to give the smallest residual. The residual from the non-faulty EKF had in four cases the lowest magnitude and indicates a running system with no faults, which in this particular case is not true.

K_{L1}	3.12E-11				
K_{L2}	6.44E-11				
50bar	25°C				
		Leak1	Leak2	Leak12	No Leak
EKF Leak 1	Level1	0.7512	0.9328	0.566	0.8808
	Level2	0.717	0.9394	0.5046	
	Level3	0.6659	0.9511	0.474	
	Level4	0.1207	0.7451	0.2966	
	Level5	0.0229	0.7886	0.1478	
EKF Leak 2	Level1	0.502	0.4744	0.4417	0.5262
	Level2	0.5424	0.4749	0.417	
	Level3	0.5742	0.4426	0.3831	
	Level4	0.3707	0.1876	0.313	
	Level5	0.3757	0.1182	0.2126	
EKF Leak 1&2	Level1	1.374	1.476	1.124	1.473
	Level2	1.355	1.492	1.057	
	Level3	1.334	1.487	1.011	
	Level4	0.8084	1.236	0.8185	
	Level5	0.7121	1.267	0.6506	
EKF No Leak	Level1	0.1008	0.069	0.1167	0.0656
	Level2	0.0961	0.0777	0.135	
	Level3	0.0941	0.0934	0.1543	
	Level4	0.3171	0.3031	0.2088	
	Level5	0.3135	0.3604	0.2911	

Table 9-6 Measurement values of the means of the total residuals at different leakages and different EKFs at operating pressure 50 bar and 25°C

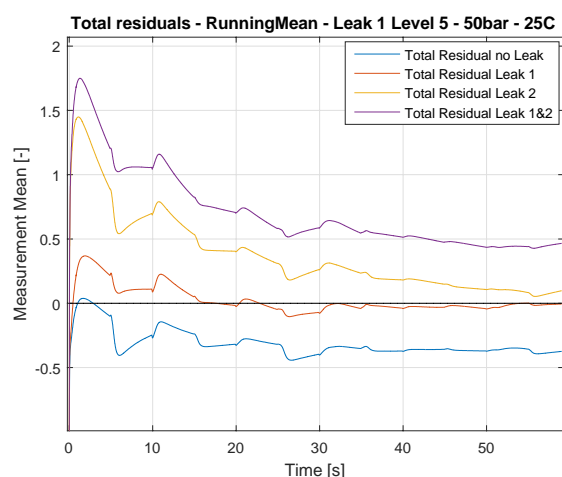


Figure 9-9 Total residuals from all EKF's at 50 bar and 25°C operating conditions with artificial Leak 1 Level 5

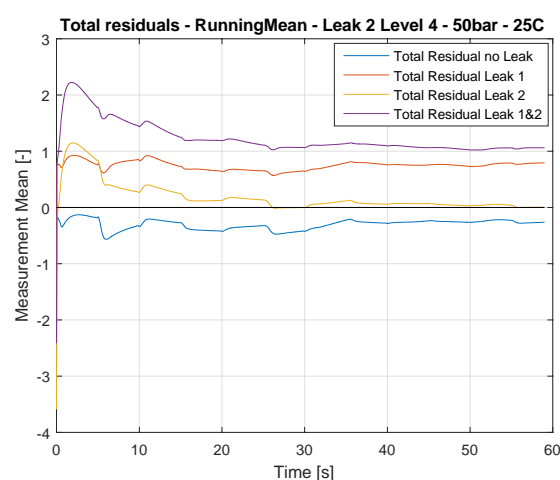


Figure 9-10 Total residuals from all EKF's at 50 bar and 25°C operating conditions with artificial Leak 2 Level 4

In Figure 9-11 and 9-12 the residuals are clearly defined and easy to identify. Depending on the leakage situation the corresponding EKF generates the smallest residual. The other residuals have a bigger deviation from the zero line, which indicates that they work as they should. More graphs related to these conditions can be found in Appendix F-a.

9.2.2. 100 bar – 25°C

Following the results given in Table 9-7, it was possible to detect Leakage 2 Level 2, 4 and 5 with the corresponding EKF. Level 1 and 3 were not possible to detect. In this case it is possible to assume that the leakage for Level 1 is too small and Level 3, due to measurement inconsistencies, is not possible to be detected using the running mean. It can also be seen, that the smallest Level 1 of Leak 1 was detectable as well as Leakage 1 Level 3, 4 and 5. Level 2 was not possible to detect which can be explained with measurement inconsistencies.

The fault simulation with Leak 1 and 2 combined shows less promising results. Here it was not possible for the corresponding EKF to give the smallest residual. The residual from the Leak 2 related EKF had in all five simulation cases the lowest magnitude and indicates a system running with Leak 2 fault. The fact that the residual from the Leak1&2 corresponding EKF shows a very small magnitude in Leakage Level 3, 4 and 5 makes it possible to assume that there is a combination of Leak 1 and Leak 2 present.

K_{L1}	2.48E-12				
K_{L2}	6.44E-11				
100bar	25°C				
		Leak1	Leak2	Leak12	No Leak
EKF Leak 1	Level1	0.0952	0.2286	0.248	0.1963
	Level2	0.1822	0.1109	0.3239	
	Level3	0.1467	0.2309	0.3791	
	Level4	0.1325	0.1458	0.3399	
	Level5	0.1052	0.2382	0.3772	
EKF Leak 2	Level1	0.1271	0.1873	0.123	0.1811
	Level2	0.1783	0.0506	0.0806	
	Level3	0.2241	0.1816	0.0084	
	Level4	0.3427	0.03973	0.0721	
	Level5	0.3755	0.0939	0.031	
EKF Leak 1&2	Level1	0.4046	0.5609	0.3347	0.5482
	Level2	0.3821	0.4253	0.2641	
	Level3	0.4111	0.5553	0.1771	
	Level4	0.4518	0.4271	0.19	
	Level5	0.459	0.5048	0.1203	
EKF No Leak	Level1	0.3734	-0.145	0.4596	0.1709
	Level2	0.3859	-0.2583	0.5073	
	Level3	0.3333	0.1426	0.5476	
	Level4	0.2503	0.2416	0.4577	
	Level5	0.1886	0.1729	0.4787	

Table 9-7 Measurement values of the means of the total residuals at different leakages and different EKFs at operating pressure 100 bar and 25°C

As seen in Figure 9-13 the EKF residual representing the combined leakage with 100 bar supply pressure with both leakages present, is closer to zero after 26 sec. It is possible to assume that there are two leakages at the same time in the system.

On the other hand, Figure 9-14 shows the residuals of the EKFs with implemented Leak 2 Level 5. It is seen, that the residual is closer to the zero line which indicates that Leak 2 is present. More information on that can be found in Appendix F-c.

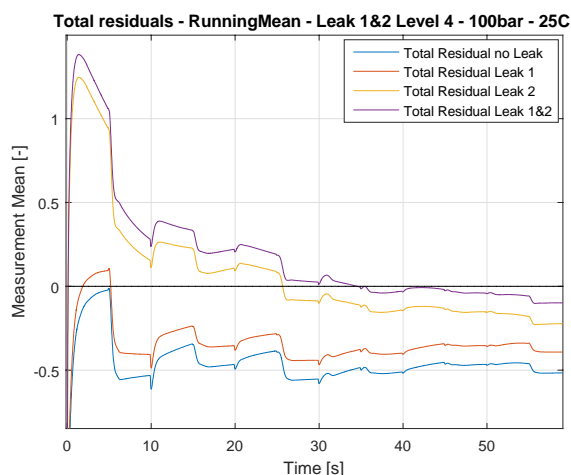


Figure 9-11 Total residuals from all EKFs at 100 bar and 25°C operating conditions with artificial Leak 1&2 Level 4

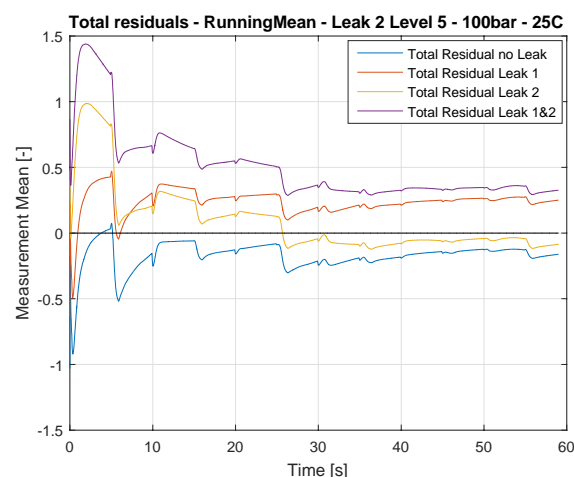


Figure 9-12 Total residuals from all EKFs at 100 bar and 25°C operating conditions with artificial Leak 2 Level 5

9.2.3. 50bar – 40°C

The following Table 9-8 shows the simulation condition with an oil temperature at 40°C and a supply pressure of 50 bar. Leak 1 and Leak 2 were only simulated on Level 4 and 5 to see if it is possible to detect leakage at the threshold of Level 4 even at 40°C and 50 bar supply pressure. It can be seen, that the leakages were not detectable. In both simulation cases the residual from the non-faulty EKF was the smallest.

In the simulation case of a fault free system the EKFs work as they should. The generated residual from the non-faulty EKF shows the smallest magnitude which indicates a running system without fault.

K_{L1}	3.12E-11				
K_{L2}	6.44E-11				
50bar	40°C				
		Leak1	Leak2	Leak12	No Leak
EKF Leak 1	Level1	X	X	X	0.836
	Level2	X	X	X	
	Level3	X	X	X	
	Level4	0.3586	0.8782	X	
	Level5	0.2463	0.8836	X	
EKF Leak 2	Level1	X	X	X	0.4375
	Level2	X	X	X	
	Level3	X	X	X	
	Level4	0.5578	0.3386	X	
	Level5	0.623	0.2407	X	
EKF Leak 1&2	Level1	X	X	X	1.319
	Level2	X	X	X	
	Level3	X	X	X	
	Level4	0.9925	1.364	X	
	Level5	0.9189	1.364	X	
EKF No Leak	Level1	X	X	X	0.0459
	Level2	X	X	X	
	Level3	X	X	X	
	Level4	0.07625	0.1476	X	
	Level5	0.0496	0.2391	X	

Table 9-8 Measurement values of the means of the total residuals at different leakages and different EKFs at operating pressure 50 bar and 40°C

The residuals from the corresponding EKF were always the second smallest. Therefore it can be assumed that the leakage coefficient needs another tuning step in order to match the leakages at 40°C. By evaluating the residual graphs Figure 9-15, which has Leak 2 Level 5 implemented, over the full 59 sec, it is possible to see that the residuals show a reasonable behavior after the 26 sec mark. More graphs can be found in Appendix F-b.

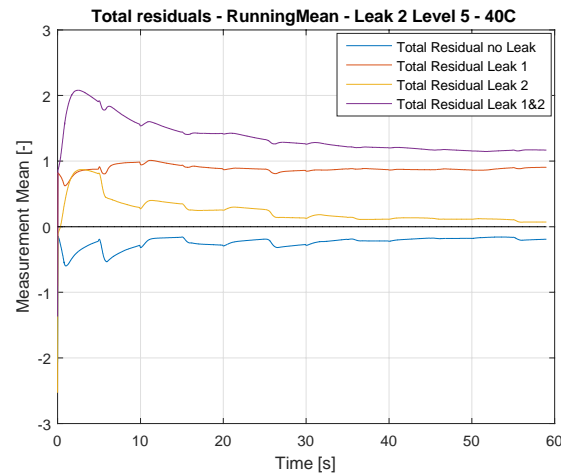


Figure 9-13 Total residuals from all EKFs at 50 bar and 40°C operating conditions with artificial Leak 2 Level 5

Plotting the artificial leakage at 40°C in comparison to the leakage at 25°C in Figure 9-16 and 9-17, it is possible to see, that the amount of leakage differs by roughly 23% or 0.4 l/min at 25 sec. The amount of leakage is smaller in the 40°C situation. This can be explained by the fact that with higher temperature the viscosity of the oil is lower [5] and the oil can flow faster through the pipes and orifices. Due to the faster flow, an increasing Reynolds number appears, and with it a turbulent flow. This will increase the pressure drop needed to create the same amount of leak as with laminar flow, which could explain that the leakages could not be detected with the chosen K_L coefficients.

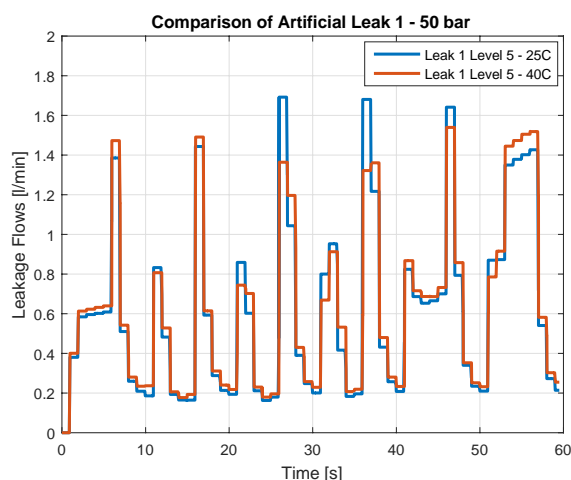


Figure 9-14 Artificial Leak 1 Level 4 comparison between different oil temperatures – 50bar

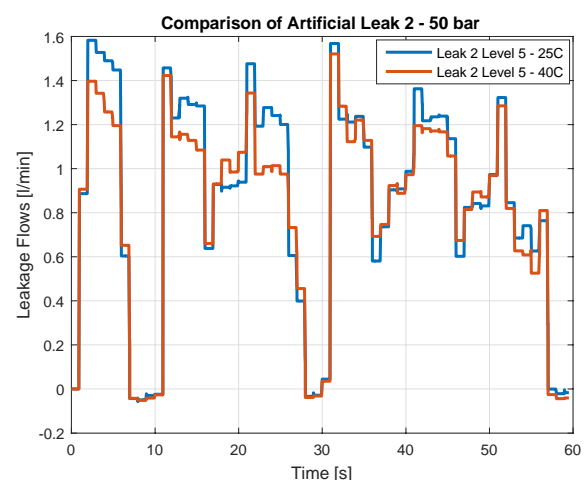


Figure 9-15 Artificial Leak 2 Level 5 comparison between different oil temperatures – 50bar

9.2.4. 100bar – 40°C

Table 9-9, with 100 bar supply pressure and 40°C of oil temperature shows that it was possible to detect Leak 1 Level 4 and 5. Leak 2 was not possible to detect. In this simulation the non-faulty EKF gave the best results. It should be mentioned that the second best residuals were generated by the Leak 2 corresponding EKF.

In the simulation case of a fault free system the EKFs work as they should. The generated residual from the non-faulty EKF shows the smallest magnitude which indicates a running system without fault.

K_{L1}	2.48E-12				
K_{L2}	6.44E-11				
100bar	40°C				
		Leak1	Leak2	Leak12	No Leak
EKF Leak 1	Level1	X	X	X	0.3434
	Level2	X	X	X	
	Level3	X	X	X	
	Level4	0.0688	0.3831	X	
	Level5	0.0585	0.3052	X	
EKF Leak 2	Level1	X	X	X	0.2744
	Level2	X	X	X	
	Level3	X	X	X	
	Level4	0.4144	0.2386	X	
	Level5	0.4507	0.1477	X	
EKF Leak 1&2	Level1	X	X	X	0.6421
	Level2	X	X	X	
	Level3	X	X	X	
	Level4	0.5253	0.632	X	
	Level5	0.5227	0.5631	X	
EKF No Leak	Level1	X	X	X	0.0245
	Level2	X	X	X	
	Level3	X	X	X	
	Level4	0.1796	0.0103	X	
	Level5	0.1312	0.1091	X	

Table 9-9 Measurement values of the means of the total residuals at different leakages and different EKFs at operating pressure 100 bar and 40°C

Figure 9-18 shows the simulation condition with no leak at 40°C and 100 bar supply pressure. Just by looking at the graph it is not possible to say if the system runs fault free or with an artificial Leak 2. By evaluating the mean of the residuals it is easy to say that the system runs fault free. More information can be found in Appendix F-d.

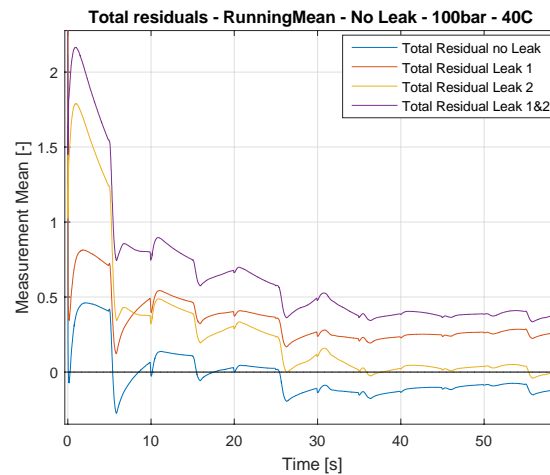


Figure 9-16 Total residuals from all EKF's at 100 bar and 40°C operating conditions with no Leak implemented

Comparing the leakages in 25°C and 40°C at 100 bar it can be seen in Figures 9-19 and 9-20, that Leak 1 has the same size in the beginning but starts to differ at 25 sec and afterwards. The difference is bigger compared to the 50 bar situation and present with a maximum size of 0.75 l/min at 35sec. Leakage 2 shows an opposite behavior. The leakage in 40°C is bigger compared to the colder simulation in 25°C. A difference of 0.5 l/min can be identified at 31 sec. The leakage difference in Leak 2 can explain that the Bank of Kalman filters could not detect the fault.

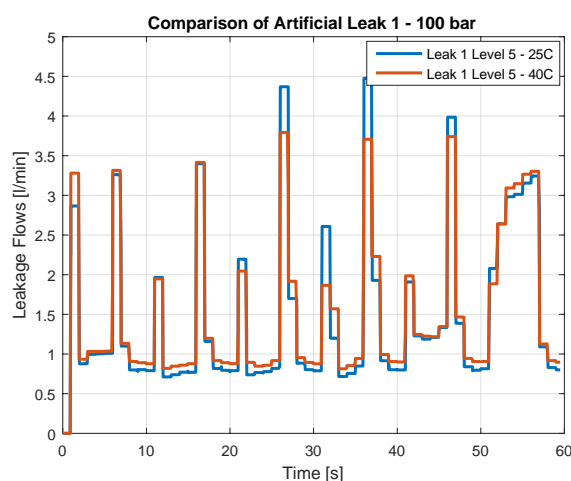


Figure 9-17 Artificial Leak 1 Level 5 comparison between different oil temperatures – 100bar

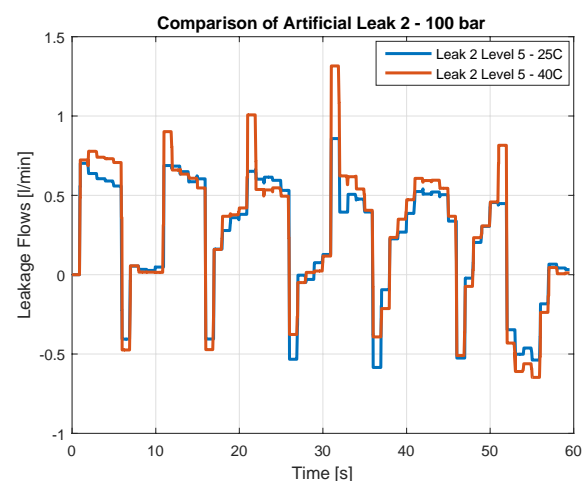


Figure 9-18 Artificial Leak 1 Level 4 comparison between different oil temperatures – 50bar

9.2.5. 50bar – 25°C – Tuned K_L 's

The K_L coefficients were tuned to each leakage level situation in order to see if the accuracy of the Bank of Kalman Filters is good enough to detect even the small leakages. Table 9-10 below shows the tuned K_L values for each leakage level. They were tuned by heuristic methods to get them as suitable as possible.

	Leak1 K_{L1}	Leak2 K_{L2}	Leak1&2 K_{L1} K_{L2}	
Level1	1,20E-12	4,40E-12	1,20E-12	4,40E-12
Level2	2,50E-12	6,10E-12	2,50E-12	6,10E-12
Level3	4,20E-12	8,80E-12	4,20E-12	8,80E-12
Level4	2,23E-11	4,89E-11	1,43E-11	2,31E-11
Level5	3,12E-11	6,44E-11	1,83E-11	3,22E-11

Table 9-10 Tuned K_L values at different Leakages and Leak Levels

		Leak1	Leak2	Leak1&2	NoLeak
EKF Leak 1	Level1	0,0571	0,9617	0,0707	0,8808
	Level2	0,0308	0,9687	0,0837	
	Level3	0,01618	0,9687	0,0697	
	Level4	0,0042	0,7451	0,0229	
	Level5	0,0229	0,7886	0,0877	
EKF Leak 2	Level1	0,5202	0,0318	0,0455	0,5262
	Level2	0,5424	0,0253	0,0826	
	Level3	0,5745	0,00218	0,0809	
	Level4	0,3707	0,0641	0,0216	
	Level5	0,3757	0,1182	0,05936	
EKF Leak 1&2	Level1	0,5652	0,9987	0,0004	1,473
	Level2	0,6074	1,021	0,0314	
	Level3	0,6839	1,044	0,0037	
	Level4	0,7851	1,143	0,2101	
	Level5	0,7121	1,267	0,3559	
EKF No Leak	Level1	0,1008	0,0689	0,1167	0,0656
	Level2	0,096	0,0776	0,135	
	Level3	0,0941	0,0776	0,1535	
	Level4	0,3171	0,3031	0,2088	
	Level5	0,3135	0,3604	0,2088	

Table 9-11 Measurement values of the means of the total residuals at different leakages and different EKFs at operating pressure 50 bar and 25°C – with Tuned K_L 's

Table 9-11 shows the residuals given by the Bank of EKF. It can be seen, that all leakage levels of Leak 1 and Leak 2 were detectable. The combined leakage of Leak 1 and 2 was detectable only in the smaller Level of 1, 2 and 3. The higher Levels did not influence the residuals from the EKF Leak 1&2. By analyzing the other residuals it possible to see, that the residuals from EKF Leak 1 and EKF Leak 2 are very small and close to zero where the residual from the non-faulty EKF show bigger differences. It can be concluded, that Leak 1 and 2 were detected by the corresponding EKF.

9.2.6. Extended Kalman Filter conclusion

The EKF and BEKF proved to be successful in detecting and in the second case isolating the fault depending on the threshold we defined. Due to the nature of the design of the EKFs, the magnitude of the leaks that can be detected was set by defining the leak coefficients in the Jacobian matrix. These non-updating coefficients limited the fault detection capabilities.

Concerning the fault isolation by the bank of EKF, it failed to perform when both leakages are present. This project results, compared to [11] differ, by the inability of our algorithm to detect both leakages at the same time. It can be assumed that this happened due to the different simulation conditions. In M. Choux, (2012) [11], the experiments are conducted under a 3 Hz sine input with amplitude of 1V, while this project uses a step input and a pseudo-random input.

When applying the EKF on the model directly, during the first steady state of the step input the residual converges to zero, while during and after the shift between the steady states the convergence stops and opposite behavior is observed. Thus, it can be assumed, that under the verification of an algorithm with an input of the same constant frequency and magnitude, could prove the algorithm correct when detecting both leakages, in addition to separate ones.

When applying the more random input, on the experimental data directly, it can be concluded that the BEKF performs well with the exception of certain leakage levels and most importantly in the case when both leakages are acting at the same time in the system.

In the case of constantly tuned leakage coefficients, it is not only possible to isolate the faults but also determine them through all the magnitudes [Chapter 9.2.5]. Both leaks can be determined by the separate Leak 1 and Leak 2 EKFs, but not the combined Leak 1 and Leak 2.

10. Spectral analysis based FDD

10.1.Introduction

Spectral analysis is based on Fast Fourier Transformation (FFT) function and is a powerful tool for data analysis and measurement of plug-in data acquisition signals. FFT is a discrete-time transformation with a reduced amount of needed computation [4]. Fourier transformation converts signals from their original domain to the frequency domain and the other way around.

10.2.Fault detection using spectral analysis

By implementing the measured pressure signals into a FTT script, it is possible to see the magnitude of the different frequencies that build up the signal. The chamber pressures p_3 and p_4 were chosen to be analyzed because the leakages will influence them the most.

By comparing the different FFT outcomes, it can be seen, that there are two frequencies that vary according to the leakage size. Both leakages influence the frequencies at 0.1008Hz and 0.2017Hz.

The result of the Leak 1 situation in different levels is seen below. Figure 10-1 shows the spectral density of the chamber pressure p_3 without any artificial leakage compared to p_3 with an artificial Leak 1 in the smallest leak Level 1 and the largest Level 5.

It can be seen, that the magnitudes of 0.1008 and 0.2017 are changing with the artificial Leak 1 present. It is possible to see how much the signal increases in 0.2017 Hz in combination with an increasing leakage level.

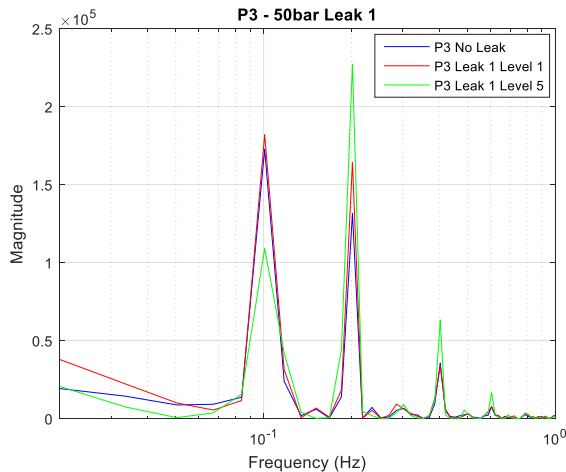


Figure 10-1 Low Frequencies spectrum of p3 with Leak 1 and 50bar input pressure

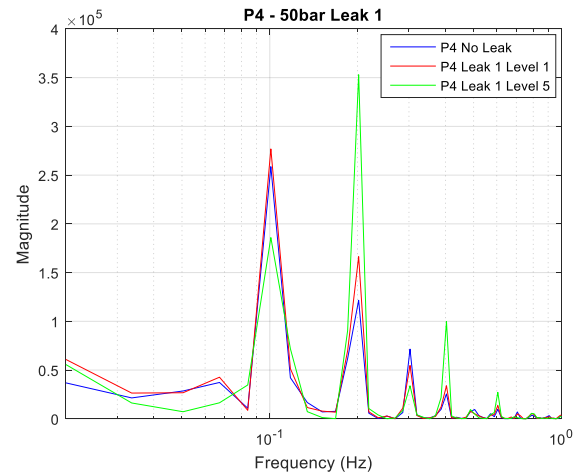


Figure 10-2 Low Frequencies spectrum of p4 with Leak 1 and 50bar input pressure

Compared to the ring side pressure p_4 it is seen that the same behavior occurs there as well. Figure 10-2 shows the spectral density of the ring side chamber pressure without any artificial leakage compared to the artificial simulations. The dominant signal frequencies are as well 0.1008 Hz and 0.2017 Hz.

It is possible to detect the same behavior in an increasing frequency magnitude at both observed frequencies. The growth in magnitude is even bigger compared to the one from the piston side pressure.

The result of the Leak 2 situation in different levels is seen below. Figure 10-3 shows the spectral density of the chamber pressure without any artificial leakage compared to the artificial leakage simulation. The characteristic frequencies are present as well. It shows the spectral density from the piston side pressure p_3 with an artificial Leak 2 in the Levels of 1 and 5. It can be seen, that the frequency component of 0.1008 Hz is increasing a lot more compared to the comparing frequency component of 0.2017 Hz. In Leak Level 5 the difference can be clearly spotted.

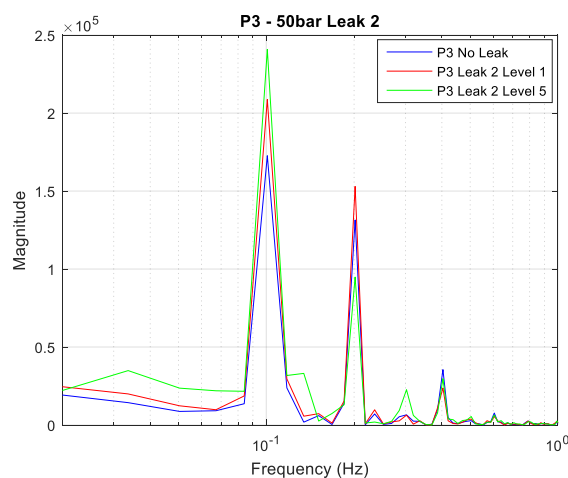


Figure 10-3 Low Frequencies spectrum of p3 with Leak 2 and 50bar input pressure

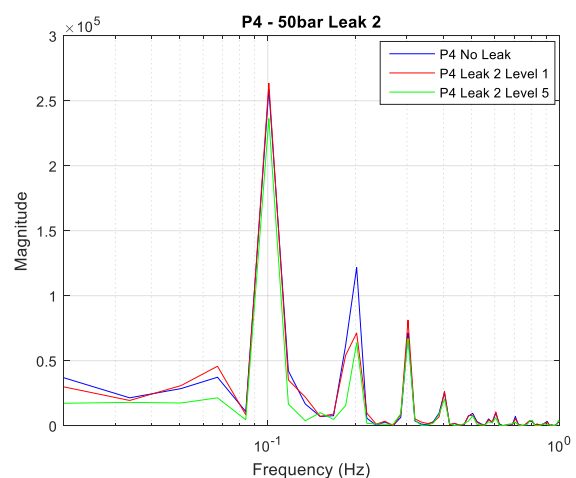


Figure 10-4 Low Frequencies spectrum of p4 with Leak 2 and 50bar input pressure

Analyzing p_4 with an artificial Leak 2 shows kind of the same behavior like p_3 . Figure 10-4 shows p_4 without any artificial leakage compared to the spectral density of p_4 which is manipulated by the artificial Leak 2 in the two different leakage sizes. It is possible to see that the characteristic frequencies of 0.1008 and 0.2017 Hz are increasing with the leakage level.

Plotting the spectral density over the entire power spectrum in dB [Figure 10-5,10-6] gives the possibility to identify a change in frequency power between 10Hz and 1000Hz. The following figures illustrate the decrease of signal power in higher frequencies according to the leakage level. It can be clearly seen, that the higher frequencies are decreasing with a leakage present. Small leakages will not change the spectral density in a big manner; the no leakage curve (blue) is nearly covered by the small leakage curve (red). A big artificial Leak of Level 5 which is represented in the green curve shows a shift to the lower magnitudes.

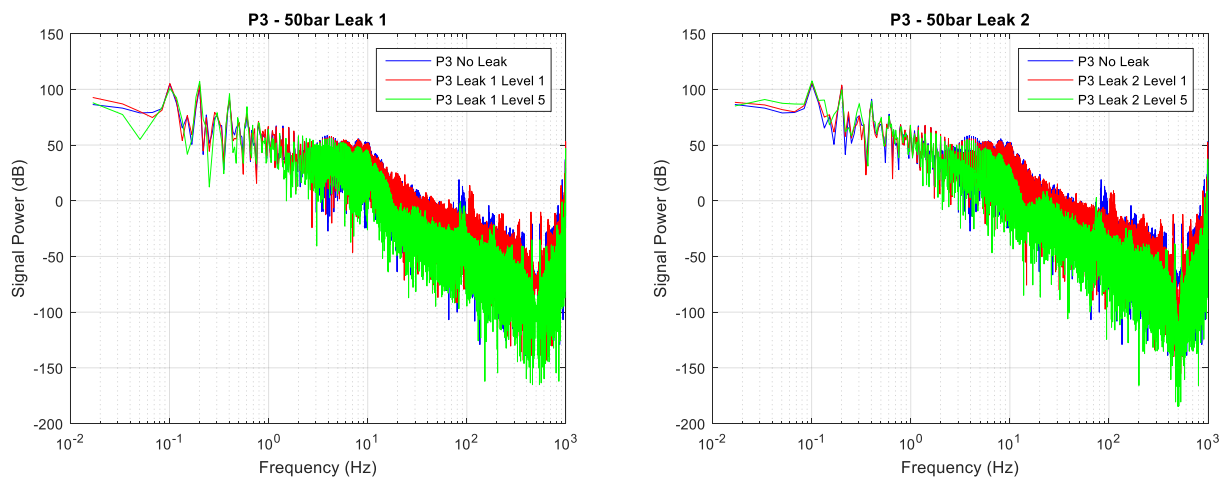


Figure 10-5 Full spectrum of p3 with Leakages 1 and 2 of and 50bar input pressure

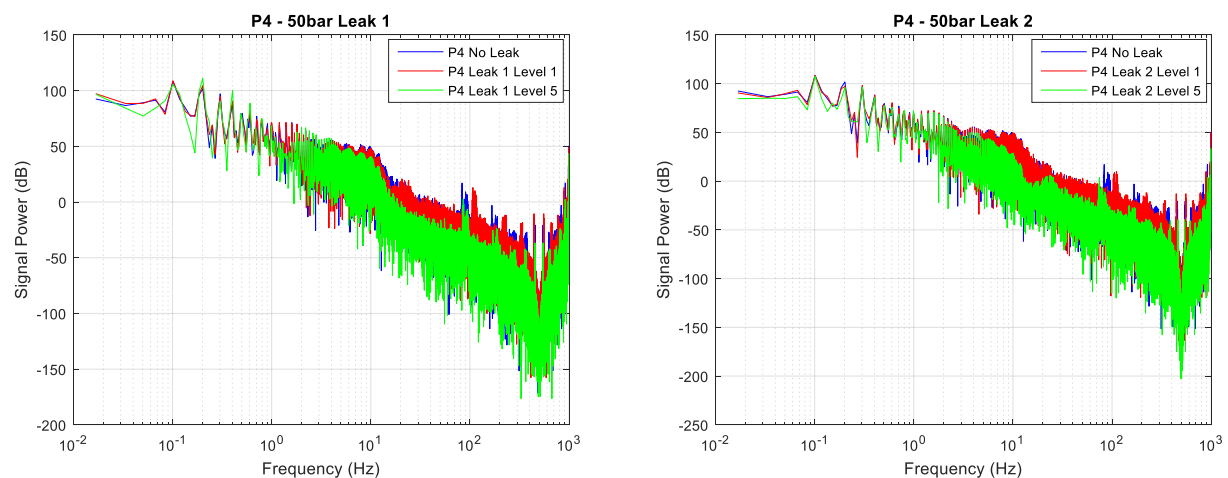


Figure 10-6 -Full spectrum of p4 with Leakages 1 and 2 of and 50bar input pressure

10.3. Residual analysis

After the single EKF has been implemented it was necessary to run the simulation with different settings. Due to the fact, that every leakage changes the residual, multiple simulations were performed. To see the development in the spectral density of each leakage, two different leak levels were simulated. The residuals of p_3 and p_4 were chosen. The artificial leakage has the biggest influence on these states. Spectral analysis was also performed experimentally on the other states but the results were not satisfactory.

Plotting the residual spectral density of the pressures p_3 and p_4 gives the possibility to detect differences in the frequencies. To isolate the fault, it is necessary to analyse the residual of p_3 and p_4 from the single EKF. It can be seen that, during the presence of a fault, the lower frequencies are increasing compared to the non faulty situation.

The graphs below show the behavior of the residual from different simulations. It can be seen, that there are not big changes in the p_3 residual. Figure 10-7 shows the residual comparison of an artificial Leak 1 in Level 1 and Level 5 compared to the non-leakage pressure. It is possible to see that the magnitude of the residual signal is lower over the whole bandwidth. Figure 10-8, which represents an artificial Leak 2 in Level 1 and 5, shows the same behavior. Comparing the two artificial leakage residuals with the normal pressure it is not possible to detect a clear pattern [Figure 10-9].

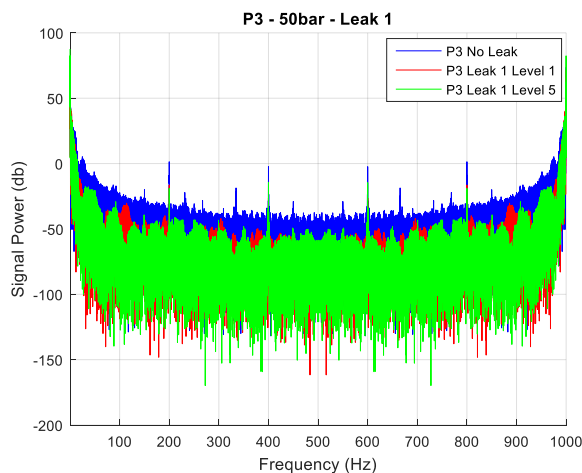


Figure 10-3 Spectral density of p_3 with Leak 1 and input pressure 50bar

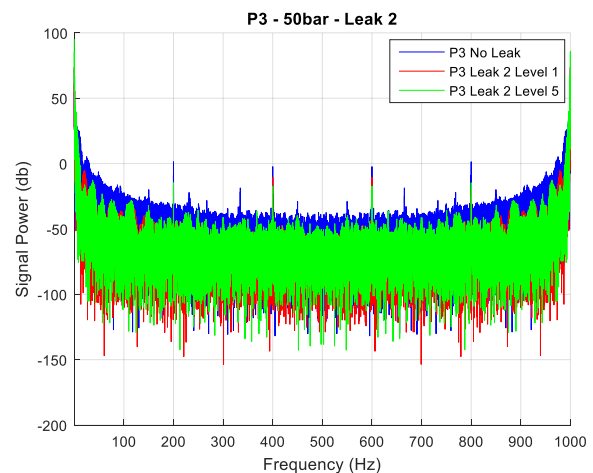


Figure 10-4 Spectral density of p_3 with Leak 2 and input pressure 50bar

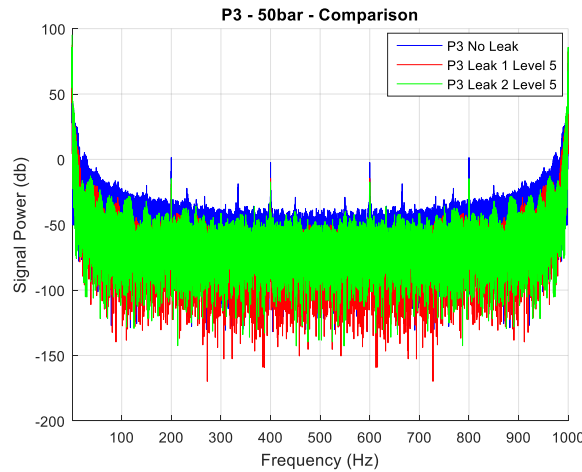


Figure 10-5 Comparison of Spectral density of p3 with Leak 1 and 2 - input pressure 50bar

The evaluation of Figure 10-10 shows that the residuals generated in p_4 with the different leakages behave in a different way. It is possible to remark that the magnitude of the Leak 1 residual is bigger over the whole bandwidth compared to the non-faulty pressure. Leak 1 in Level 1 shows a decrease in fluctuation where Level 5 gives an even more steady behavior between 200 Hz and 850 Hz.

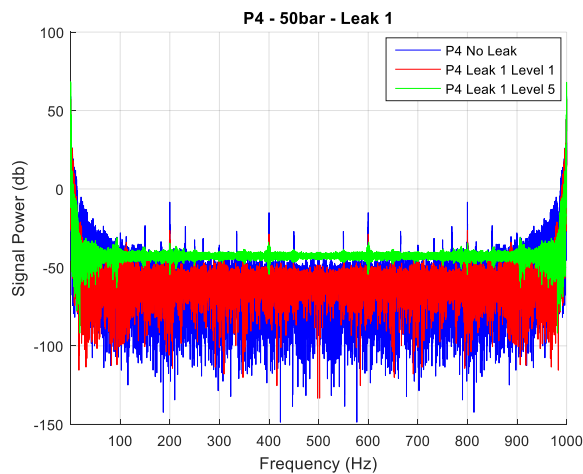


Figure 10-6 Spectral density of p4 with Leak 1 and input pressure 50bar

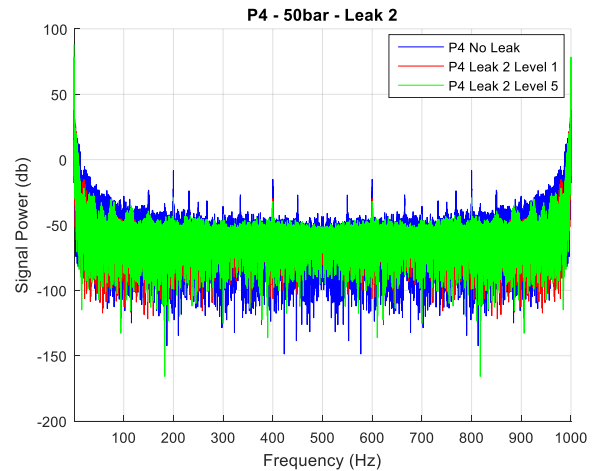


Figure 10-7 Spectral density of p4 with Leak 2 and input pressure 50bar

Leak 2 in Figure 10-11 shows a different pattern. There is not a lot of change in the signal density in leakage situations compared to the non-leakage pressure.

Figure 10-12 shows the comparison of p_4 with Leak 1 and p_4 with Leak 2 to the normal p_4 residual. The difference between Leak 1 and Leak 2 can be seen. As the residual from the EKF detects the Leak it is possible to isolate the fault to Leak 1.

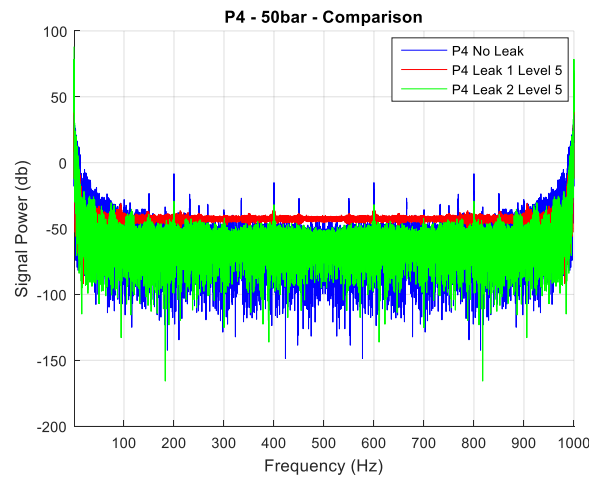


Figure 10-8 Comparison of Spectral density of p_4 with Leak 1 and 2 - input pressure 50bar

The same behavior can be seen with 100 bar supply pressure. The only difference is that p_4 is less accurate compared to p_3 , meaning more fluctuations in frequency density are present in p_4 , especially in the range of 250 Hz to 750 Hz. Leak 1 is better to observe in the p_3 residual which has less fluctuations compared to the non-faulty and Level 1 residual. Figure 10-13 and 10-14 show the comparison between the artificial simulation of Leak 1 and Leak 2 Level 5 in p_3 and p_4 .

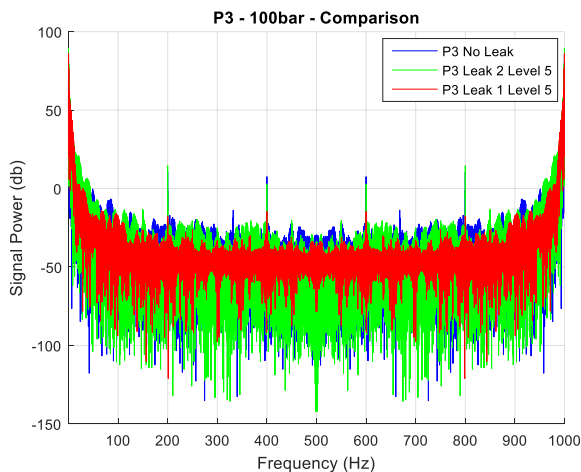


Figure 10-10 Comparison of Spectral density of p_3 with Leak 1 and 2 - input pressure 100bar

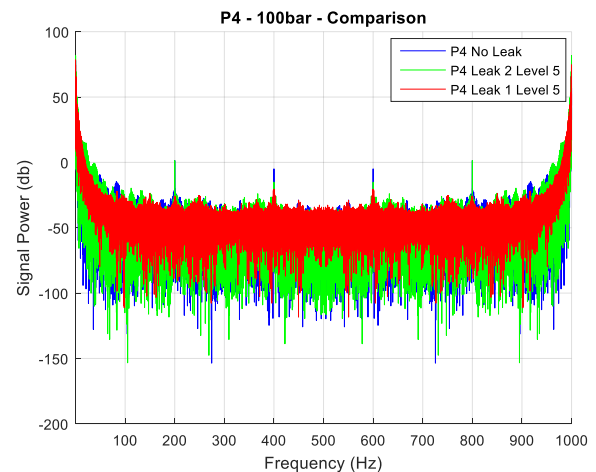


Figure 10-9 Comparison of Spectral density of p_4 with Leak 1 and 2 - input pressure 100bar

10.4. Spectral Analysis conclusion

The experiments show, that the SDA is suitable to detect leakages in the modeled system on its own [Chapter 10-2]. It was chosen to use the SDA as an additional tool to isolate the fault in a detected residual. By the use of the SDA it was possible to isolate the Leak 1 in the residual of the state $x_5(p_3)$ and state $x_6(p_4)$. The big change in higher frequencies makes it possible to detect a different behavior in the system.

One aspect should be considered: SDA would work better in a system, which operates in a cyclic matter, meaning there is not much alteration during the whole operating time. This could be the case if the crane would be running under a sinusoidal input. Having this, would make it easier to identify the natural frequency of the system and thus to interpret the FFT of the signals, both of the direct measurement and as an add-on, to the EKF or other filter.

The stochastic behavior makes the SDA not the first and not the most reliable option, compared to other FDD methods. SDA proves a data distribution, without showing the behavior throughout the whole simulation, for example how the residual does. Thus makes it impossible to see how the convergence goes throughout the whole process.

The last point, the fact that it shows the final data distribution only, gives a good background to use SDA as a side tool for additional, secondary analysis, rather than the primary for hydraulic systems.

11. Comparison of the FDD methods

Due to the fact that the SDA is an offline method and the EKF is an online method it is not possible to compare them directly in terms of application process. The possibility to combine the EKF with the SDA gives the opportunity to convert the online EKF to an offline detection method.

Analyzing the results of the detection methods, it is possible to observe that the EKF shows a more precise residual. By the use of a single EKF it is possible to detect the leakage. By using multiple EKF in a bank it was possible to detect and to isolate the leakage. By tuning of the K_L coefficients the precision can be adjusted accordingly. With further research it will be possible to analyze a relationship between the residual and the leakage size.

The SDA is less powerful in terms of leakage detection in a hydraulic system. By using the SDA method to detect a leakage it was possible to see a difference between Leak 1 and Leak 2 in higher frequencies. Due to the fact, that the operating conditions in the real world are never as stable as the one used in the lab it will be difficult to obtain a clear detection. It will be difficult to obtain characteristic frequencies as reported for a bearing case in [10]. There it was possible to detect certain frequencies by evaluating the fault. This will be more challenging with hydraulics being part of the system. SDA is more a quantitative method. It requires a big amount of analyzed data, to see the behavioral patterns, to later determine and possible isolate the leak. Without this prerequisite SDA will give confusing and hard to interpret results.

Combining the single EKF with the SDA gave the possibility to increase the performance of the EKF. The SDA gave the possibility to separate the Leak 1 from Leak 2 in frequency behavior. It was possible to isolate the leakage. But taking into account, that simple statistical tools, such as the RMS or the running mean give the same results, it gives an amount of uncertainty to whether this more complex method should be utilized.

12. Conclusion

In the introduction, the focus of the project was described to be on modeling the system, which precision would be high enough to be suitable for FDD purposes. The FDD would be focused solely on fault identification and isolation, fault estimation not being a primary objective.

Artificial faults were implemented on the experimental rig and mathematically modeled. In the project, we considered artificial faults of internal and external nature. External include leak across the valve, while internal include leak across the cylinder seal.

The experimental rig consisted of a pantograph crane, which was driven by a hydraulic system. The crane would be lifted by a hydraulic cylinder through one of the lower joints, while the other lower joint was fixed and the crane revolved around it making it a one degree of freedom system.

The modeling part of the project consists of a combination of a mechanical model and a hydraulic model.

The mathematical model of the mechanical system, constructed by the use of the Lagrangian method, proved to be accurate to the extent, where the calculated and the measured trajectories were identical. The load change due to position proved to be accurate enough for FDD purposes, leaving only one minor adjustment that could be made, which is the deeper investigation into the mass and mass moment of inertia of the cranes components. Weights of the bolts and nuts were estimated, while the welds and the paint, which also contributes to it, were taken into account.

The hydraulic system proved to be the hardest to model precision wise. While acceptable accuracy was achieved with the position and flows, the pressures proved to need a deeper analysis. The problem occurred in the transition between lifting and lowering, during the valve shift, when the valve got into the closed position. With further investigation, it was discovered that additional leakages had to be modeled, which were: supply to port to tank, for each side of the valve. Magnitudes of these leakages were chosen so they seem logical and realistic, due to the fact that real magnitudes were not measured. Concerning the accuracy of the modeled pressures, this definitely made a positive impact, but still remains the biggest part to be taken into consideration, if accuracy is to be increased even more. This would involve fine-tuning the leakage coefficients.

The fault detection and diagnosis part of the project consists of implementation of the bank of EKF and further analysis by the use of spectral analysis.

A continuous-discrete Extended Kalman Filter was implemented. It was implemented in a same way that a bank of observers is made. Four EKFs were present in each simulation, each

representing an individual leak, lack of leak or a combination of leaks. Based on these filters a residual was calculated, which is the difference between the predicted and the measured selected states. Summation of the ring, piston pressures and position residuals was used for analysis. Artificial leakages were divided into Levels 1 to 5, depending on their magnitudes. Once a threshold was set, for our EKF's according to the simulation conditions, results that were obtained showed, that it was possible to detect and isolate all leakages at Level 4 (eg. 50bar – 25°C – external Leak: 0.1293 to 0.9853 l/min and internal Leak: 0.0012 to 0.8062 l/min) and above, unless both leakages happen at the same time. When both leaks were implemented, the filter provided confusing results, as different residuals were converging to 0 at the beginning of the simulation, compared to the ones at the end of the simulation.

Separately tuning the leak coefficients allowed to increase the detection performance by adjusting the coefficients for every single threshold. While, this seems to be working, it is unlikely to be implemented in the real world scenario, such that you will not adjust your model every time the operating conditions are changed.

The use of a Spectral Density Analysis (SDA) on the single EKF residual as an addition to isolate the fault turned out to be a successful method to difference between Leak 1 and Leak 2. It was possible to isolate the fault in this way. Isolation of a combined Leakage 1 and 2 was not possible with the use of SDA.

Using SDA as a standalone detection method showed that it was possible to detect a leakage by the change of frequency density in lower and higher frequencies, where in lower frequencies an increasing magnitude is observed and in higher frequencies a decreasing one. To use this detection method alone it is necessary to have a reference of a non-faulty signal to be able to observe changes in frequency density. Furthermore, SDA is usually used for cyclic processes, where as our setup under the inputs that were used proved to be rather stochastic.

Further research

Improvements can be applied on top of the models and algorithms presented in this project, in order to further analyze and possibly achieve greater results.

Discharge coefficient analysis

- Due to the fact that the data sheet for the valve is non-existent and that it might be a one-way assembly, a deeper analysis and more simulations can be conducted concerning valves discharge coefficient.

Leakage coefficients analysis

- Leakage coefficients can be tried to be fine-tuned more, this way increasing the accuracy of the pressure from the mathematical model, which could lead to better FDD results.

Analysis into weight and inertia of the crane

- Taking into account exact mass of bolts, welds and possibly paint, to get an even more accurate load versus piston position curve.

Make an EKF with leakages as states

- Leakages being state estimates, it would be possible to get the exact magnitude of each leak. For this, a new non-linear state space has to be constructed together with a new Jacobian matrix.

Different thresholds

- Different thresholds, such as new ones which would be between the represented level 3 and 4 could set a new bar for the level of leakage that can be identified.

Spectral analysis

- Spectral analysis used to analyze the signals from the sensors could be considered as an alternative, to the residual analysis.

13. References

- [1] Y. Wang. (2015) *Dynamic Modeling and Simulation of Marine Satellite Tracking Antenna Using Lagrange Method*
- [2] H. Goldstein, C. Poole, J. Safko (2002) *Classical Mechanics, 3rd Edition*, Edison - Wesley
- [3] J.P. Corriou (2004) *Process control: Theory and applications*, Springer, page(s) 665-667
- [4] R. Isermann (2006) *Fault-Diagnosis Systems: an introduction from fault detection to fault tolerance*, Springer
- [5] E.C.Fitch, I.T.Hong (2004) *Hydraulic Component Design and Selection*, BarDyne.Inc, page. 29
Figure 2-3
- [6] T.O. Andersen, M.R. Hansen (2007) *Fluid power circuits: system design and analysis*
- [7] L. An, N. Sepehri (2006) *Hydraulic actuator leakage quantification Scheme using extended Kalman filter and sequential test method*
- [8] L. An, N. Sepehri (2005) *Hydraulic Actuator Leakage Fault Detection using Extended Kalman Filter*
- [9] M. Karpenko, N. Sepehri (2005) *Fault-Tolerant Control of a Servohydraulic Positioning System with Crossport Leakage*
- [10] Z. Yang (2015) *Automatic Condition Monitoring of Industrial Rolling-Element Bearings Using Motor's Vibration and Current Analysis*
- [11] M. Choux, I. Tyapin, G. Hovland (2012) *Leakage-Detection in Blade Pitch Control Systems for Wind Turbines*
- [12] J.Liniger, H.C. Pedersen, M.Soltani (2015) *Reliable fluid power pitch systems - a review of state of the art for design and reliability evaluation of fluid power systems*
- [13] D. Lassen, S. T. Pedersen (2014) *Fault detection using unscented Kalman Filters for Wind Turbine Hydraulic Pitch System*, Master Thesis AAU
- [14] L. Schmidt (2014) *Robust Control of Industrial Hydraulic Cylinder Drives - with Special Reference to Sliding Mode- & Finite-Time Control*
- [15] A. C. Valdiero, D. Bavaresco & P. L. Andrighetto (2014) *Experimental Identification of the Dead Zone in Proportional Directional Pneumatic Valves*

[16] B. Armstrong, C.C. de Wit (1995) *Friction Modeling and Compensation, The Control Handbook*, CRC Press

[17] Sketch of a pantograph crane [Online]:

http://www.meccanoindex.co.uk/Mmanuals/Mmodels.php?Srow=40&M_era=22&id=1378594219

[Accessed 02-June-2016]

A. Appendix

$$\theta_1 = 162.5 \cdot xp - 19.99 \quad (\text{A.1})$$

$$\theta_2 = -664.6 \cdot xp^2 + 163.9 \cdot xp + 87.71 \quad (\text{A.2})$$

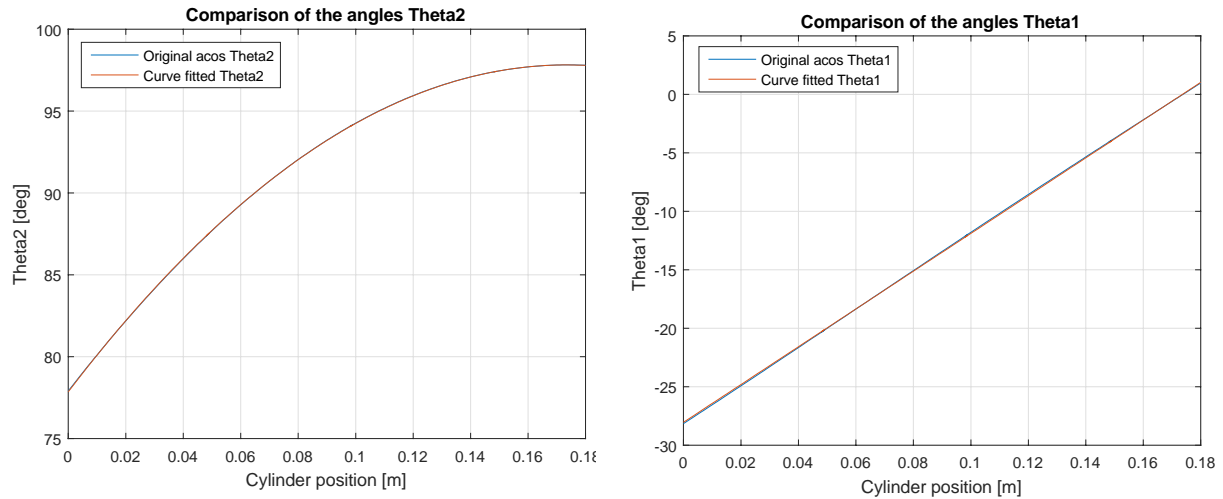


Figure A-1 - Graphs showing comparison between calculated θ and curve fitted

Curve fitting was done as a necessity to get the angular velocity, due to the fact that the derivation of the constraint gave a result with imaginary numbers. Furthermore, the curve fit has reduced the equation size more than 4 times, making it easier to work with. The curve fit equation is represented in terms of the piston position, and when derived, provides angular velocity in terms of the piston velocity.

It is possible to see that our angles go through the 0 and 90 degree angle value. During simulations we can expect not reliable results during these values, due to the gimbal lock effect of the Euler angles.

B. Appendix

Plotting the rod1 vector coordinates in terms of the full stroke of the piston:

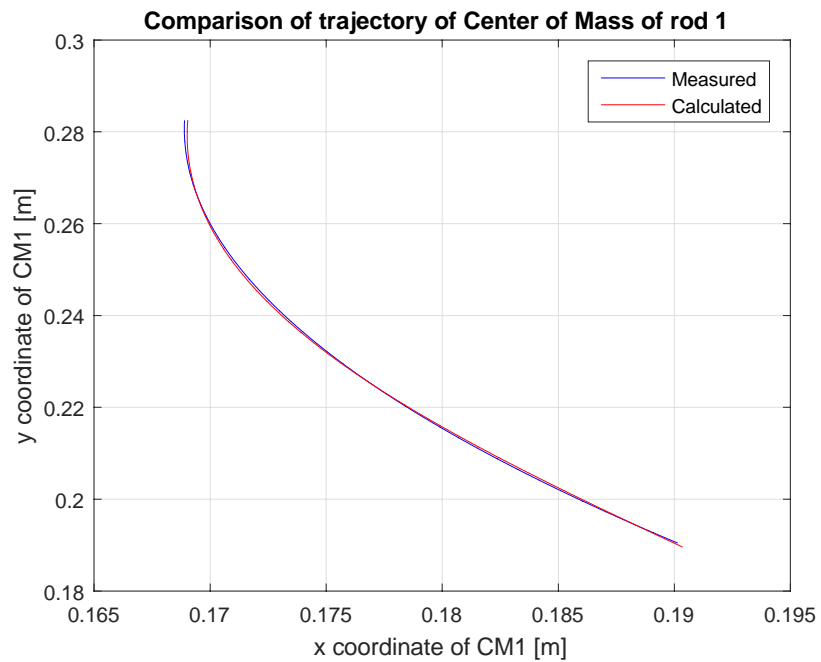


Figure B-1 Comparison between trajectories of centers of masses of rod 1

Plotting the rod3 vector coordinates in terms of the full stroke of the piston:

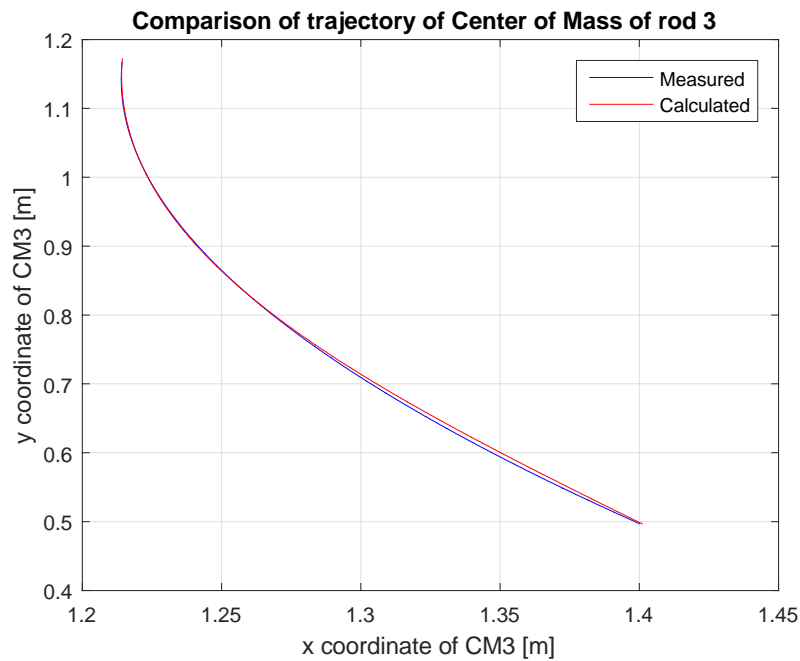


Figure B-2 Comparison of trajectories of centers of mass of rod 3

Plotting the rod21 vector coordinates in terms of the full stroke of the piston:

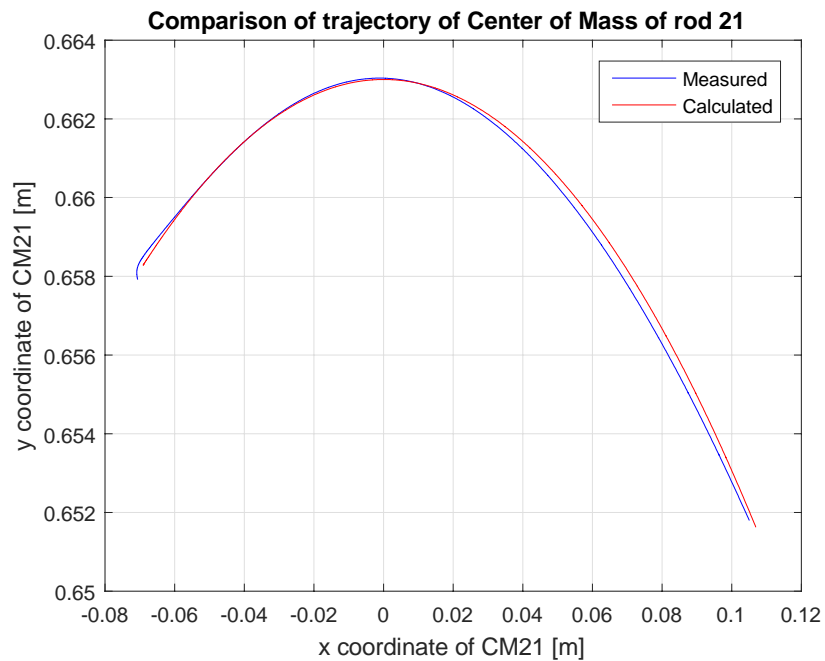


Figure B-3 Comparison of trajectories of centers of mass of rod 21

Plotting the rod22 vector coordinates in terms of the full stroke of the piston:

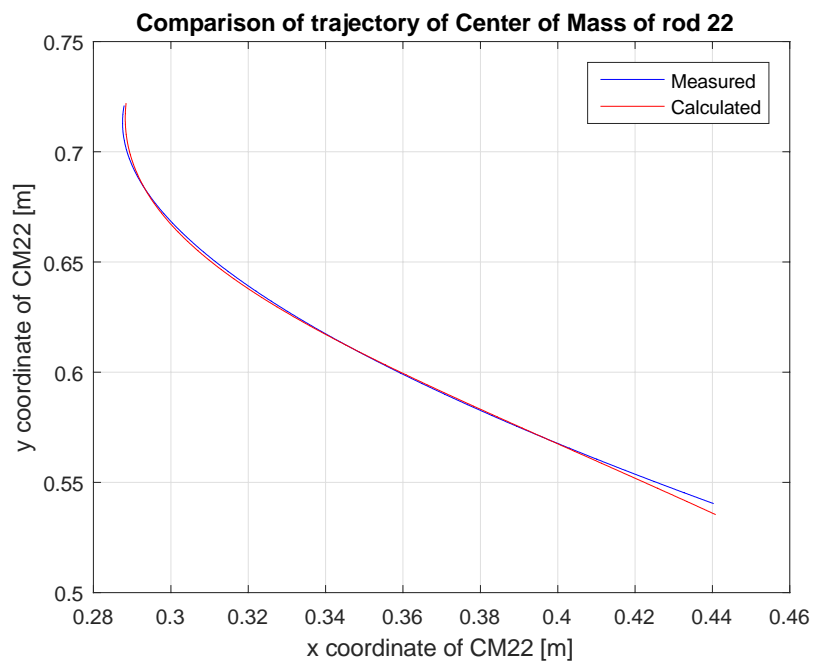


Figure B-4 Comparison of trajectories of centers of mass of rod 22

C. Appendix

- **Alternative mechanical model**

Rod1

Rod1 coordinate shift with angles:

$$x_1 = L_{21} \cdot \cos(\theta_2) + L_{1cg1} \cdot \cos(\theta_1)$$

$$y_1 = L_{21} \cdot \sin(\theta_2) + L_{1cg1} \cdot \sin(\theta_1)$$

Velocity of rod1:

$$V_{r1} = \sqrt{\left(\frac{dy_1}{dt}\right)^2 + \left(\frac{dx_1}{dt}\right)^2}$$

Rotational kinetic energy:

$$TKE_{r1} = \frac{1}{2} \cdot m_{r1} \cdot V_{r1}^2$$

Translational kinetic energy:

$$RKE_{r1} = \frac{1}{2} \cdot I_{n_{r1}} \cdot \frac{d\theta_1}{dt}$$

Potential energy:

$$PE_{r1} = m_{r1} \cdot g \cdot y_1$$

Rod3

Rod3 coordinate shift with angles:

$$x_3 = L_{21} \cdot L_3 \cdot \cos(\theta_2) + L_{3cg3} \cdot \cos(\theta_1)$$

$$y_3 = L_{21} \cdot L_3 \cdot \sin(\theta_2) + L_{3cg3} \cdot \sin(\theta_1)$$

Velocity of rod1:

$$V_{r3} = \sqrt{\left(\frac{dy_2}{dt}\right)^2 + \left(\frac{dx_2}{dt}\right)^2}$$

Rotational kinetic energy:

$$TKE_{r3} = \frac{1}{2} \cdot m_{r3} \cdot V_{r3}^2$$

Translational kinetic energy:

$$RKE_{r3} = \frac{1}{2} \cdot I_{n_{r3}} \cdot \frac{d\theta_1}{dt}$$

Potential energy:

$$PE_{r3} = m_{r3} \cdot g \cdot y_3$$

Rod21

Rod21 coordinate shift with angles:

$$x_{21} = L_{21cg21} \cdot \cos(\theta_2)$$

$$y_{21} = L_{21cg21} \cdot \sin(\theta_2)$$

Velocity of rod1:

$$V_{r21} = \sqrt{\left(\frac{dy_{21}}{dt}\right)^2 + \left(\frac{dx_{21}}{dt}\right)^2}$$

Rotational kinetic energy:

$$TKE_{r21} = \frac{1}{2} \cdot m_{r21} \cdot V_{r21}^2$$

Translational kinetic energy:

$$RKE_{r21} = \frac{1}{2} \cdot I_{n_{r21}} \cdot \frac{d\theta_2}{dt}$$

Potential energy:

$$PE_{r21} = m_{r21} \cdot g \cdot y_{21}$$

Rod22

Rod22 coordinate shift with angles:

$$x_{22} = L_{21} \cdot L_1 \cdot \cos(\theta_2) + L_1 \cdot L_{22} \cdot \cos(\theta_1) + L_{22cg22} \cdot \cos(\theta_2)$$

$$y_{22} = L_{21} \cdot L_1 \cdot \sin(\theta_2) + L_1 \cdot L_{22} \cdot \sin(\theta_1) + L_{22cg22} \cdot \sin(\theta_2)$$

Velocity of rod22:

$$V_{r22} = \sqrt{\left(\frac{dy_{22}}{dt}\right)^2 + \left(\frac{dx_{22}}{dt}\right)^2}$$

Rotational kinetic energy:

$$TKE_{r22} = \frac{1}{2} \cdot m_{r22} \cdot V_{r22}^2$$

Translational kinetic energy:

$$RKE_{r22} = \frac{1}{2} \cdot I_{n_{r22}} \cdot \frac{d\theta_2}{dt}$$

Potential energy:

$$PE_{r22} = m_{r22} \cdot g \cdot y_{22}$$

Lagrangian

$$L = (TKE_{r1} + RKE_{r1} + TKE_{r3} + RKE_{r3} + TKE_{r21} + RKE_{r21} + TKE_{r22} + RKE_{r22}) \\ - (PE_{r1} + PE_{r3} + PE_{r21} + PE_{r22})$$

$$Force = \frac{d}{dt} \left(\frac{dL}{dxp} \right) - \frac{dL}{dxp}$$

Position Transducer: HBM 500 – Inductive displacement transducer

The position transducer was used in collaboration with a Measuring amplifier in desktop housing from the same company: HBM SCOUT55, this allowed us to convert the signal given by the transducer, into measurable voltage signal.

- Amplifiers input: 230 V
- After setting up using the procedure mentioned in the datasheet (the settings for inductive displacement transducer did not work, however the settings for “piezorezistive” transducer did work, so those were used: output 0...1.45 V

• **Pressure sensors (Total number : 6): Danfoss model:**

MBS 3050-3411-1AB04

- Input: 9...34 VDC
- Signal output: 4...20 mA

MBS 30..

Standard	0 0
With pulse-snubber	5 0

Measuring range

0 – 1 bar	10
0 – 1.6 bar	12
0 – 2.5 bar	14
0 – 4 bar	16
0 – 6 bar	18
0 – 10 bar	20
0 – 16 bar	22
0 – 25 bar	24
0 – 40 bar	26
0 – 60 bar	28
0 – 100 bar	30
0 – 160 bar	32
0 – 250 bar	34
0 – 400 bar	36
0 – 600 bar	38

Pressure connection

AB04	G ¼ A (EN 837) (MBS 3000 only)
AB06	G ⅜ A (EN 837) (MBS 3000 only)
AB08	G ½ A (EN 837)
AC04	¼ – 18 NPT
AC08	½ – 14 NPT (MBS 3000 only)
GB04	DIN 3852-E-G ¼, Gasket: DIN 3869-14 NBR
FA09	DIN 3852-E-M14 x 1.5, Gasket: DIN3869-14-NBR (MBS 3050 only)

Electrical connection
Figures refer to plug and standard PIN configuration – see page 5

1	Plug Pg 9 (EN 175301-803-A)
2	* Plug, AMP Econoseal, J Series, male, excl. female plug
3	Screened cable, 2 m
5	* Plug, EN 60947-5-2, M12 x 1; 4-pin; male, excl. female plug
8	* Plug, AMP Superseal 1.5 series male, excl. female plug

Pressure reference

Gauge (relative)	1	1
Absolute	2	2

Output signal

1	4 – 20 mA
2	0 – 5 V
3	1 – 5 V
4	1 – 6 V
5	0 – 10 V
7	1 – 10 V

☐ Preferred versions

*) Gauge versions only available as sealed gauge versions

Performance (EN 60770)

Accuracy (incl. non-linearity, hysteresis and repeatability)		≤ ± 0.5% FS (typ.)
		≤ ± 1% FS (max.)
Non-linearity BFSL (conformity)		≤ ± 0.2% FS
Hysteresis and repeatability		≤ ± 0.1% FS
Thermal zero point shift		≤ ± 0.1% FS / 10K (typ.)
		≤ ± 0.2% FS / 10K (max.)
Thermal sensitivity (span) shift		≤ ± 0.1% FS / 10K (typ.)
		≤ ± 0.2% FS / 10K (max.)
Response time	Liquids with viscosity < 100 cSt	< 4 ms
	Air and gases (MBS 3050)	< 35 ms
Overload pressure (static)		6 × FS (max. 1500 bar)
Burst pressure		6 × FS (max. 2000 bar)
Durability, P: 10 – 90% FS		> 10 × 10 ⁶ cycles

Reference: Pressure sensor: Danfoss MBS 3050

<http://products.danfoss.com/productrange/documents/industrialautomation/pressure-transmitters/mbs-3050-compact-pressure-transmitters-with-pulse-snubber/> [Accesed 04-June-2016]

- **Flow sensor: Parker SCQ -60l/min to 60l/min**
- Input: 7...12VDC
- Signal output: -3...0...3 VDC

Technical data

Type	SCQ-060	SCQ-150
Flow range Q_N	-60...+60 l/min	-150...+150 l/min
Q_{max}	-66...+66 l/min	-165...+165 l/min
Media connection	M24 (NG10)	M42 (NG16)
Weight (g)	670	1,050

Accuracy	
Deviation from characteristic curve	± 2 % FS @ 46cSt.
Response time	2 ms
Thermal drift	± 0.05 % FS*/°C
Repeat accuracy	± 0.5 % FS*
Resistance to pressure	
Pressure range	3...420 bar
Operating pressure P_N	315 bar
Overload pressure P_{max}	420 bar
Pressure drop ΔP (bar) @ (FS*)	see diagram
Material	
Housing	Steel
Seal	NBR
Parts in contact with media	Steel, NBR
Type of protection	IP54 EN 60529
* FS = Full Scale (measuring range end value)	

Ambient conditions	
Ambient temperature (°C)	+10...+60
Storage temperature (°C)	-20...80
Media temperature (°C)	+80
Filtration	25 μ m
Viscosity range	15...100 cSt.
Electrical connection to handheld measuring device	
Plug connection	5 pin, push-pull
Electromagnetic compatibility	
Interference emissions	EN 61000-6-3
Interference resistance	EN 61000-6-2

Reference: Flow sensor: Parker SCQ -60l/min to 60l/min

<http://www.parker.com/literature/Tube%20Fittings%20Division%20Europe/New/CAT-4054-3-UK.pdf> [Accessed 04-June-2016]

• Technical specifications VSI 0.02 / IPF – VSI 4 / IPF

Size	Measuring range l/min	Frequency Hz	Pulse value cm ³ /pulse	R-factor pulse/litre
VSI 0.02	0.002 ... 2	1.667 * IPF ... 1666.67 * IPF	0.02 / IPF	50 000 * IPF
VSI 0.04	0.004 ... 4	1.667 * IPF ... 1666.67 * IPF	0.04 / IPF	25 000 * IPF
VSI 0.1	0.01 ... 10	1.667 * IPF ... 1666.67 * IPF	0.1 / IPF	10 000 * IPF
VSI 0.2	0.02 ... 18	1.667 * IPF ... 1500.00 * IPF	0.2 / IPF	5 000 * IPF
VSI 0.4	0.03 ... 40	1.250 * IPF ... 1666.67 * IPF	0.4 / IPF	2 500 * IPF
VSI 1	0.05 ... 80	0.833 * IPF ... 1333.33 * IPF	1 / IPF	1 000 * IPF
VSI 2	0.1 ... 120	0.833 * IPF ... 1000.00 * IPF	2 / IPF	500 * IPF
VSI 4	1.0 ... 250	4.167 * IPF ... 1041.67 * IPF	4 / IPF	250 * IPF

Adjustable interpolation factors IPF: 1; 2; 3; 4; 5; 8; 10; 12; 16

Measurement accuracy	: up to 0.3 % of measurement value (with viscosity > 20mm ² /s)	
Repetition accuracy	: ± 0.05 % under the same operating conditions	
Material	: Cast iron EN-GJS-400-15 (EN 1563) or stainless steel 1.4305	
Meter bearing	: Ball bearings or steel plain bearings (medium-dependent)	
Seals	: FPM (standard), NBR, PTFE or EPDM	
Max. operating pressure	Cast iron EN-GJS-400-15 (EN 1563)	315 bar
	stainless steel 1.4305	450 bar
Medium temperature	: -40 ... +120°C (-40 °F ... 248 °F)	
Ambient temperature	: -20 ... +50°C (-4 °F ... 122 °F)	
Viscosity range	: 1 ... 100 000 mm ² /s	
Installation position	: any	
Flow direction	: any	
Running noise	: max. 72 db(A)	
Power supply version	: 10 to 30 volts/DC	
Pulse output	: 3 current limiting and short-circuit-proof high-level stages low signal: 0 = GND; high signal: 1 = U _b -1	
Channel offset	: 90° ± 30° max.	
Pulse-width repetition rate	: 1/1 ± 15° max.	
Pre-amplifier housing	: Aluminium	
Protection type	: IP 65	

Reference: Leak Flow sensor: VSE High definition flow meter model

<http://www.vse-flow.com/downloads-en.html#technical-documents> [Accessed 04-June-2016]

Because of the fact that the Voltage going into the I/O card was recommended to be kept at a maximum of 12V, it was required to reduce the output signal from the leakage flow valve from a maximum of 28 V to a value which would accommodate the card requirements.

Using a resistive divider as seen in [Figure C.1] and the formula listed below, the voltage was reduced significantly.

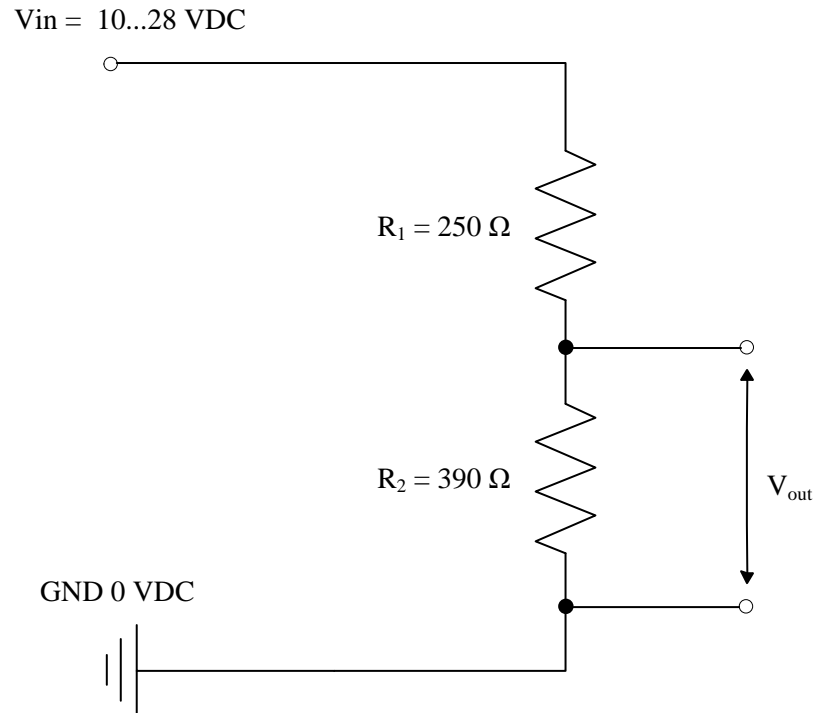


Figure D-1 Electrical diagram of a voltage divider

$$V_{out} = 10 \dots 28 \text{ VDC} = V_{in} \frac{R_2}{R_1 + R_2} \rightarrow$$

$$V_{in} \approx 3.9 \dots 10.9 \text{ VDC} \quad (D.1)$$

- **Directional Control valve: MOOG Direct drive servo valve**

Model: D633-313A

Type designation: R16KO1M0NSM2

- Input supply signal: 18...32 VDC
- Input command signal: -10...10 VDC
- Signal output: 4...20 mA

Model-Number		Type designation	
D 63			

Series		Supply voltage	
3	Size 03	2 24 VDC (19 to 32 VDC)	
4	Size 05		

Specification-Status		Signals for 100% spool stroke*	
-	Series specification	Command	Output
E	Preseries specification	M ± 10 VDC	+4 to +20 mA
K	explosion proof version upon request	X ± 10 mA, floating	+4 to +20 mA deadband compensation on request
Z	Special specification		

Model designation		Valve connector	
assigned at the factory		S 6+PE pole EN 175201 Part 804	

Factory Identification		Seal material	
		N NBR (Buna)	
		V FPM	
		others on request	

Valve version		Y- port	
R with integrated electronics		0 closed with plug $P_{Tmax} = 50$ bar (715 psi)	
		3 open, with filter insert $p > 50$ bar (715 psi)	

Rated flow			
	Q_N [l/min] at $\Delta p_N = 35$ bar	$\Delta p_N = 5$ bar per land	Series
	$(Q_N$ [gpm] at $\Delta p_N = 500$ psi)		
02	5 (1.3)	2	D633
04	10 (2.6)	4	D633
08	20 (5.3)	8	D633
16	40 (10.6)	16	D633
24	60 (15.8)	24	D634
40	100 (26.3)	40	D634

Maximum operating pressure	
K	350 bar (5000 psi)

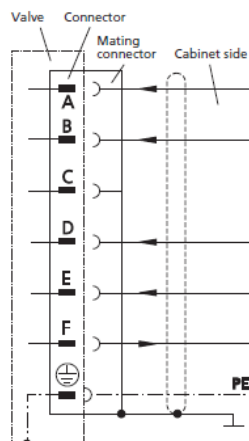
Spool position without electric supply	
M	mid position
F	P \blacktriangleright B, A \blacktriangleright T connected (10% open)
D	P \blacktriangleright A, B \blacktriangleright T connected (10% open)
	other openings on request

Linear motor		Series
1	Standard	D633
2	Standard	D634

Bushing / Spool type	
O	4-way: axis cut, linear characteristic
A	4-way: 1,5 to 3% overlap, linear characteristic
D	4-way: 10% overlap, linear characteristic
Z	2x2-way: P \blacktriangleright A, B \blacktriangleright T, with Y-port only
X	Special spool on request

Options may increase price and delivery.
All combinations may not be available.
Preferred configurations are highlighted.
Technical changes are reserved.

*(input voltage limited, see page 6)

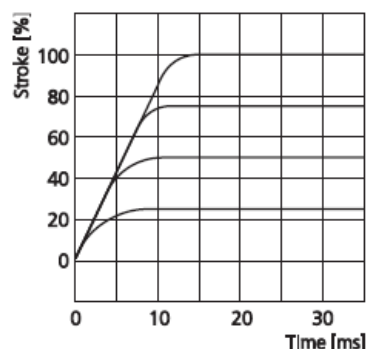


Function	Current command 0 to ± 10 mA floating	Voltage command 0 to ± 10 VDC
Supply	24 VDC (19 to 32 VDC)	
Supply / Signal ground	\perp (0 V)	
not used		
Input rated command (differential)	Input command $I_0 = -I_1$; 0 to ± 10 mA Input command (inv.) $I_2 = -I_3$; 0 to ± 10 mA ($R_e = 200$ K Ω)	$U_{0-3} = 0$ bis ± 10 V $R_e = 10$ K Ω
Output actual valve spool position	$I_{0-3} = 4$ to 20 mA. At 12 mA spool is in centred position, $R_i = 300$ to 500 Ω	
Protective earth		

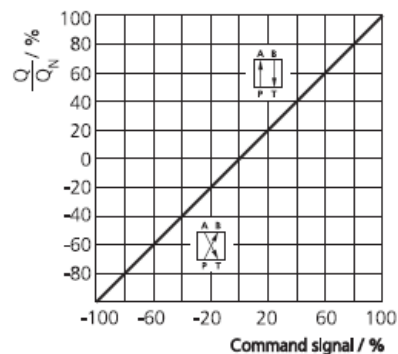
¹⁾ formerly DIN 43563

CHARACTERISTIC CURVES (TYPICAL)

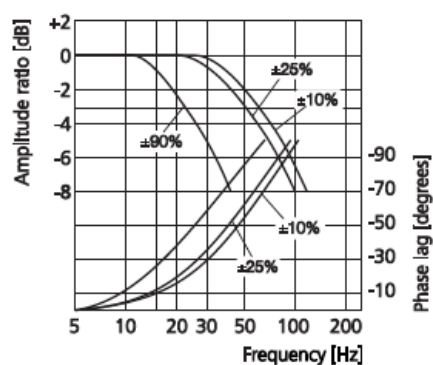
Step response



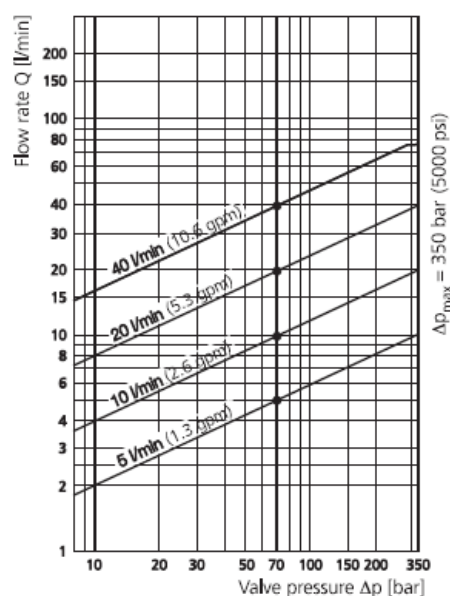
Flow signal characteristic curve



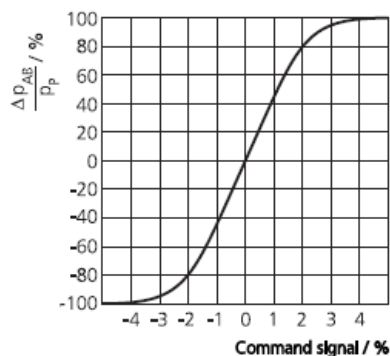
Frequency response



Valve flow diagram



Pressure signal characteristic curve



Reference: Directional Control valve: MOOG Direct drive servo valve

http://www.moog.com/literature/ICD/Moog-Valves-D633_D634-Catalog-en.pdf [Accessed 04-June-2016]

- **National Instruments I/O card model: NI 6229**

- 32 analog inputs
- 4 analog outputs
- 48 digital inputs/outputs which can be used as counters

The data acquisition PCI card can receive analog input signals from the sensors only in Voltage. It can be seen from the previous mentioned technical data that some of the sensors analog signal output is measured in Ampere (current signal).

In this case we have converted the signal which generally was from 4...20 mA, to a Voltage signal with the range of 1...5V using a 250 ohm resistor in the following manner, using Ohms law:

$$1 \dots 5V = 250\Omega \cdot (4 \dots 20)e - 3 A \quad (D.2)$$

Applying this physically on the setup would change the regular sensor output wires in such a manner:

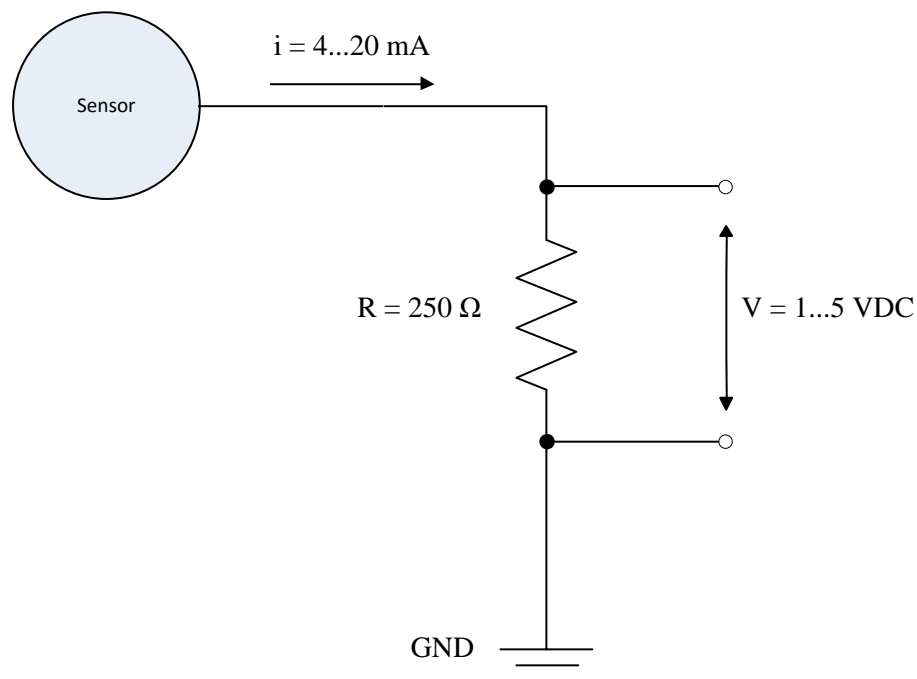
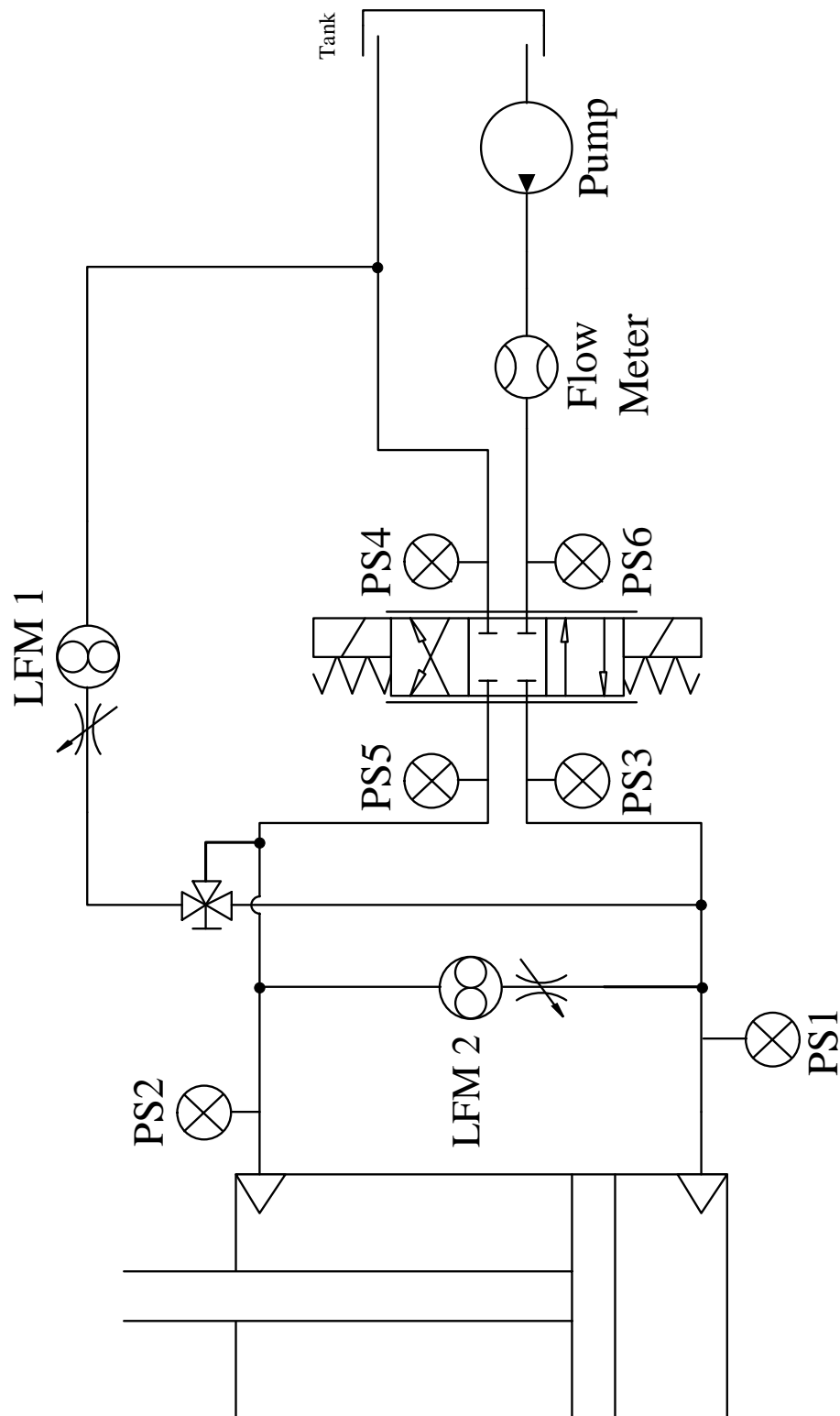


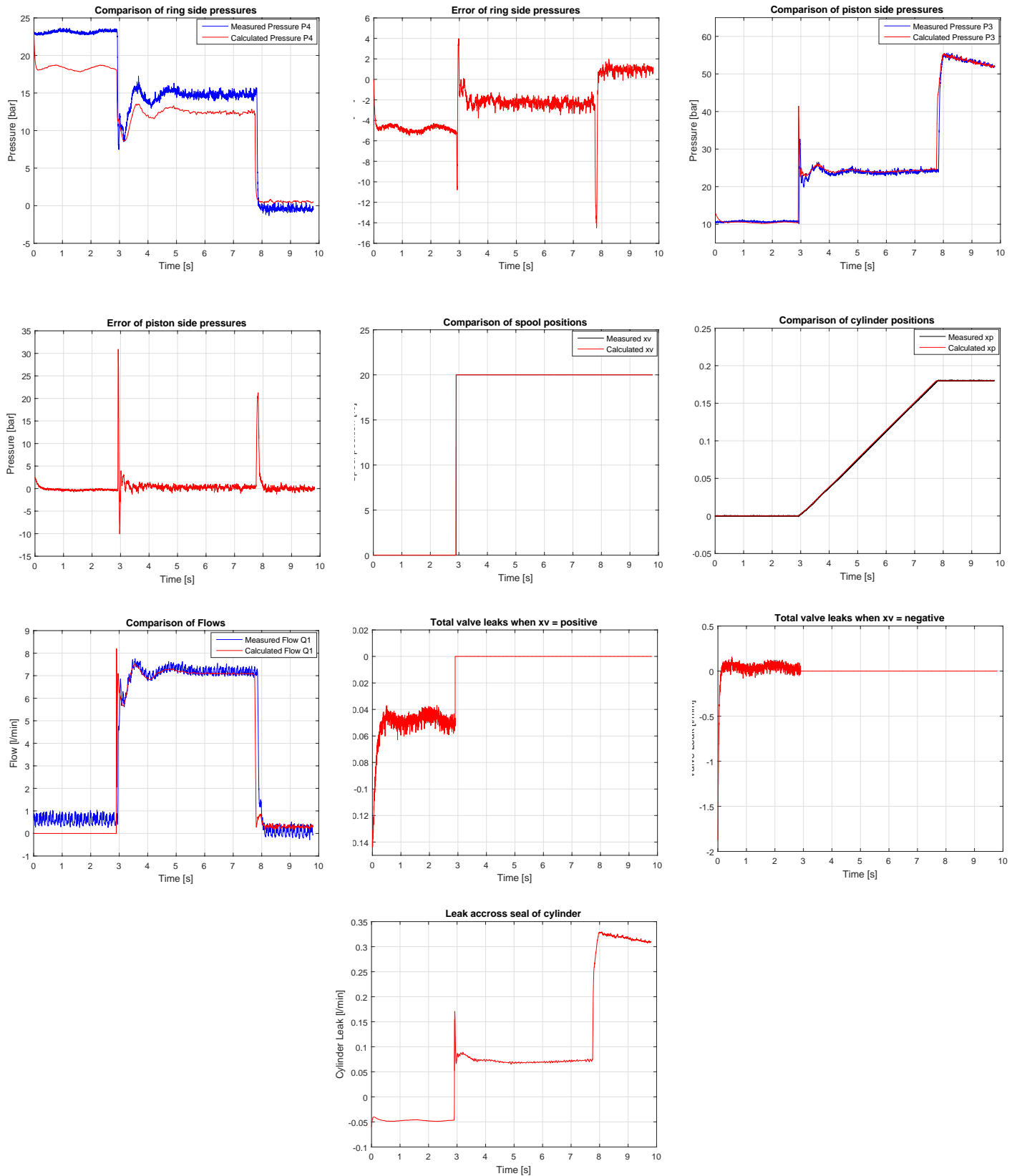
Figure D-2 Electrical diagram of signal conversion

- Hydraulic diagram of the setup used in the laboratory, with the proper notations used, similar to the ones in the database.



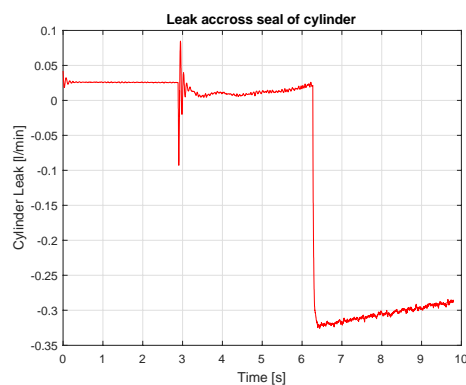
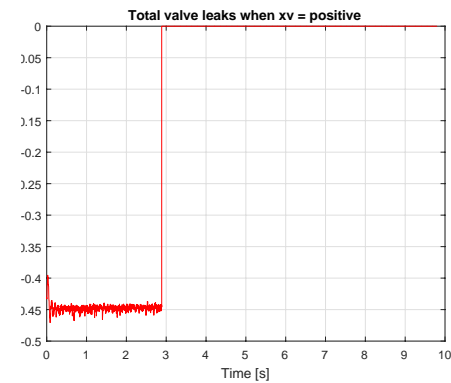
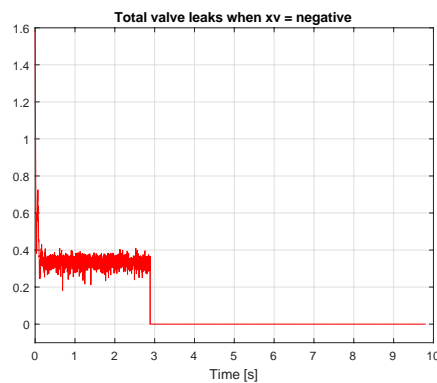
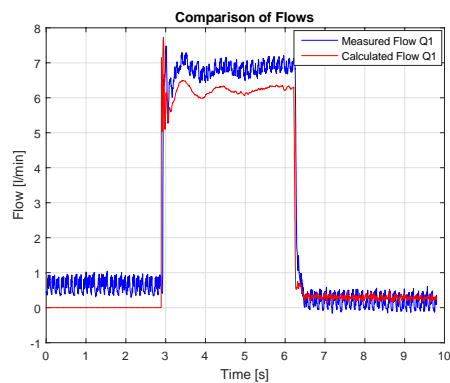
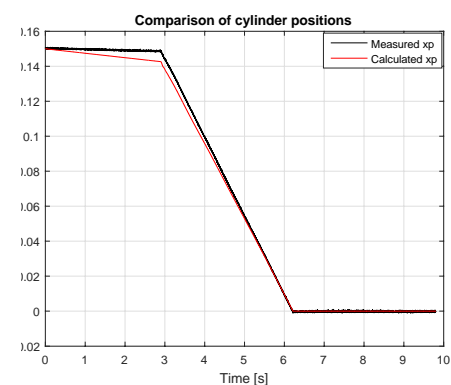
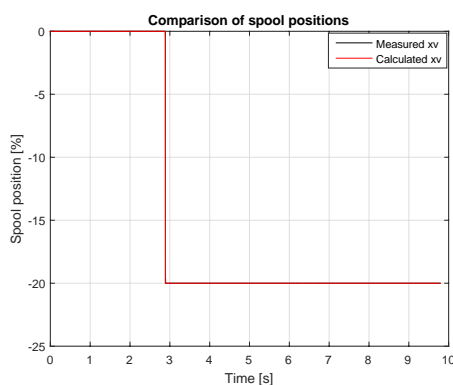
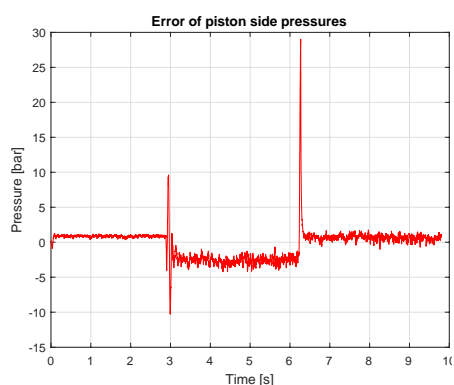
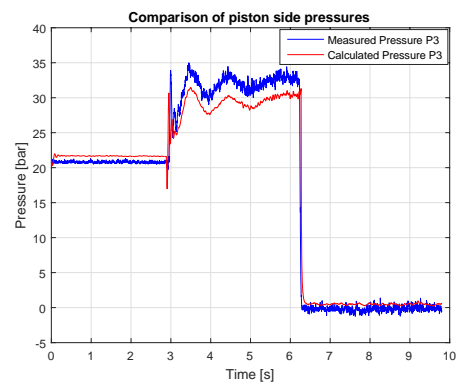
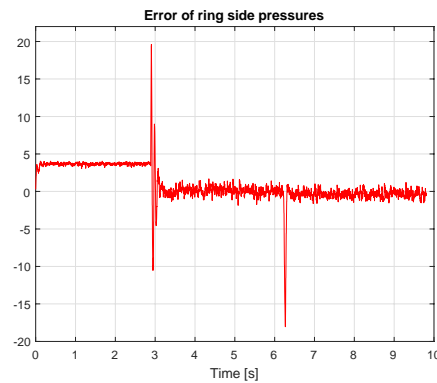
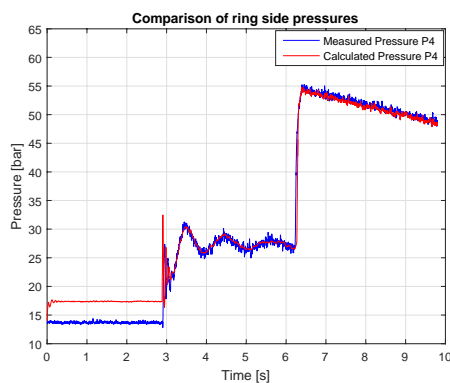
E. Appendix

a. Step input 20%, 50 bar

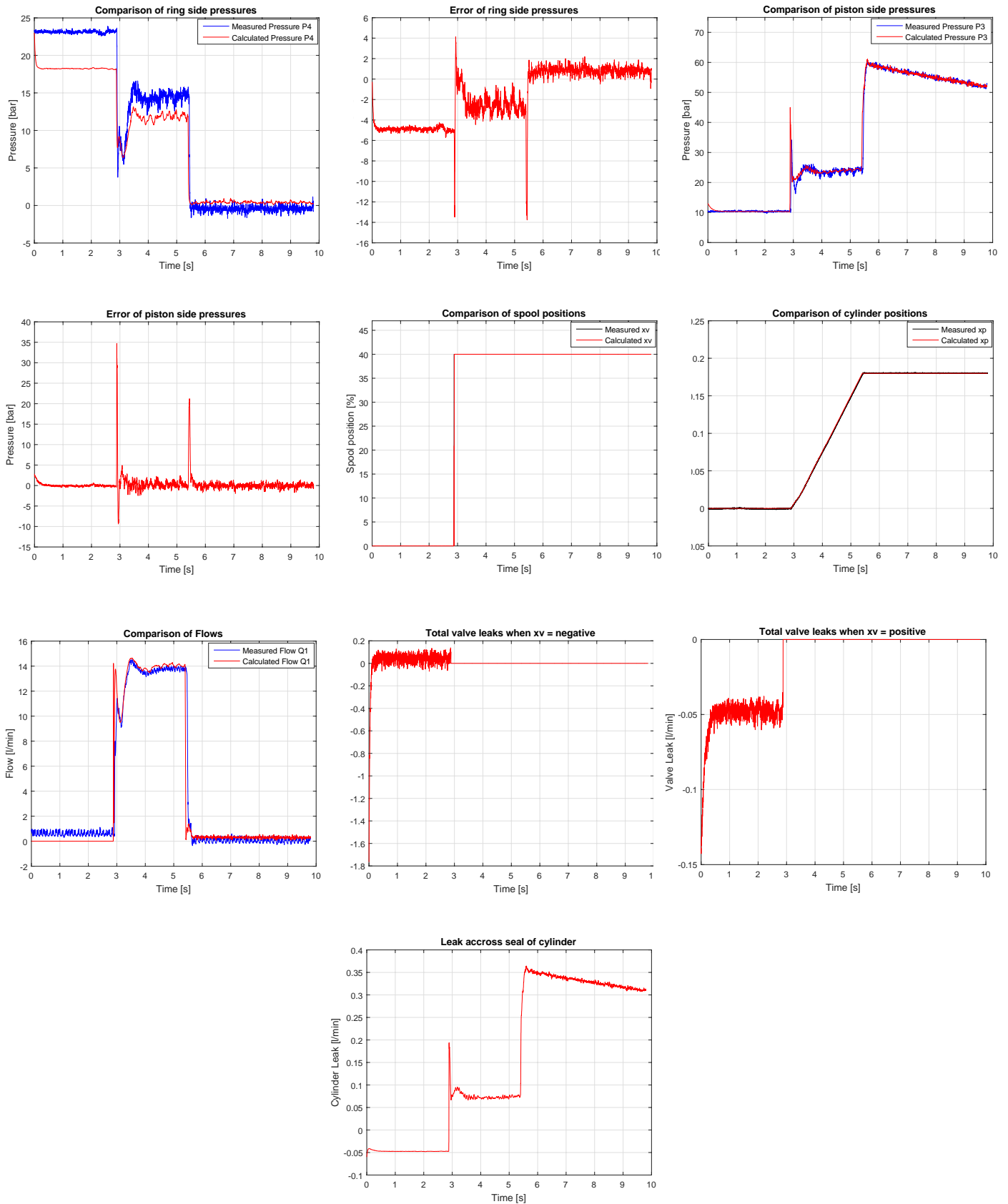




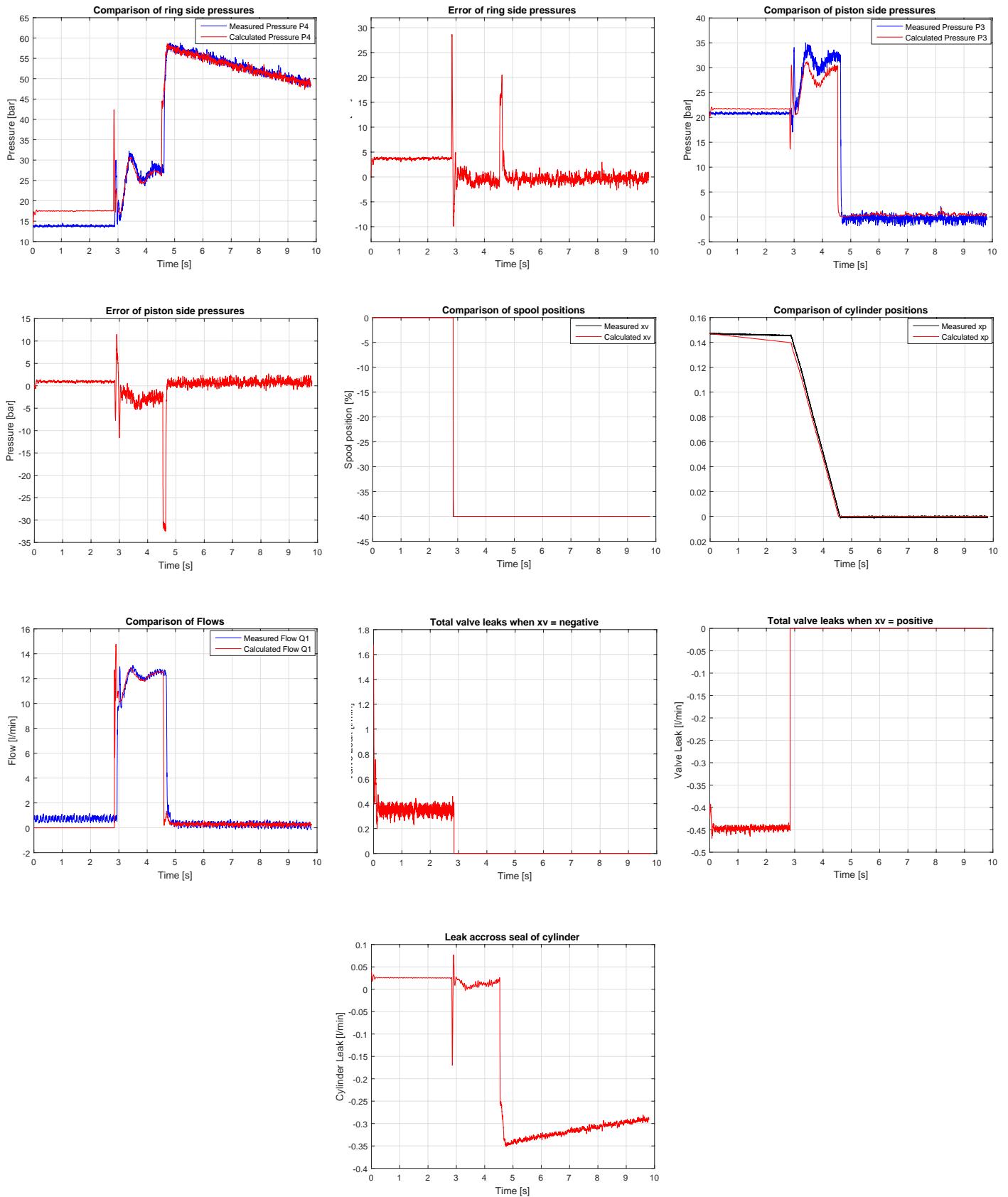
b. Step input -20%, 50 bar



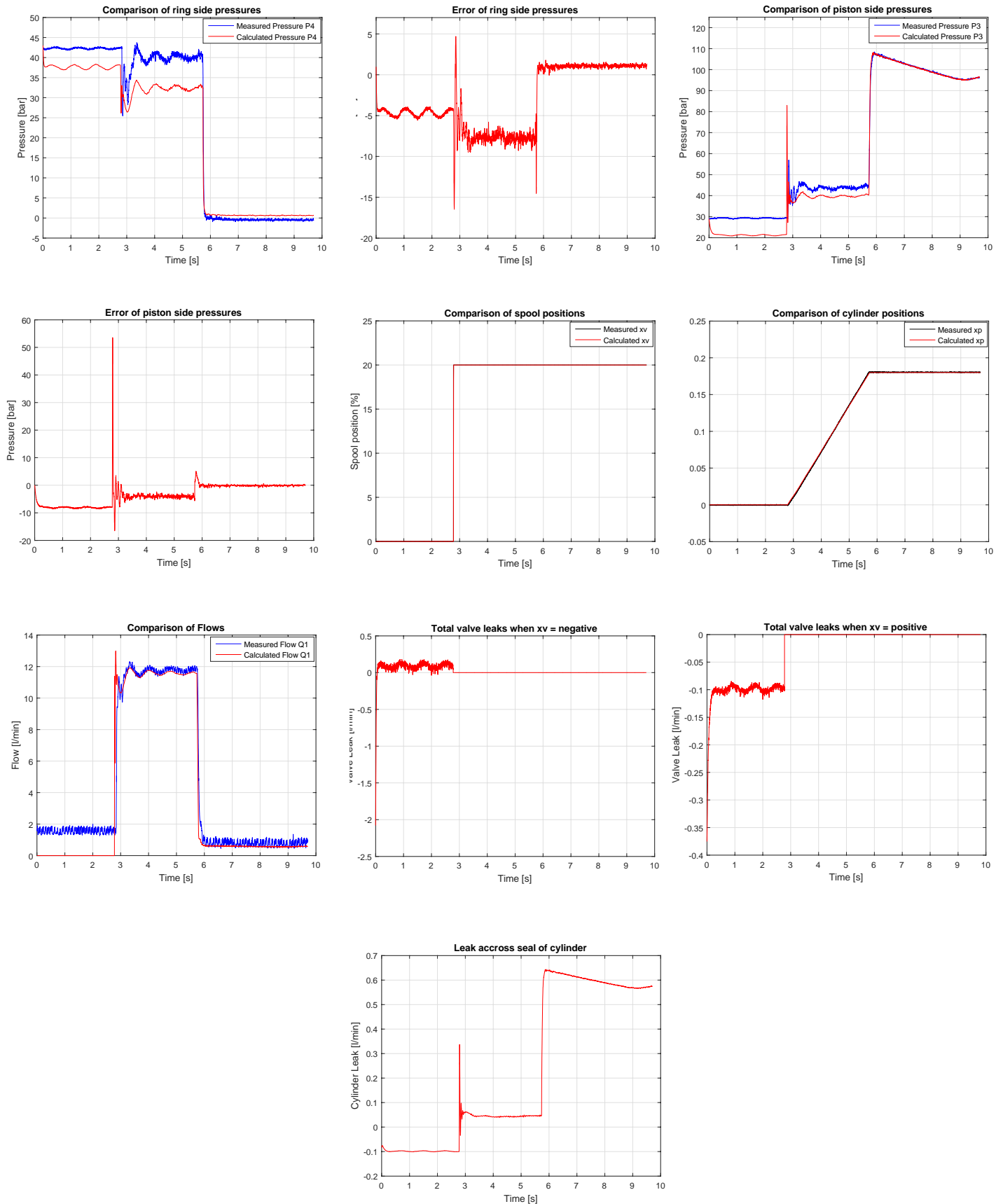
c. Step input 40%, 50 bar



d. Step input -40%, 50 bar



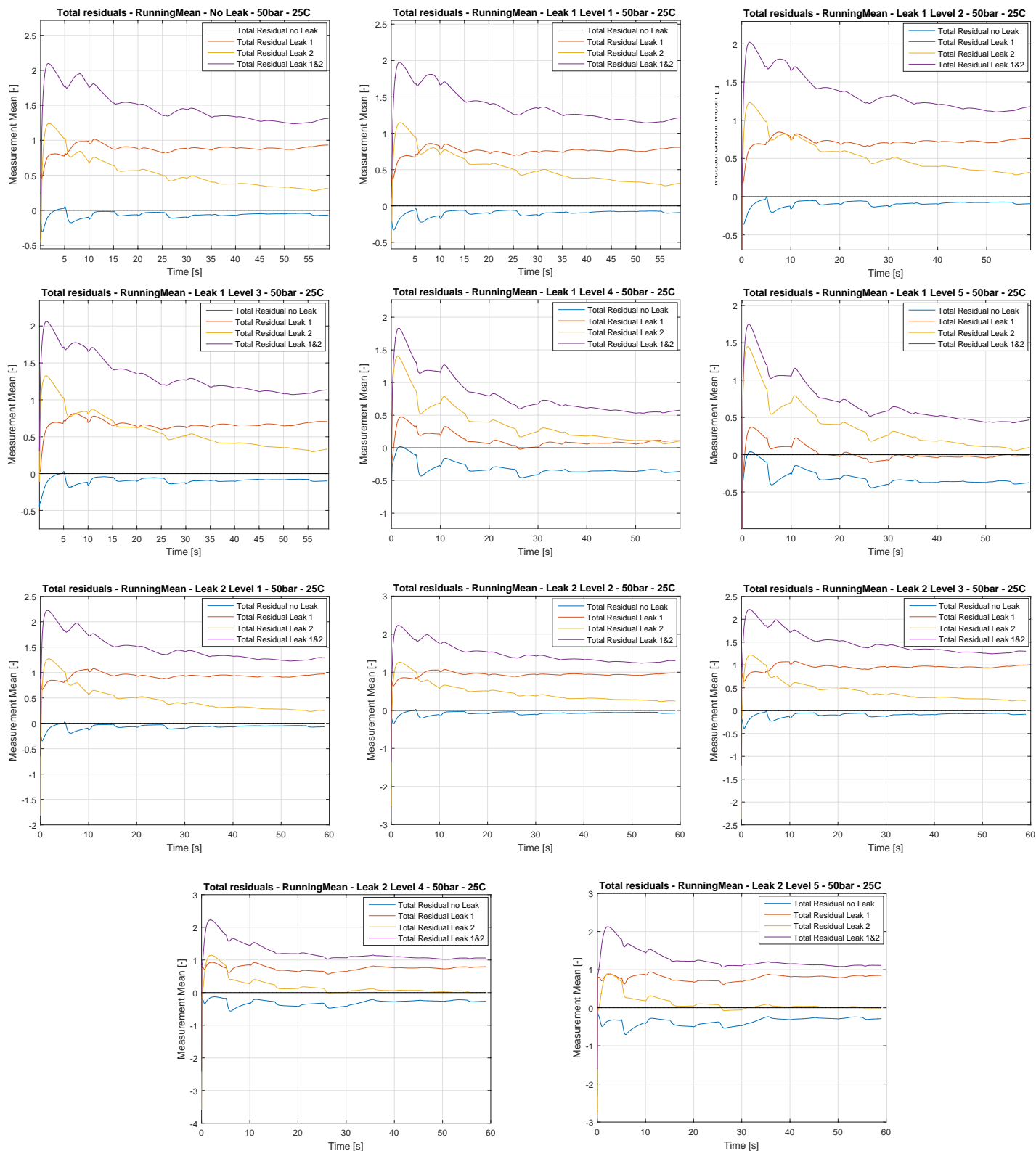
e. Step input 20%, 100 bar

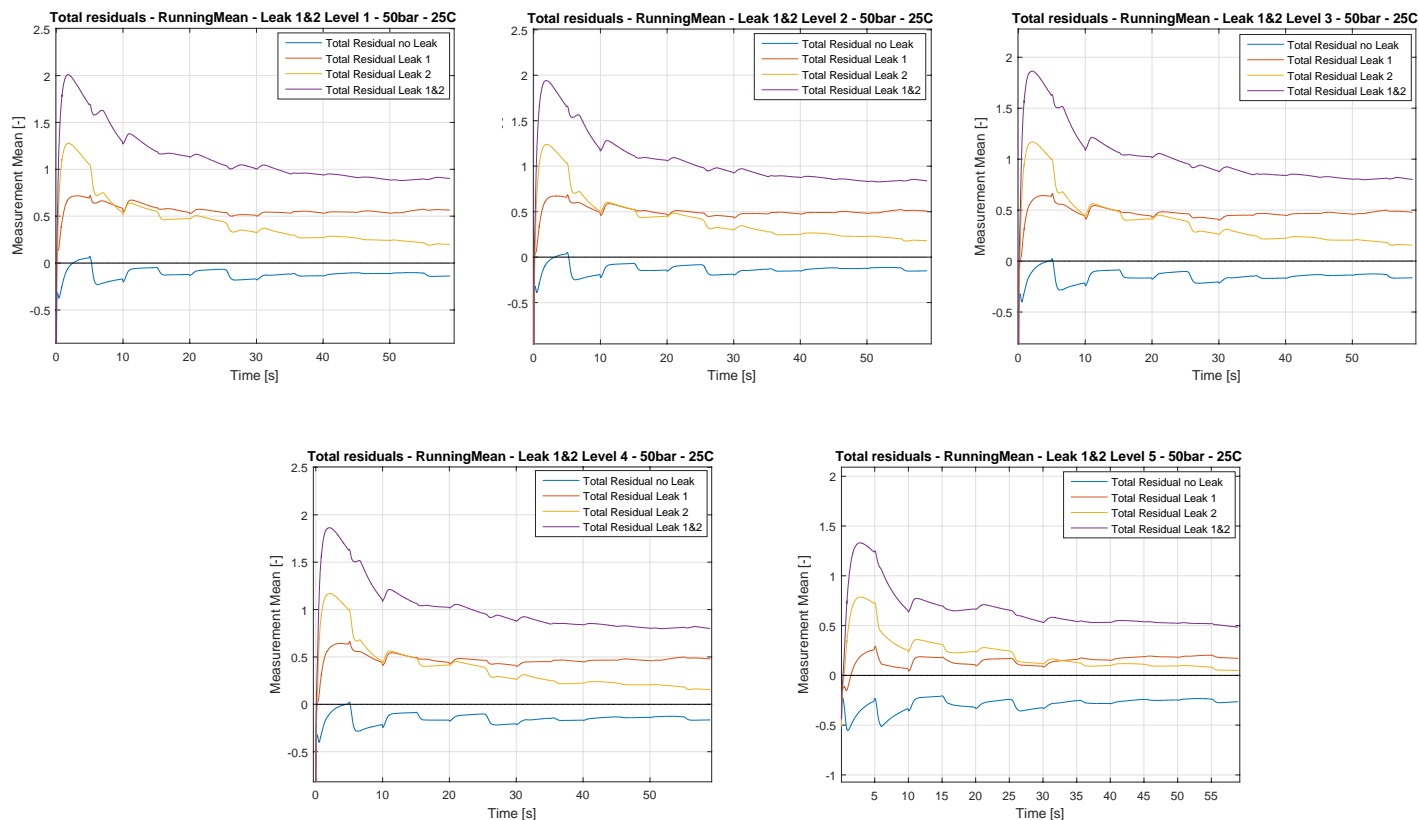




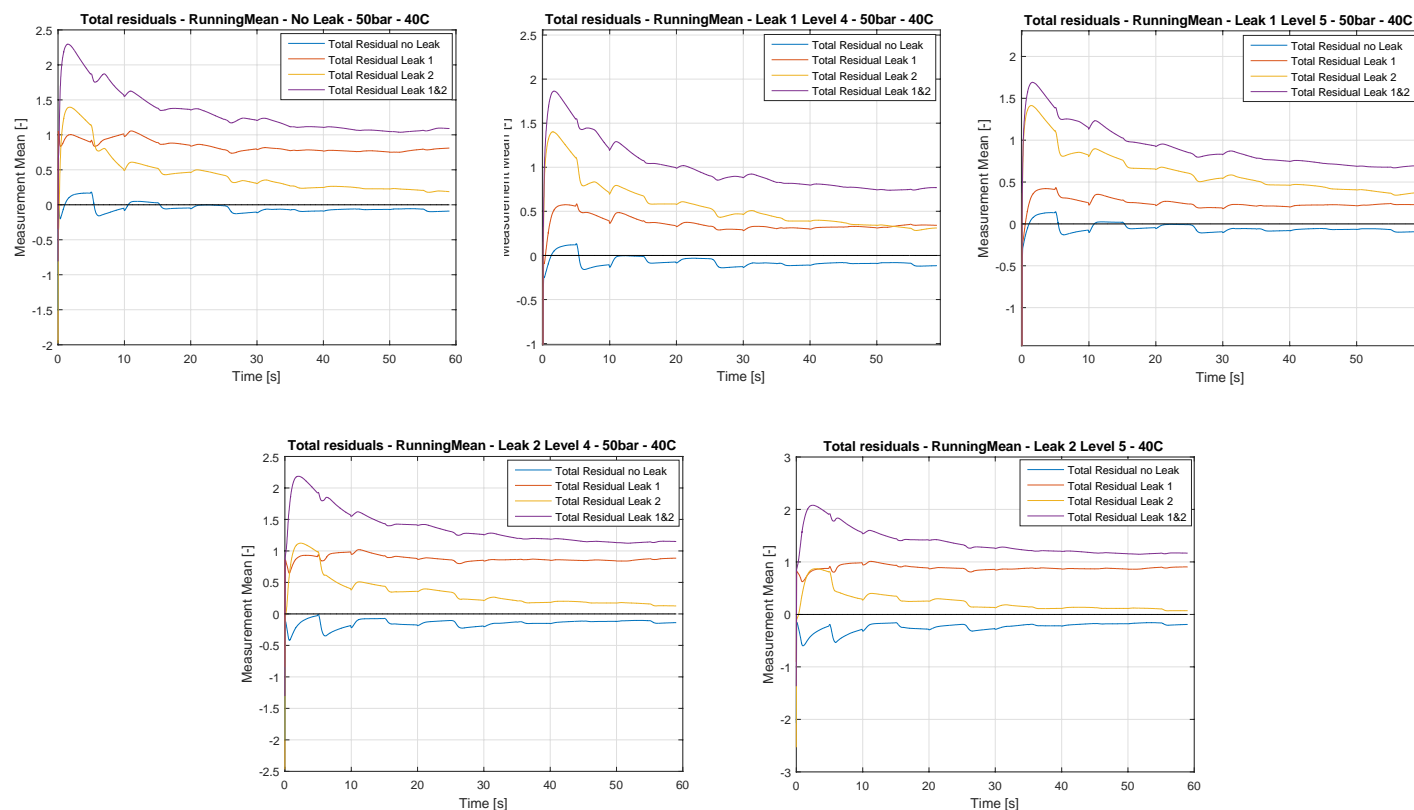
F. Appendix

a. EKF analysis – 50 bar – 25°C



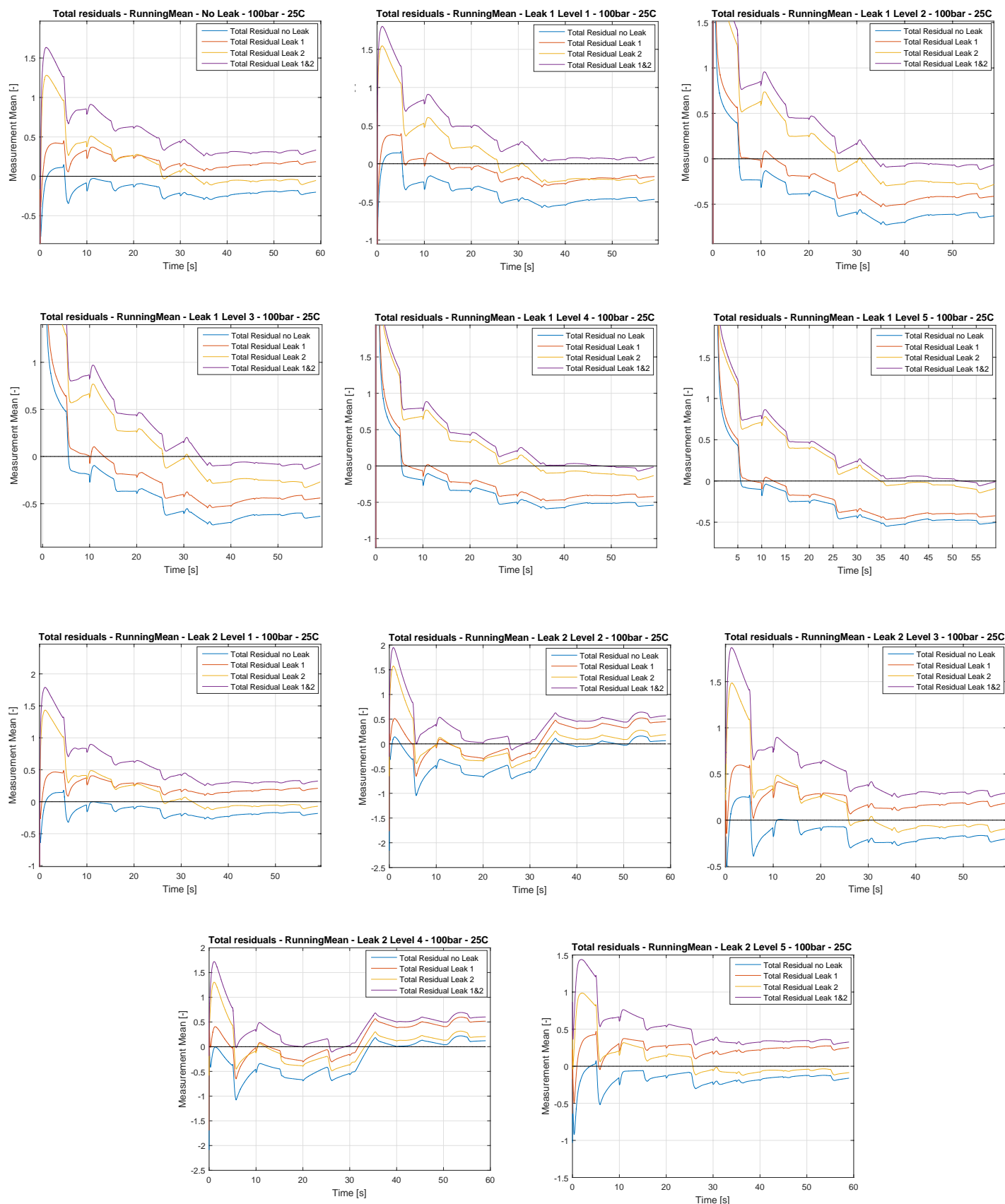


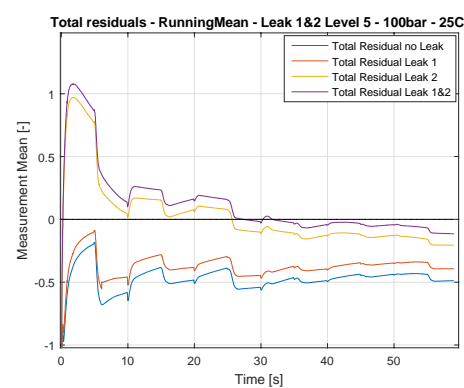
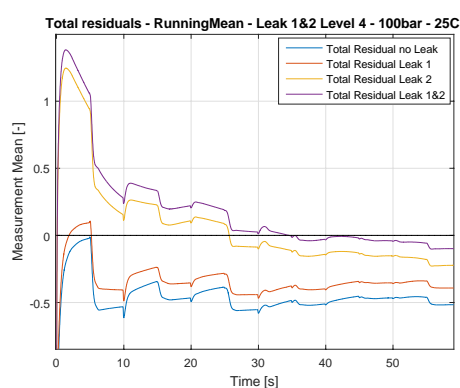
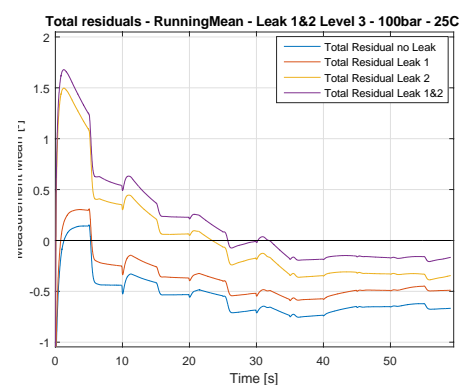
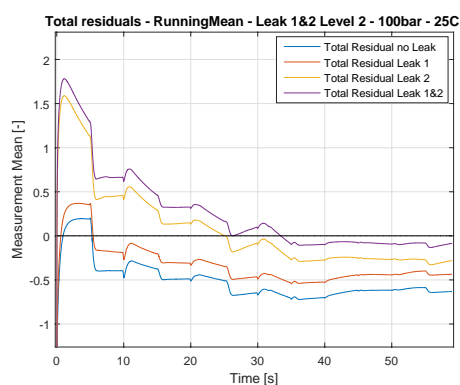
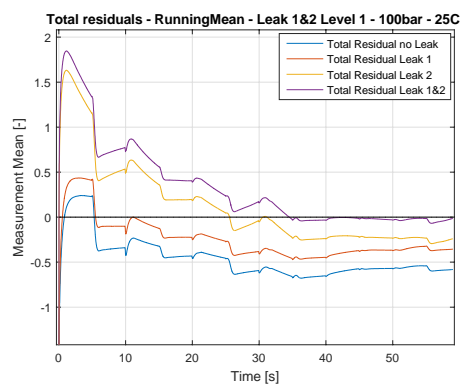
b. EKF analysis – 50bar – 40°C



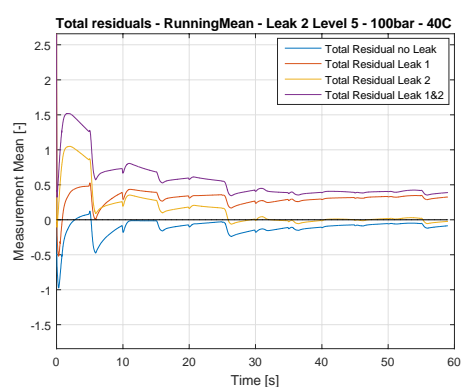
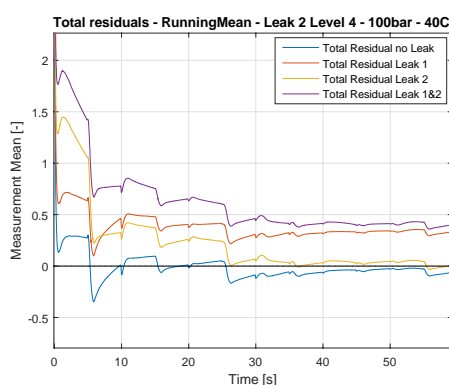
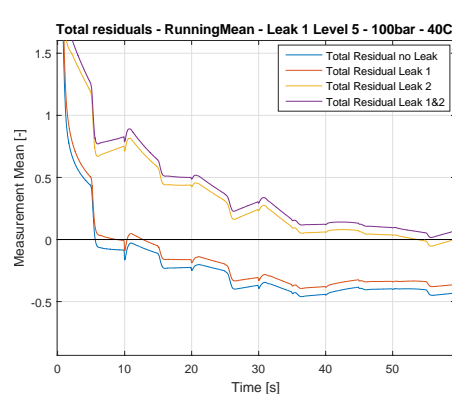
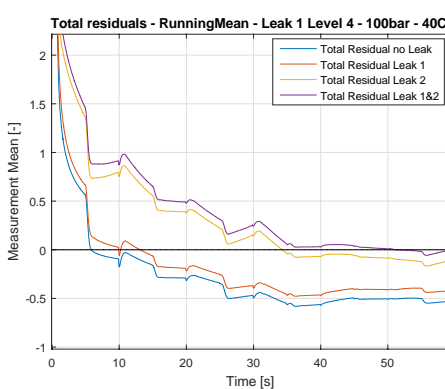
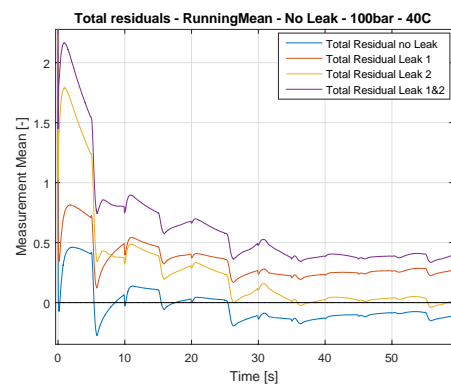


c. EKF analysis – 100bar – 25°C





d. EKF analysis – 100bar – 40°C



G.Simulink diagrams

